TARGET DISCRIMINATION/CLASSIFICATION RADAR

FINAL REPORT

J. Skinner, Ph.D.
F. Ingels, Ph.D.
P. Donohoe, Ph.D.

August 1, 1995

U.S. Army Research Office
Contract: EPSCoR Grant Number
DAAL03–92–G–0355
(ARO Proposal No. P–30691–RT–EP5)

Mississippi State University
Box 9571
MS State, MS 39762
(601+325–2063)

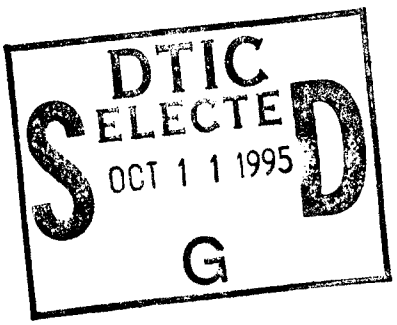

APPROVED FOR PUBLIC RELEASE

DISTRIBUTION UNLIMITED

Submitted To:

U.S. Army Research Office
P. O. Box 12211
Research Triangle Park, NC 27709–2211

TARGET DISCRIMINATION/CLASSIFICATION RADAR

FINAL REPORT

J. Skinner, Ph.D.
F. Ingels, Ph.D.
P. Donohoe, Ph.D.

August 1, 1995

U.S. Army Research Office
Contract: EPSCoR Grant Number
DAAL03–92–G–0355
(ARO Proposal No. P–30691–RT–EP5)

Mississippi State University
Box 9571
MS State, MS 39762
(601+325–2063)

Submitted To:

U.S. Army Research Office
P. O. Box 12211
Research Triangle Park, NC 27709–2211

MASTER COPY KEEP THIS COPY FOR REPRODUCTION PURPOSES

REPORT DOCUMENTATION PAGE

Form Approved
OMB No. 0704-0188

1. AGENCY USE ONLY (Leave blank)	2. REPORT DATE	3. REPORT TYPE AND DATES COVERED
	1 Aug 95	Final Report: 1 Aug 92 - 31 July 95

4. TITLE AND SUBTITLE

Target Discrimination/Classification Radar

5. FUNDING NUMBERS

C: 30691-RT-EPS

G: DAAL03-92-G-0355

6. AUTHOR(S)

B. Jeffrey Skinner, Frank Ingels, P. Donohoe

7. PERFORMING ORGANIZATION NAME(S) AND ADDRESS(ES)

Mississippi State University
Department of Electrical & Computer Engineering
Box 9571
MS State, MS 39762

8. PERFORMING ORGANIZATION REPORT NUMBER

9. SPONSORING/MONITORING AGENCY NAME(S) AND ADDRESS(ES)

U. S. Army Research Office
P. O. Box 12211
Research Triangle Park, NC 27709-2211

10. SPONSORING/MONITORING AGENCY REPORT NUMBER

11. SUPPLEMENTARY NOTES

The view, opinions and/or findings contained in this report are those of the author(s) and should not be construed as an official Department of the Army position, policy, or decision, unless so designated by other documentation.

12a. DISTRIBUTION/AVAILABILITY STATEMENT

Approved for public release; distribution unlimited.

12b. DISTRIBUTION CODE

13. ABSTRACT *(Maximum 200 words)*

Adaptive FSK/PSK is a spectrally agile pulse compression radar signaling scheme that learns target-specific information over time & integrates that information into the design of its radar signal processor in real-time. This use of target-specific information into the real-time transmitter signal design process enhances the return from the target, thus improving the performance of the radar system in both additive noise environments (jamming) & ground clutter limited environments (low altitude targets). Since FSK/PSK signaling is a pseudorandom pulse compression scheme with a large time-bandwidth product, it has inherent low probability of intercept characteristics. Additionally, adaptive FSK/PSK signaling is able to learn target-specific information which can be used to identify the target using existing target identification techniques. In this study, the cross-ambiguity function of a general FSK/PSK waveform is derived and analyzed in a probabilistic manner. The results of this probabilistic analysis are used to develop a design methodology that allows the signal to be matched to an arbitrary target. It is shown that both the signal to clutter ratio and signal to noise ratio of a matched FSK/PSK radar are superior to those of a conventional signaling radar that utilizes no target-specific information.

14. SUBJECT TERMS

LPI, Target Discrimination/Classification Radar Adaptive FSK/PSK Radar Signals

15. NUMBER OF PAGES

151

16. PRICE CODE

17. SECURITY CLASSIFICATION OF REPORT	18. SECURITY CLASSIFICATION	19. SECURITY CLASSIFICATION OF ABSTRACT	20. LIMITATION OF ABSTRACT
UNCLASSIFIED	UNCLASSIFIED	UNCLASSIFIED	UL

NSN 7540-01-280-5500

Standard Form 298 (Rev. 2-89)
Prescribed by ANSI Std. Z39-18
298-102

THE VIEWS, OPINIONS, AND/OR FINDINGS CONTAINED IN THIS REPORT ARE THOSE OF THE AUTHOR(S) AND SHOULD NOT BE CONSTRUED AS AN OFFICIAL DEPARTMENT OF THE ARMY POSITION, POLICY, OR DECISION, UNLESS SO DESIGNATED BY OTHER DOCUMENTATION.

FORWARD

The authors are very grateful to the U.S. Army for providing support for this research. It is believed the result is interesting and vital to those interested in the topic of target detection and discrimination using radar.

TABLE OF CONTENTS

TARGET DISCRIMINATION/CLASSIFICATION RADAR

1.0 PURPOSE OF STUDY

It was proposed to investigate the use of Low Probability of Detection/Super Wide Band (LPI/SWB) radar systems operating from airborne platforms for target discrimination/classification. These LPI/SWB radar systems would have a transmitted percent bandwidth on the order of 1% to 10%, and they would make use of pulse compression techniques. The radar envisioned would obtain its target discrimination/classification capability by exploiting the dissimilarities that exist between the scattering characteristics of various radar targets of interest. In other words, the radar would have a library of target specific signals that it would be capable of transmitting and processing. Each signal in the library would be constructed in such a manner as to excite a large reflection from a specific target while exciting a minimal reflection from other targets. Therefore, when a target is detected, the entire library could be used to interrogate the target, and the signal that excited the largest response would have the highest probability of being the target associated with the target specific signal.

The system would achieve its LPI characteristics by passing the target specific waveforms generated by the target library through a pulse expansion filter. The expanded waveform would then be up–converted and transmitted. The expanded target specific signal would then excite the target and the reflected energy would be received and down–converted. The down–converted signal would then be passed through a pulse–compression filter (which is the time reversal of the pulse–expansion filter) to obtain the minimally corrupted response of the target to the target specific signal. The system would be similar to a conventional pulse compression system, and it differs only in that the standard pulse compression system excites the pulse expansion filter with an impulse and the LPI/SWB system excites the pulse expansion filter with the target specific signal.

It was anticipated that this investigation would be achieved in three steps:

1) Various LPI/SWB radar implementations would be rigorously investigated to determine which method has the most promise in the application described above.

2) The scattering characteristics of various target geometries of interest would be investigated to determine exactly how they may be exploited.

3) The information learned in the studies outlined above would be combined to determine guidelines that can be used in the design of specific radar systems to accomplish the target discrimination/ classification task described above.

Task 1 involved an investigation into various types of pulse compression radar systems (PSK, FSK and Hybrid FSK/PSK) to determine their limitations and beneficial qualities. Some of these qualities investigated were achievable bandwidth, low probability of intercept capability, and the spectral purity of the pulse expansion filter. Task 2 involved the development of accurate computer models of generic targets for generation of target scattering characteristics. This involved the use of existing exact solution techniques that could be used for resonant region analysis (or the region at which the target size is on the order of a wavelength), and the development of approximate solution programs for optical region analysis (or the frequency region where the target extends for many wavelengths). Task 3 involved using the tools developed in Tasks 1 and 2 to determine the optimum implementation of a LPI/SWB radar. This was basically an analysis of model systems to determine performance levels as target discrimination/classification systems.

2.0 SUMMARY AND CONCLUSIONS OF RESEARCH

The purpose of this study was to develop a signal processing scheme that would combine the separate research efforts of low probability of intercept signaling, low altitude low observable target tracking, and non-cooperative target recognition into a single research effort. The end result of this fusion is a new radar design concept designated adaptive FSK/PSK signaling. An adaptive FSK/PSK radar system makes use of matched FSK/PSK signals in conjunction with a gradient descent adaptive signal design algorithm. Matched FSK/PSK signals are ultra wideband pseudorandom multiple frequency bi–phase modulated signal sequences that have spectral content specifically matched to the target under track. This use of target–specific information in the design of radar signals is the salient point of this research effort. It allows for more efficient use of signal power and results in a performance improvement over existing radar technologies that are matched to the transmit signal only. Since the spectral content of the target is not known a priori, the target range profile must be learned by the radar. This matching of the signal to the target is accomplished through the use of an iterative (adaptive) algorithm that is based on gradient descent. Once the radar has adapted to the target (learned the target), the range profile of the target is known and target identification can take place based on the learned range profile. Therefore, an adaptive FSK/PSK radar system can be thought of as a learning system as opposed to a measurement system. In other words, the radar measurement is improved as a result of the learning process.

The pseudorandom sequence structure of the matched FSK/PSK signal, along with its high time–bandwidth product, makes the radar inherently difficult to detect. Therefore, the signals can be classified as low probability of intercept. Additionally, since the transmitter power is used in a most effective manner (signal efficiency is maximized by target matching), lower peak power signals can be utilized by the radar. This results in an additional improvement in LPI performance.

In an additive noise environment, matched FSK/PSK signaling provides a signal processing gain over a baseline radar that utilizes a signal with an impulse–like ambiguity function. This performance improvement results from the fact that the signal power is utilized in an efficient manner and the target reflection is enhanced without enhancing the additive noise. The level of signal processing gain is dependent upon the spectral complexity of the target. If the target reflects all frequencies equally well, little processing gain is seen. On the other hand, if the target reflectivity is concentrated in a few isolated frequency bands, then the processing gain can be large (on the order of the square of the number of frequencies used in the signal).

In a ground clutter limited environment, matched FSK/PSK signaling performs better than conventional radar technologies that do not take into account any target specific information. This occurs because the matched FSK/PSK radar system is capable of achieving a theoretical target enhancement of between 1 and K^2 while the integrated sidelobe level is increased by a factor of between 1 and K where K is the number of frequencies used in the construction of the signal. Therefore, in a clutter limited environment, adaptive FSK/PSK radar systems can achieve performance improvement factors of between 1 and K. It should be noted that a matched FSK/PSK radar system and a conventional radar system using a matched filter post–processor are able to achieve identical performance in a clutter limited environment.

Analysis of predicted real target signature data shows that the use of target–specific information in the design of the radar signal typically yields average signal to noise ratio improvements of between 3 dB and 6 dB depending on the target. In a clutter limited environment, typical improvements are between 2 dB and 5 dB. These improvements are closer to the low end of the theoretically possible performance improvements. This is result of the uniform nature of optical region target spectra. The gains, however, are significant and provide a significant performance increase. It should be pointed out that in the resonance region, greater gains are expected since resonance region spectra are typically impulse–like.

The adaptation algorithm derived in the research (See Chapter VIII of the Appendix) provides a method of not only designing the optimum signal to excite the maximum response from the target, but also for measuring the best mean squared estimate of the target range profile. Through computer simulations, it was shown that the adaptation algorithm removes additive noise. The level of noise removal is dependent on the value of the learning parameter. The smaller the learning parameter (slower the learning rate), the better the

mean squared estimate. The simulations also show that the random fluctuations of the target range profile due to random range motion and random incidence angle motion increase the mean squared error of the estimate. If the learning rate is high enough for the adaptive algorithm to learn the target range profile before the profile decorrelates, then the errors are small. If on the other hand, the target decorrelates more rapidly than the algorithm can learn, range profile estimation errors are increased. This results in decreased target enhancement due to matched FSK/PSK signaling. It should be pointed out that the performance metric used in this study (the mean squared range profile error) is biased towards stationary (nonfluctuating) targets. It is difficult to ascertain the deleterious effects of range profile fluctuations on an actual target identification algorithm. The effects may be insignificant since the adaptation algorithm determines a best mean squared fit to the second order statistics of the random target fluctuation process within the learning period of the algorithm. It is of interest to note that a linear averaging scheme would yield a zero result for range profile estimation since the phase angle of the returns is random from measurement to measurement.

In conclusion, adaptive FSK/PSK signaling radar is an excellent platform for fulfilling the future mission of radar: low probability of intercept noncooperative target recognition. It utilizes low probability of intercept signals in a spectrally adaptive manner. The ability of the radar to adapt its spectrum makes it possible to enhance targets thus improving system performance in additive noise environments and ground clutter limited environments. Finally, the adaptation scheme derived in this study is capable of extracting the range profile of the target under track. This is important for target identification since it is the range profile that is the feature vector used by most target identification algorithms.

In the work performed, a series of equations were derived to model the Radar Performance for Target Return, Signal–to–Clutter and Bandwidth Loss for three cases. These three cases are a Baseline Radar (Correlation) Receiver, a Matched Filter Radar Receiver, and a Matched FSK/PSK Radar Receiver. The Table below summarizes the equations with equation numbers referencing Chapter VII of the Appendix.

Performance estimates for specific target scenarios are contained in Chapter VII for Appendix, Table 7.1, page 91.

Summary of Radar Performance Equations.

	Baseline	Matched Filter	Matched FSK/PSK
Target Return	$\frac{1}{K}\max_{\cdot}\left\lvert\sum_{k=0}^{K-1}\sqrt{\sigma_k}\;e^{j(2\pi k\cdot\cdot+\phi_k)}\right\rvert$	$\frac{\sum_{k=0}^{K-1}\sigma_k}{K\sqrt{\sum_{k=0}^{K-1}\sigma_k}}$	$\frac{\sum_{k=0}^{K-1}\sigma_k}{\sum_{k=0}^{K-1}\sqrt{\sigma_k}}$
	Equation (7.4)	Equation (7.9)	Equation (7.18)
Signal to Clutter	$\frac{1}{K}\max_{\cdot}\left\lvert\sum_{k=0}^{K-1}\sqrt{\sigma_k}\;e^{j(2\pi k\cdot\cdot+\phi_k)}\right\rvert^2$	$\sum_{k=0}^{K-1}\sigma_k$	$\sum_{k=0}^{K-1}\sigma_k$
	Equation (7.7)	Equation (7.15)	Equation (7.22)
Bandwidth Loss	None	None	$\frac{1}{K\max\{p_k\}}$
			Equation (5.14)

3.0 PUBLICATIONS; PRESENTATIONS RESULTING DIRECTLY FROM THIS CONTRACT

Correlation Properties of Gaussian FSK/PSK Radar Signal," B. Jeffrey Skinner, J. Patrick Donohoe, and Frank Ingels, Proceedings of IEEE Southeastcon '93, Charlotte, NC, April 1993. (REFEREED CONFERENCE PROCEEDINGS)

"Simplified Performance Estimation of FSK/PSK Hybrid Signalling Radar Systems," B. Jeffrey Skinner, J. Patrick Donohoe, and Frank Ingels, NAECON'93, Dayton, OH, May 1993.[1]

"Simulation of Target Response to High Frequency Ultra Wideband Radar Signals Using the Physical Optics Impulse Response," B. Jeffrey Skinner, J. Patrick Donohoe, and Frank Ingels, 25th SSST, Tuscaloosa, AL, March 1993.

"The Effect of Radar Signal Construction on Detectability," B.J. Skinner, F.M. Ingels and J.P. Donohoe, 1994, Proceedings of Southeastern Symposium on System Theory, Athens, OH, March 1994.

"Matched FSK/PSK Radar," B.J. Skinner, J.P. Donohoe and F.M. Ingels, Proceedings of the 1994 IEEE National Radar Conference, Atlanta, GA, April 1994. (REFEREED CONFERENCE PROCEEDINGS)

"Gradient Descent Method for Designing Optimum Radar Signals," B.J. Skinner, J.P. Donohoe, F.M. Ingels, 1995 IEEE International Radar Conf., Washington, DC, May 1995. (REFEREED CONFERENCE PROCEEDINGS)

1. Mr. B.J. Skinner was awarded first prize in the NAECON'93 Student Paper Competition.

4.0 PERSONNEL WHO PARTICIPATED IN THIS PROJECT

The personnel who participated in this research were:

J.P. Donohoe, Ph.D., Associate Professor of Electrical Engineering

F.M. Ingels, Ph.D., Professor of Electrical Engineering

B.J. Skinner, Ph.D.*, Research Investigator (Electrical Engineering)

*Dr. B.J. Skinner received his Doctorate of Philosophy (Electrical Engineering) while employed in this project. The project research was the foundation of his dissertation (Appendix of this report).

APPENDIX

The appendix is a reproduction of the dissertation that resulted from the research for this project. Publications that occurred during the course of the research are listed in Section 3.0. The appendix is a self contained document that gives full background details and results. It is the desire of the authors that the work be readable and useable to those who are interested in this interesting and vital topic.

ADAPTIVE FSK/PSK RADAR WITH APPLICATION TO LOW PROBABILITY OF INTERCEPT NONCOOPERATIVE TARGET RECOGNITION

A Dissertation
by
BURNICE JEFFREY SKINNER

for the
Doctorate of Philosophy
in
Electrical Engineering

Mississippi State University
Box 9571
Mississippi State, MS 39762

TABLE OF CONTENTS

LIST OF TABLES

LIST OF FIGURES

CHAPTER I

INTRODUCTION

Radar was first used as a military sensor system during World War II when it came into prominence during the air war over Britain. These early radar systems were able to locate the direction and distance (azimuth and range) of attacking waves of German bombers while they were still well beyond visual range. This location information made it possible to deploy the outnumbered Royal Air Force fighter wings in a more effective manner and thus, the Battle of Britain was won. By the end of the war, the state-of-the-art in radar had advanced significantly and included fire control radar for anti-aircraft artillery. These radar systems were able to automatically track the range, range-rate, azimuth, and elevation of a target.

During the late 1940's and 1950's, the role of radar technology remained basically unchanged. Developments in radar were primarily devoted to codifying radar design principles [1] and expanding the underlying mathematical theory of radar [2]. During the 1960's and 1970's, the new technologies of solid state devices and digital computing were implemented into radar systems making them smaller, more power efficient, and basically more capable. Still, technology had not advanced to the extent that the role of World War II era radar would be changed significantly change.

The 1970's and 1980's saw the advent of two new radar design requirements: tracking of stealth (or low observable) aircraft and anti-radiation missiles. Stealth technology drove research into the area of radar signal designs capable of tracking low radar cross section targets buried in ground clutter returns. The goal of these signal designs was waveforms capable of rejecting the range extended ground clutter return [3, 4, 5, 6] primarily by lowering the range sidelobes of the radar signal ambiguity function. These clutter suppression efforts assumed that the radar target of interest was localized to a point-like range extent (point target assumption) and therefore, reflected all waveforms equally well. Anti-radiation missiles drove research into the area of signal designs that made it more difficult for a radar warning receiver to detect the existence of the radar signal (low probability of intercept signaling) [7]. In other words, the radar signals themselves were forced to become stealthy. This led to pulse compression signals that utilized random frequency and phase coding to provide a signal processing gain to the radar. This signal processing gain was typically measured by the time-bandwidth product of the waveform [7, 8, 9].

The late 1980's and 1990's have seen an interest in expanding the role of radar. Instead of radar simply being a detection device, radar systems capable of identifying targets [10] are of interest. In other words, modern radar systems will be required to extract more information from targets. Therefore, there is an increased interest in so-called ultra wideband radar concepts [10]. Ultra wideband radar concepts can be classified into two types of radar signaling regimes [11]: impulse radar for resonant frequency extraction and high range resolution waveform signaling.

Resonant region radars try to identify targets based on the extraction of the natural resonant frequencies excited by a broadband pulse of electromagnetic radiation [12, 13, 14, 15, 16]. These resonant frequencies are target-specific and are therefore good classification features. The problem with this technique is that the radars are required to operate in the VHF and low UHF frequency bands and therefore, the radar systems are very large and unwieldy. Additionally, the percent bandwidth of the waveforms used must be very high (multi-octave signaling desirable) and Doppler processing becomes ineffective for ground clutter removal.

High range resolution radar systems identify radar targets based on the location of scattering centers [17, 18]. In other words, the range resolution of the radar is such that the individual scattering components of the target can be resolved. These radar systems operate in typical radar frequency bands (above 1 GHz), but use higher than typical signal bandwidths. High range resolution radar systems have the advantage of small size, narrow antenna beamwidths, and a higher degree of Doppler precision. The disadvantage of high range resolution radar systems is that the range profiles are highly dependent upon target aspect angle and a large amount of data is required to describe each individual target in a target database [17, 18].

1.1. Combining Goals

Future radar systems will use low probability of intercept (LPI) waveforms to track and identify low observable targets. Therefore, the development of radar target identification techniques must be accomplished within the confines of the requirements on low observable target tracking and signal detectability by hostile interceptors. In

the past, research in these three areas has progressed in separate directions. Research into low observable target tracking has been based on the assumption that radar targets are point targets (single point scatterer) while ground clutter is range extended. Therefore, design techniques have focused on designing waveforms that are matched to point targets yet reject distributed clutter targets. Target identification algorithms, on the other hand, make use of the range extended nature of radar targets [17, 18] (i.e., each target scatters radiation differently). A question therefore arises; should low observable target tracking research focus on enhancing the return from distributed radar targets by making use of target-specific information as well as suppressing clutter? In short, is it possible for the range extended target-specific information to be utilized to the radar's advantage?

1.2. Scope of Study

The purpose of this study is to combine the three different research efforts related to low observable target tracking in clutter, LPI signal design, and target identification into a single research effort. In this study, a pulse compression technique designated "matched FSK/PSK" [21] is introduced. Unlike conventional signaling techniques, matched FSK/PSK signaling makes it possible to not only suppress clutter returns, but also to enhance the target return. The target return enhancement is accomplished by making use of target-specific information in the signal design process. Since target enhancement requires a priori knowledge about the range profile of the particular target, an iterative signal design technique [22] is introduced. This is a nonlinear design technique that effectively extracts the target's

range profile over time and can be thought of as a measurement technique. The extracted target range profile is a usable feature for target identification purposes. When matched FSK/PSK is used in conjunction with the iterative design algorithm, the resulting system is designated "adaptive FSK/PSK". This study is theoretical in scope since a treatment of hardware implementation issues would tend to mask the fundamental principles involved. Realistic target modeling is used, however, to acquaint the reader with typical achievable performance improvements.

1.3. Organization of Study

This study is organized in the following manner. Some fundamentals of radar and radar signal processing are presented briefly in Chapter II. The concepts of pulse compression, radar-interceptor advantage, range smearing, ground clutter analysis with the cross-ambiguity function, as well as radar scattering regimes are discussed in general terms in order to standardize terminology and to develop a basis for presenting and solving the problem. In Chapter III, the cross-ambiguity function [20] is discussed in general with respect to radar-target interaction, noise removal and resolution, and specifically with respect to FSK/PSK signaling. The cross-ambiguity function of the FSK/PSK waveform is analyzed probabilistically in Chapter IV. This analysis includes a mean and mean squared analysis of the mainlobe of the cross-ambiguity function, mean and mean squared analysis of the cross-ambiguity function sidelobes, and evaluation of the integrated mean square sidelobe level of the cross-ambiguity function (a baseline measure of clutter rejection). The power spectral density and equivalent time-bandwidth product of an FSK/PSK radar signal are

derived in Chapter V. In Chapter VI, the probabilistic analysis of Chapter IV is used to develop a design methodology for matched FSK/PSK radar based on a known arbitrary range profile. The performance gain of matched FSK/PSK over a conventional signaling radar system that utilizes no target-specific information is determined in Chapter VII. The performance metrics used in the study are the target enhancement, signal to noise ratio, and signal to clutter ratio of matched FSK/PSK relative to a baseline conventional radar. These performance gains are calculated for both theoretical target scattering distributions and for some predicted target data. An iterative signal design technique is derived in Chapter VIII. This technique is derived based on gradient descent optimization of the mean squared reflected voltage. This gradient descent adaptive signal design scheme is also studied parametrically in Chapter VIII. This parametric study illustrates the effect of additive white noise, target range motion, and target angular motion. Concluding remarks and suggestions for future work are discussed in Chapter IX.

1.4. References

1. Radiation Laboratory Reports

2. P. M. Woodward, Probability and Information Theory, with Applications to Radar, Pergamon Press, New York, 1953.

3. A. W. Rihaczek and R. L. Mitchell, "Radar Waveforms for Suppression of Extended Clutter", IEEE Transactions on Aerospace and Electronic Systems, May 1967, pp. 656-663.

4. D. F. DeLong, Jr. and E. M. Hostetter, "On the Design of Optimum Radar Waveforms for Clutter Rejection", IEEE Transactions on Aerospace and Electronic Systems, January 1967, pp. 138-141.

5. M. Ares, "Optimum Burst Waveforms for Detection of Targets in Uniform Range-Extended Clutter", IEEE Transactions on Aerospace and Electronics Systems, January 1967, pp. 138-141.

6. T. K. Bhattacharya and P. R. Mahapatra, "A Versatile and Powerful Method of Designing Optimum Signals Against Arbitrary Range-Doppler Clutter", 1989 International Radar Conference,

7. G. Schrick and R. G. Wiley, "Interception of LPI Radar Signals", 1990 IEEE International Radar Conference, pp. 108-111.

8. D. C. Schleher, "Low Probability of Intercept Radar", 1985 IEEE International Radar Conference, pp. 346-349.

9. S. L. Johnston, "Radar Operability/Survivability in the 1990's", 1989 International Radar Conference,

10. M. Skolnik, "Status of Ultra Wideband (UWB) Radar and its Technology", Proceedings of the 1992 IEEE Antennas and Propagation Society International Symposium, Vol. 3, pp. 1224-1227.

11. L. S. Riggs and C. R. Smith, "Bayesian Probability Theory Applied to the Problem Radar Target Discrimination", Proceedings of the 1992 IEEE Antennas and Propagation Society International Symposium, Vol. 3, pp. 1246-1249.

12. A. J. Berni, "Target Identification by Natural Resonance Estimation", IEEE Transactions on Aerospace and Electronics Systems, March 1975, pp. 147-154.

13. A. A. Ksienski, Y.T. Lin, and L. J. White, "Low-Frequency Approach to Target Identification", Proceedings of the IEEE, December 1975, pp. 1651-1660.

14. C. W. Chuang and D. L. Moffatt, "Natural Resonances of Radar Targets Via Prony's Method and Target Discrimination", IEEE Transactions on Aerospace and Electronics Systems, September 1976, pp. 583-589.

15. E. W. Kennaugh, "The K-Pulse Concept", IEEE Transactions on Antennas and Propagation, March 1981, pp. 327-331.

16. E. K. Rothwell, D. P. Nyquist, K. M. Chen, and B. Drachman, "Radar Target Discrimination Using the Extinction-Pulse Technique", IEEE Transactions on Antennas and Propagation, September 1985, pp. 929-936.

17. S. Hudson and D. Psaltis, "Correlation Filters for Aircraft Identification From Radar Range Profiles", IEEE Transactions on Aerospace Electronics Systems, July 1993, pp. 741-748.

18. H. J. Li and S. H. Yang, "Using Range Profiles as Feature Vectors to Identify Aerospace Objects", IEEE Transactions on Antennas and Propagation, March 1993, pp. 261-268.

19. E. J. Kelly and R. P. Wishner, "Matched-Filter Theory for High-Velocity, Accelerating Targets", IEEE Transactions on Military Electronics, January 1965, pp. 56-69.

20. A. W. Rihaczek, Principles of High Resolution Radar, Peninsula Publishing, Los Altos, CA, 1985.

21. B. J. Skinner, J. P. Donohoe, and F. M. Ingels, "Matched FSK/PSK Radar", Proceedings of the 1994 National Radar Conference, pp. 251-255.

22. B. J. Skinner, J. P. Donohoe, and F. M. Ingels, "Gradient Descent Method for Designing Optimum Radar Signals", accepted for publication Proceedings of the 1995 International Radar Conference.

CHAPTER II

RADAR FUNDAMENTALS

In this chapter, several fundamentals of radar systems analysis are discussed primarily to introduce notation and for proper problem formulation. These fundamental topics are: 1) signal to noise ratio (SNR) at the radar receiver and at the intercept receiver (receiver-interceptor advantage), 2) pulse compression, 3) range resolution, 4) velocity or Doppler resolution, 5) range smearing, 6) range-doppler trade-offs, and 7) ground clutter analysis with the cross-ambiguity function. Additionally, an overview of radar scattering fundamentals, as related to target identification, is given. These limits and bounds are not derived in detail, only discussed in relation to the problem of LPI tracking and identification of low observable radar targets.

Figure 2.1 graphically shows all components of the problem that are points of interest in this study. A waveform $y(t)$ is transmitted from the radar antenna. A portion of the energy is reflected by the target while another portion is reflected by the surface of the earth. The energy reflected from the earth is referred to as clutter as it is an unwanted return. The received signal and clutter is also contaminated with additive noise from various sources such as thermal noise, the sun, other radars and communication equipment in the area, and hostile jamming equipment. Once the

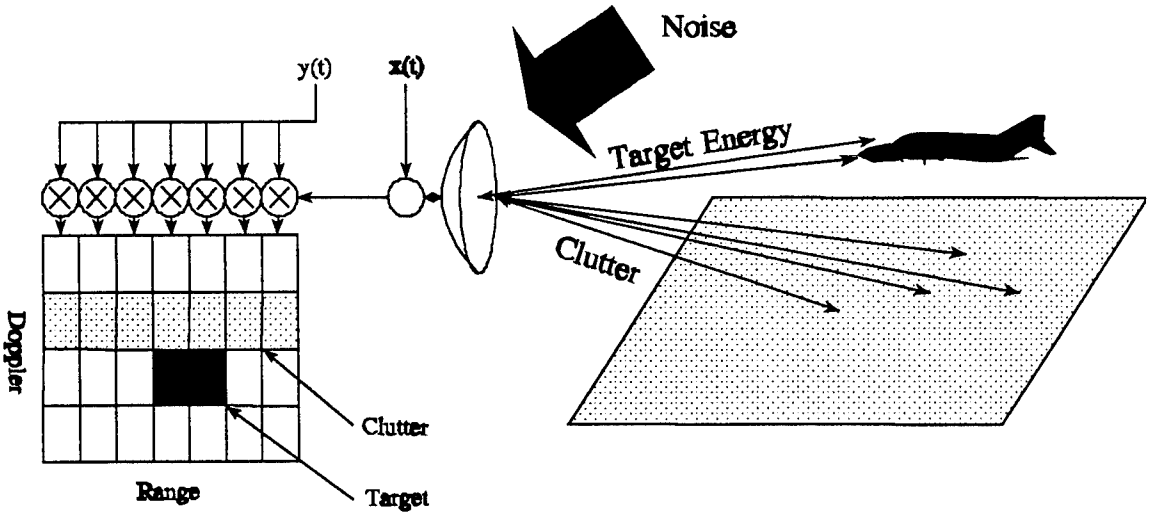

Figure 2.1. General Radar Block Diagram Showing the Target and a Clutter Contaminant.

signal is received by the antenna, it is passed to a signal processor that processes the waveform and separates out the returns by range and Doppler (velocity). Typically the clutter is stationary whereas the target is moving toward or away from the radar. Therefore, the target and clutter theoretically can be separated based on relative velocity. In reality, however, measurement of range and velocity are not perfect, and clutter can obscure the moving target. This will be discussed in more detail later in this chapter.

2.1. The Radar Equation

The radar equation, which describes the signal to noise ratio of the processed received waveform is given by

$$SNR_r = \frac{P_t G_r^2 \lambda^2 \sigma}{(4\pi)^3 R^4 N_o B_p} \tag{2.1}$$

where P_t is the transmitter peak power, G_r is the antenna gain, λ is the radar wavelength, σ is the effective radar cross section of the target within the radar bandwidth, N_o is the noise power spectral density, B_p is the processor bandwidth, and R is the range to the target. A substitution of

$$G_r = \frac{4 \pi A_e}{\lambda^2} \tag{2.2}$$

where A_e is the antenna effective aperture, into (2.1) yields the following equation in terms of the antenna aperture and wavelength

$$SNR_r = \frac{P_t A_e^2 \sigma}{(4\pi) \lambda^2 R^4 N_o B_p} \tag{2.3}$$

Therefore, for a fixed antenna aperture A_e, the received power increases with decreasing wavelength.

The signal to noise ratio for a intercept receiver on board the target being illuminated by the radar is given by

$$SNR_i = \frac{P_t G_r G_i \lambda^2}{B_r (4\pi) R^2 N_o} \tag{2.4}$$

where G_i is the antenna gain of the intercept receiver and B_r is the radiated bandwidth of the radar signal. In Equation (2.4), the noise levels are assumed to be the same in both the intercept receiver and the radar receiver and the intercept receiver is assumed

to be in the mainlobe of the radar antenna. It is also assumed that the radiated bandwidth of the radar signal is much greater than the bandwidth of the intercept receiver signal processor. An important quantity is the ratio of the radar SNR to the intercept receiver SNR. This is known as the radar-interceptor advantage α and is given by

$$\alpha = \frac{SNR_r}{SNR_i} = \left(\frac{G_r}{G_i}\right)\sigma\left(\frac{B_r}{B_p}\right)\left(\frac{1}{4\pi}\right)\left(\frac{1}{R^2}\right) \quad . \tag{2.5}$$

The radar-interceptor advantage is important because it relates the performance of the radar to the performance of the radar's enemy (the intercept receiver). Signal to noise ratios are used because they typically describe the "bottom line" of system performance. Therefore, if the radar requires a minimum signal to noise ratio of SNR_{rmin} to meet its specified performance level, and the intercept receiver requires a minimum signal to noise ratio of SNR_{imin} to meet its specified performance criterion, the radar system will have an advantage over the intercept receiver if

$$\alpha > \frac{SNR_{rmin}}{SNR_{imin}} \tag{2.6}$$

(assuming the minimum radar SNR has been achieved). Otherwise, the intercept receiver is said to have the advantage. Solving Equation (2.5) for the range R_o at which the radar achieves an advantage over the intercept receiver yields

$$R_o = \sqrt{\left(\frac{G_r}{G_i}\right)\sigma\left(\frac{B_r}{B_p}\right)\left(\frac{1}{4\pi}\right)\left(\frac{1}{\alpha_o}\right)} \tag{2.7}$$

where α_o is the minimum radar-interceptor advantage satisfying Equation (2.6). Therefore, if the minimum SNR for the radar can be lowered, the operable range of the radar can be increased. Notice that there is a 5 dB/decade improvement in range versus radar signal to noise ratio improvement. Notice also that there are three factors available to the radar designer in Equation (2.7) that improve radar performance: antenna gain G_r relative to the intercept receiver antenna gain G_i, radar radiated bandwidth B_r relative to the radar receiver processor bandwidth B_p, and possibly the effective radar cross section σ of the target. The antenna gain parameter is a hardware parameter that is fixed by the operating frequency of the radar along with the physical dimensions of the antenna. The ratio of radiated bandwidth to processor bandwidth is a signal processor dependent parameter that can be improved by utilizing advanced signal processing schemes such as pulse compression. The effective radar cross section of the target is typically thought of as a parameter that is fixed by the target. In this study, however, signal processing schemes will be introduced that make use of target-specific information in order to increase the effective radar cross section of the target thus increasing the LPI performance of the radar. Therefore, effective radar cross section can be thought of as a design parameter available to the radar designer. In this study, only signal processing gains are investigated.

2.2. Pulse Compression

Pulse compression is a signaling technique in which a signal of duration T_d and bandwidth B_r is transmitted and the reflected waveform is compressed through a matched filter into a pulse of duration $1/B_r$. This makes it possible for a radar to

transmit a long duration low peak power signal that can be compressed into a short duration high peak power signal. This is shown graphically in Figure 2.2. Another interpretation and implementation of pulse compression involves the use of a correlator. When a correlator is used for despreading, the signal of bandwidth B_r is collapsed into a signal of bandwidth $1/T_d$. This is shown graphically in Figure 2.3.

For a pulse compression radar, Equation (2.5) becomes

$$\alpha = \left(\frac{G_r}{G_i} \right) \sigma \left(B_r \, T_d \right) \left(\frac{1}{4\pi} \right) \left(\frac{1}{R^2} \right) . \tag{2.8}$$

Since $B_r T_d$ is always greater than unity if there is any pulse compression effect, the radar-interceptor advantage is always increased. Pulse compression is desirable because it allows a radar to have the range resolution of a short pulsewidth radar signal with the peak power requirements of a long pulsewidth radar signal.

2.3. Range Resolution

The range resolution of a radar is defined to be the minimum distance between two point targets at which the radar can determine that there are two targets and not one. This is shown graphically in Figure 2.4. The range resolution ΔR of a radar transmitting a signal with a bandwidth B_r is given by [1, 2]

$$\Delta R = \frac{c}{2B_r} \tag{2.9}$$

where c is the speed of light. Therefore, as the bandwidth of the signal increases, the range resolution increases.

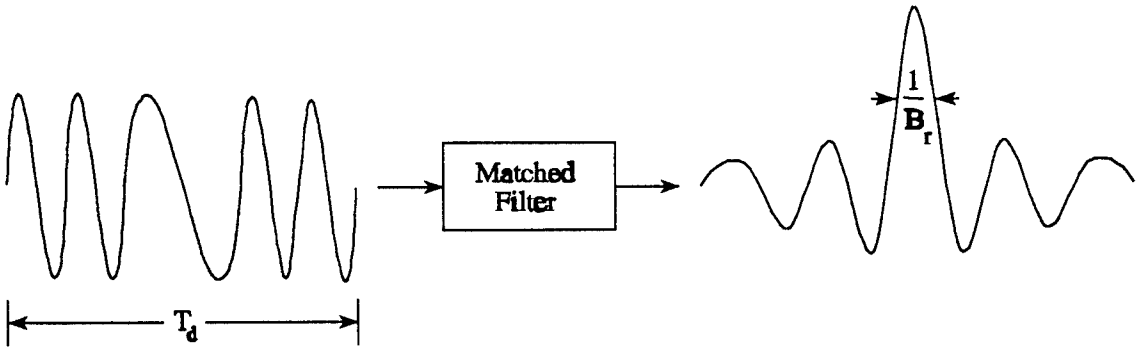

Figure 2.2. Matched Filter Implementation of Pulse Compression.

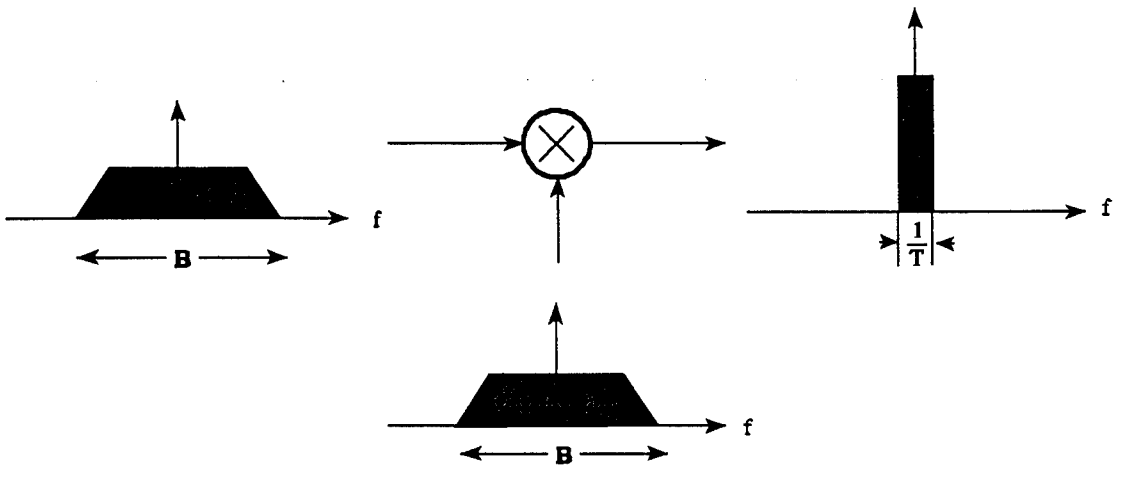

Figure 2.3. Correlator Implementation of Pulse Compression.

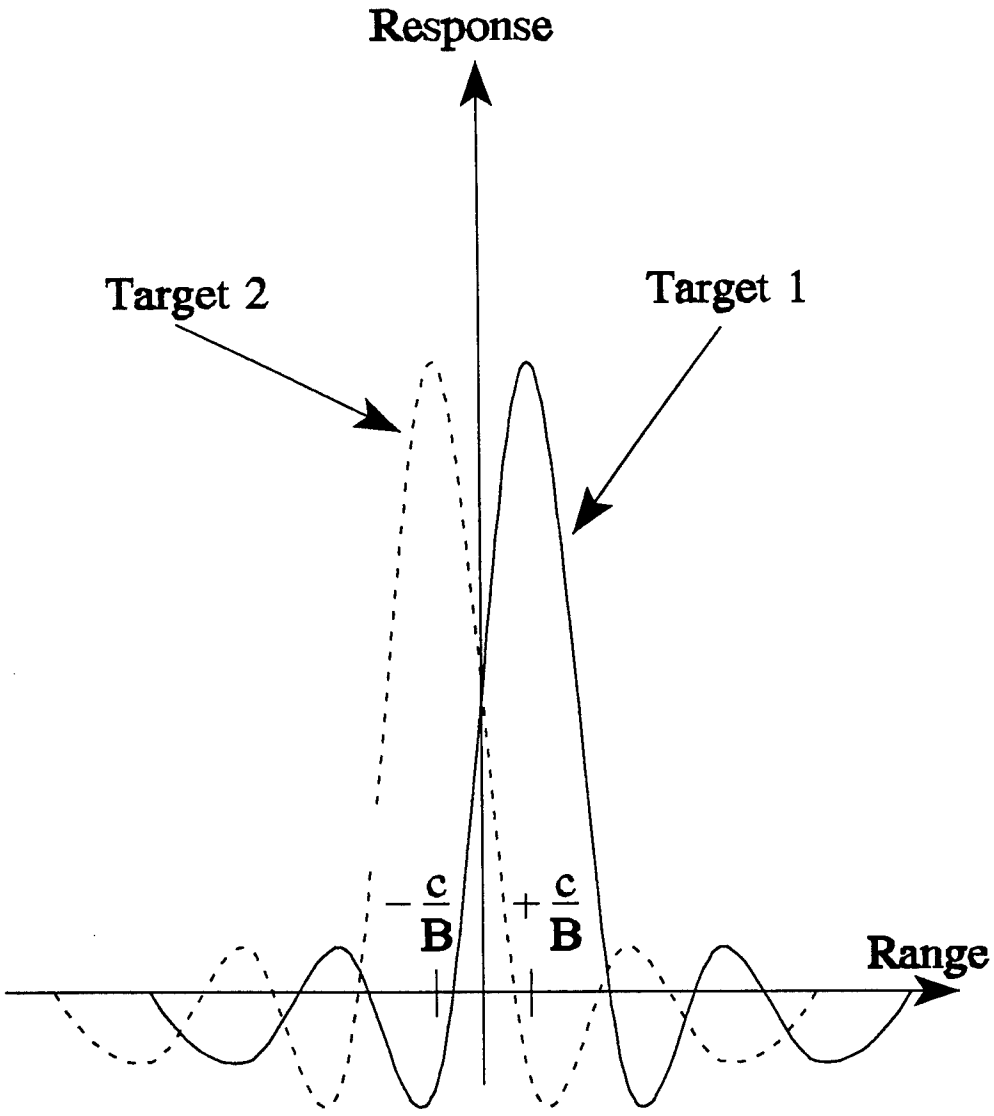

Figure 2.4. Radar Range Resolution.

2.4. Doppler Resolution

Doppler resolution (or precision) is the minimum difference in the velocity of two targets at which the radar can determine that there are two targets and not one. This is shown graphically in Figure 2.5. The Doppler resolution Δv of a radar transmitting a signal of duration T_d is given by

$$\Delta v = \frac{c}{2 f_o T_d} \quad . \tag{2.10}$$

Therefore, the ability of a target to discriminate (or separate) two targets moving at two different velocities is related directly to the duration of the signal and the carrier frequency of the radar.

2.5. Range Smearing

The previous two identities would lead one to believe that the key to radar performance would be to have an infinite bandwidth infinite duration signal. Physically this cannot occur because of range smearing. Range smearing occurs with pulse compression radars when a target moves an appreciable portion of a range resolution cell during the signal duration. To prevent range smearing the following equation must be satisfied

$$\frac{v T_d}{2} \ll \frac{c}{2B_r} \tag{2.11}$$

where v is the target velocity where the $\ll$ is interpreted as less than by a factor of at least 10. Solving Equation (2.11) for the velocity in terms of the time-bandwidth product $B_r T_d$ yields

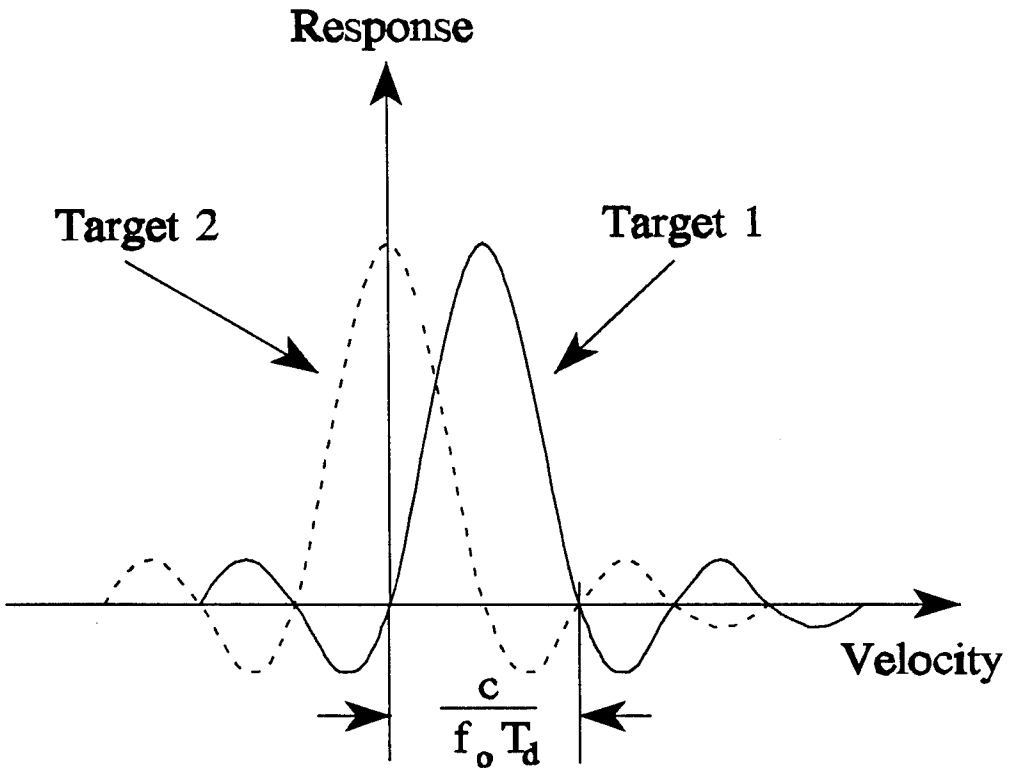

Figure 2.5. Radar Velocity (Doppler) Resolution.

$$v \ll \frac{c}{B_r T_d} \quad . \tag{2.12}$$

Therefore, the maximum time-bandwidth product of a signal is limited by the maximum target velocity of interest.

According to Equation (2.12), if a radar is to process targets that have a maximum velocity of v_{max}, then the time-bandwidth product should be chosen to be

$$B_r T_d \approx .1 \frac{c}{v_{max}} \quad . \tag{2.13}$$

Substituting this value of $B_r T_d$ into Equation (2.6) yields

$$\alpha = \left(\frac{G_r}{G_i} \right) \sigma \left(.1 \frac{c}{v_{max}} \right) \left(\frac{1}{4\pi} \right) \left(\frac{1}{R^2} \right) \quad . \tag{2.14}$$

As seen in Equation (2.14), the larger the velocity of interest, the lower the radar-interceptor advantage. Notice that the maximum achievable time-bandwidth product for a 300 m/s target is 100,000. This is equivalent to a 50 dB processing gain. Also notice that the maximum possible processing gain decreases at 10 dB/decade with increasing velocity. This results in a 5 dB/decade usable range improvement.

2.6. Range-Doppler Trade-Off

It is of interest to investigate the product of range resolution and Doppler resolution. The range-Doppler resolution product is given by

$$\Delta v \, \Delta R = \frac{c^2}{4 f_o B_r T_d} \quad . \tag{2.15}$$

Since the speed of light is constant, and it is assumed that the carrier frequency f_o is fixed by the radar hardware, the range-Doppler resolution product is fixed by the time-bandwidth product. Therefore, for a fixed time-bandwidth product $B_r T_d$, range resolution must be traded for Doppler resolution or vice versa. So, for a fixed time-bandwidth product, a high range resolution radar signal will have to come at the expense of reduced Doppler resolution.

2.7. The Cross-Ambiguity Function and Clutter Analysis

When a radar transmits a signal, the reflections do not come from the target alone. There are other competing reflections that tend to obscure the wanted target reflection. These unwanted reflections are typically referred to as clutter returns.

A general analysis tool that is used to describe the response of a radar to any given clutter distribution is the cross-ambiguity function [3] of the radar. The cross-ambiguity function χ_{xy} describes the output of a radar to a point target located at any arbitrary range delay τ and Doppler frequency f_D and is given by

$$\chi_{xy}(\tau \, , f_D) = \frac{1}{T_d} \int_{-\infty}^{\infty} x(t) \; y(t-\tau) \; e^{j2\pi f_D t} \; dt \quad . \tag{2.16}$$

Properties of the cross-ambiguity function will be discussed in detail in Chapter III.

The ideal radar signal would have an impulsive cross-ambiguity function. In other words, targets at the appropriate range and velocity would give a maximum

response, while all other targets would yield no response. The ideal signal, however, is impossible to generate. Stewart and Westerfield [4] investigated the cross-ambiguity functions four general signal classes: long pulses, short pulses, linear frequency modulated pulses, and pseudo-random coded pulses. Density plots of these four signal cross-ambiguity functions are sketched in Figure 2.6. The shaded portions of the plots represent the range-Doppler regions to which the radar will respond. The long pulse, short pulse, and frequency modulated cross-ambiguity densities are confined to a single ellipsoidal mainlobe that is $1/B_r$ in width along the range axis and $1/T_d$ in width along the Doppler axis. The ellipsoid, however, spans over a portion of the surface B_r wide in Doppler and T_d wide in range. It should be noted that for the uncoded signals (the long pulse and short pulse) that $B_rT_d = 1$ (i.e., no pulse compression). The pseudo-random cross-ambiguity function density has a central spike with a width of $1/B_r$ along the range axis and $1/T_d$ along the Doppler axis. Additionally, it has a uniform pedestal region that is $1/B_rT_d$ high and spans over a width of B_r in Doppler and T_d in range. In other words, the long pulse, short pulse, and frequency modulated radars will respond strongly to targets or clutter at range and Doppler values within the mainlobe only. For the pseudo-random signal, the radar will respond strongly to targets at the appropriate mainlobe range and Doppler, and will respond in a weak random manner for targets or clutter in the pedestal region.

Typically, it is assumed that the wanted target is a point at the origin of the range-Doppler plane, while clutter is distributed in range and Doppler. Most often, it is assumed that clutter is localized in Doppler and distributed along the range axis as

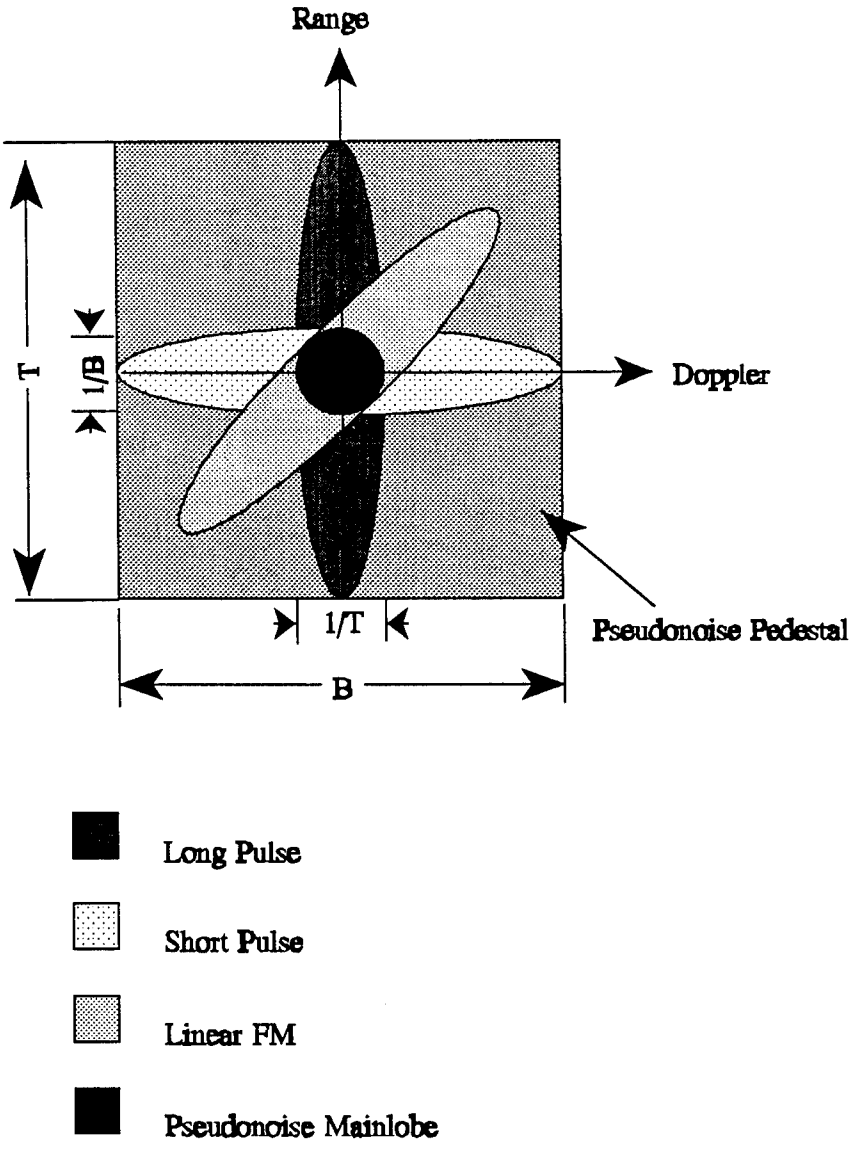

Figure 2.6. Generic Cross-Ambiguity Functions for Four Signal Types.

shown in Figure 2.7. A good measure of clutter rejection for this clutter distribution (for waveform comparison purposes only) is therefore, the integrated sidelobe level (ISL)

$$ISL\ (f_D) = \int_{-\infty}^{\infty} |\ \chi_{xy}(\tau\ ,\ f_D)\ |^2\ d\tau \quad . \tag{2.17}$$

The integrated sidelobe level is the clutter rejection figure of merit that will be used throughout this study. It is not a generalized figure of merit, and does not apply to every specific clutter distribution. It does, however, serve as a useful figure of merit for the purposes of comparing the performance of different waveforms.

2.8. Radar Scattering Phenomenology

The scattering of radar waves from targets is characterized by three different regions that are dependent upon the ratio of the target's size L to the radar wavelength λ. The Rayleigh region is associated with target lengths that are much less than a wavelength, or $L \ll \lambda$. The resonance region is associated with targets whose lengths are on the order of a wavelength $L \sim \lambda$. The optical region is associated with targets that are much larger than a wavelength $L \gg \lambda$.

2.8.A. Rayleigh Region Scattering Characteristics

In the Raleigh region, scattering phenomena are described by the quasi-static dipole moment of the target [5]. In general, the scattered field changes with square of

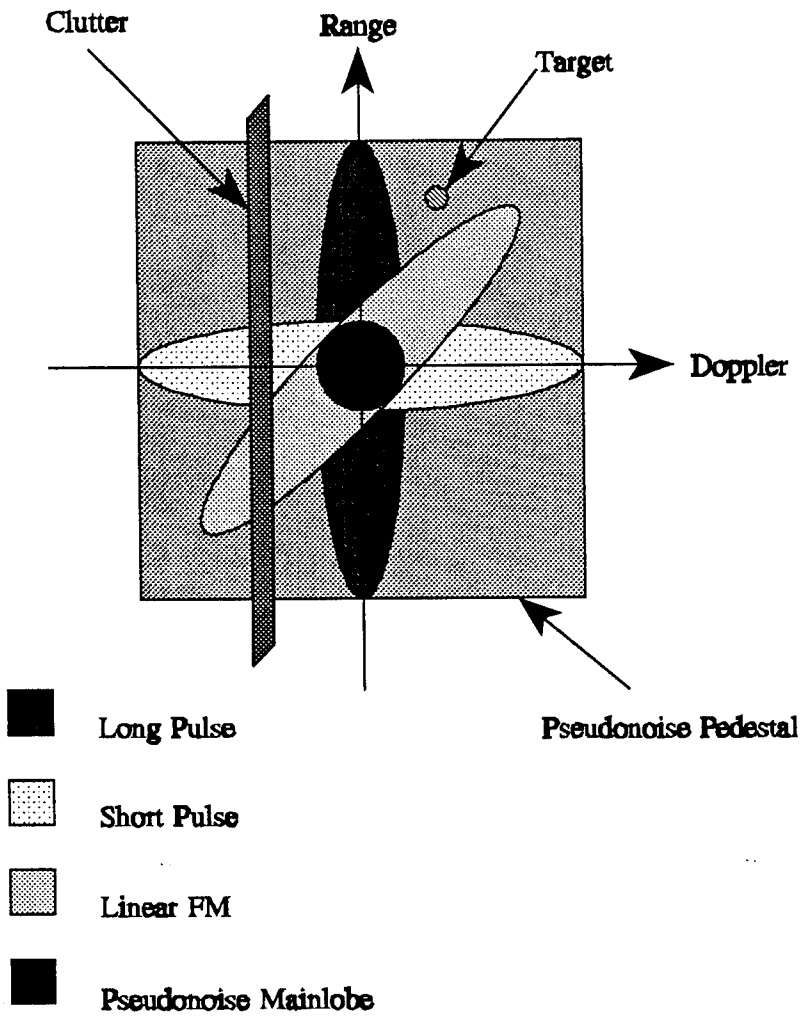

Figure 2.7. Clutter Distribution Along a Constant-Doppler Line.

the frequency of the excitation

$$E_s \propto f_o^2 \quad . \tag{2.18}$$

Since the wavelength is much larger than the target length, Rayleigh scattered returns have the advantage of being aspect independent but they convey little target-specific information. Additionally, low frequency signals make it difficult to perform Doppler processing and high-gain narrow-beamed antennas are almost impossible to build since the half-power beamwidth is given roughly as the ratio of wavelength to aperture length (Equation (2.2)). As an example of a Rayleigh scattering target, a target that is 15 meters in length would exhibit Rayleigh scattering for frequencies lower than 2 MHz. Therefore, the Rayleigh region is not of interest for target identification purposes.

2.8.B. Resonance Region Scattering Characteristics

The resonance region is defined by the ratio of target length to wavelength on the order of 1 so that

$$1 < \frac{L}{\lambda} < 10 \quad . \tag{2.19}$$

Resonant region scattering is typically described by highly damped resonant modes. These modes result from the waves circumnavigating the various portions of the target. Therefore, the frequencies of the modes are related to the physical size of the different scattering structures. Theoretically, since the resonant modes are related to the physical scattering structure dimensions, resonant mode scattering is excellent for

target identification purposes [6, 7, 8, 9, 10]. The mode locations are relatively aspect dependent since the scattering structures are still a small number of wavelengths in physical dimension. A radar to excite resonant modes, however, would have similar problems to a Rayleigh region radar. Since the wavelength is on the order of the target's physical dimension, the radar antenna would have to be much greater than the target dimensions for the antenna to achieve a narrow beamwidth and high gain. Additionally, Doppler resolution would not be sufficient for clutter rejection. As an example of a resonant mode radar, the radar would operate in a band from 20 MHz to 200 MHz for a 15 meter target. From Equation (2.2), the radar antenna would have to be on the order of 200 meters per dimension to achieve a 30 dBi gain at the low end of the frequency spectrum.

2.8.C. Optical Region Scattering Characteristics

The optical region is defined by

$$\frac{L}{\lambda} > 1 \quad . \tag{2.20}$$

Optical region scattering is defined by impulses in the time domain and complex exponentials in the frequency domain. The location of the impulses in the time domain are associated with physical scattering centers of the target. These scattering centers vary rapidly with target aspect angle, but they do provide good features for target identification purposes [11, 12]. Since the wavelength is small, radar antenna sizes can be reduced and Doppler processing can be used for clutter removal. The disadvantage is that the scattering centers are highly aspect dependent (more so at

higher and higher frequency), and therefore, a large amount of data is required to describe the target. The aspect dependence is given by the angular sampling criterion [11]

$$\Delta\theta \ll \frac{\lambda}{4L} \quad . \tag{2.21}$$

Equation (2.21) is required for coherent data processing. For noncoherent processing, the criterion can be relaxed to [11]

$$\Delta\theta < \frac{\Delta R}{L} \tag{2.22}$$

where ΔR is the range resolution of the radar. Coherent scattering data provides a better feature vector for target identification than noncoherent data [12] but at the expense of a much larger data storage requirement. As an example, consider a 15 meter target and a .15 meter wavelength (corresponding to f_o = 2.0 GHz). The angular sampling criterion of Equation (2.21) says that for the target to be sampled properly in angle, the target signature must be sampled every

$$\begin{aligned} \Delta\theta \ll \frac{.15}{(4)\ (15)} &= 0.0025 \ \textit{radians} \\ &= 0.14^\circ \quad . \end{aligned} \tag{2.23}$$

Therefore, the high antenna gain and Doppler processing capability come at the expense of a rapidly varying target. For a 15 meter target and 1 meter resolution, noncoherent processing would require

$$\Delta\theta < \frac{1}{15} = 0.067 \; radians \qquad (2.24)$$
$$= 3.84° \quad .$$

Therefore, coherent processing means that 3.84/0.14 = 27.4 more data is required for database storage purposes per angular dimension for a target identification algorithm. To describe the entire target, $(27.4)^2 = 751$ times more data is required for coherent data. In general, the ratio of coherent discritization to noncoherent discritization is given by

$$\frac{\Delta\theta_n}{\Delta\theta_c} = \frac{4\ \Delta R}{\lambda} \quad . \qquad (2.25)$$

Therefore, the larger the number of wavelengths per range resolution cell, the more data will be required for target storage.

It is important to note that target identification requires a signal bandwidth sufficient to resolve individual scattering centers on a given target (i.e., UWB waveforms). This typically has not been assumed in studies aimed at improving signal to clutter ratios. For this reason, signal to clutter ratios have been improved only by suppressing clutter returns (lowering the ISL). It seems that a logical fusing of signal to clutter enhancement and target identification should include enhancing the target return as well as suppressing the clutter return. This enhancement could be accomplished by designing signals with cross-ambiguity functions with mainlobes that cause the scattering centers to sum coherently rather than simply measuring the location and energy from each. This enhancement would have to come without

increasing the ISL in a like manner. This concept will be addressed in detail in this study.

2.9. Conclusions

The range at which an LPI radar obtains an advantage over an intercept receiver is extended by increasing the time-bandwidth product of the radar waveform and by enhancing the reflectivity of the target. The time-bandwidth product is limited by maximum velocity of interest to the radar, therefore the radar-interceptor advantage gained from increasing the time-bandwidth product is limited by target velocity. The next logical step in improving the radar-interceptor advantage is therefore, target enhancement through the use of target-specific information.

The clutter rejection performance of a waveform is quantified, for general comparative purposes, by the integrated sidelobe level (ISL) of the cross-ambiguity function. This is true specifically for the case of range-distributed Doppler-concentrated clutter. Additionally, the cross-ambiguity of a pseudo-random LPI waveform is comprised of an impulse-like target-specific and a uniformly distributed pedestal. The pedestal region is the primary source of clutter contamination.

Finally, to implement a realistic radar target identification technique, the only practical target scattering regime is the optical region because of the requirements on Doppler resolution and antenna gain. This advantage comes at the expense of an increasingly complex target scattering description. Additionally, the target description for a coherent processor is much more complex that of a noncoherent processor assuming that the range resolution of the radar is many wavelengths.

2.10. References

1. J. L. Eaves and E. K. Reedy, Editors, Principles of Modern Radar, Van Nostrand Reinhold Publishing, 1987.

2. D. R. Wehner, High Resolution Radar, Artech House, 1987.

3. A. W. Rihaczek, Principles of High-Resolution Radar, Peninsula Publishing Co., 1985.

4. J. L. Stewart and E. C. Westerfield, "A Theory of Active Sonar Detection", Proceedings of the IRE, pp. 872-881, May 1959.

5. E. F. Knott, J. F. Shaeffer, and M. T. Tuley, Radar Cross Section, Second Edition, Artech House, 1993.

6. A. J. Berni, "Target Identification by Natural Resonance Estimation", IEEE Transactions on Aerospace and Electronics Systems, March 1975, pp. 147-154.

7. A. A. Ksienski, Y. T. Lin, and L. J. White, "Low-Frequency Approach to Target Identification", Proceedings of the IEEE, December 1975, pp. 1651-1660.

8. C. W. Chuang and D. L. Moffatt, "Natural Resonances of Targets Via Prony's Method and Target Discrimination", IEEE Transactions on Aerospace and Electronics Systems, September 1976, pp. 583-589.

9. E. W. Kennaugh, "The K-Pulse Concept", IEEE Transactions on Antennas and Propagation, March 1981, pp. 327-331.

10. E. K. Rothwell, D. P. Nyquist, D. M. Chen, and B. Drachman, "Radar Target Discrimination Using the Extinction-Pulse Technique", IEEE Transactions on Antennas and Propagation, September 1985, pp. 929-936.

11. S. Hudson and D. Psaltis, "Correlation Filters for Aircraft Identification From Radar Range Profiles", IEEE Transactions on Aerospace Electronic Systems, July 1993, pp. 741-748.

12. H. J. Li and S. H. Yang, "Using Range Profiles as Feature Vectors to Identify Aerospace Objects", IEEE Transactions on Antennas and Propagation, March 1993, pp. 261-268.

CHAPTER III

ANALYSIS OF A GENERAL FSK/PSK RADAR SYSTEM

In this chapter, the radar cross-ambiguity function [1, p. 153-157] will be discussed. The cross-ambiguity function describes the response of a radar system to an impulse-like target (or point target) located at an arbitrary range and Doppler shift. In this sense, the cross-ambiguity function can be thought of as the impulse response of the radar. The cross-ambiguity function is the general case of the radar ambiguity function [1, pp. 118]. The ambiguity function is also referred to as the matched-filter response, and the uncertainty function [2]. The cross-ambiguity function is also related to the cyclic cross-correlation function as discussed in [3, pp. 369-373].

In Section 3.1, general properties of the cross-ambiguity function that are particularly applicable to radar system analysis is be derived First, the cross-ambiguity function of two signals is defined along with a discussion of the underlying assumptions made during its derivation. Second, the volumetric distribution of the cross-ambiguity function is analyzed for a general system. Third, the property of linearity is proven. Fourth, the effect of convolving one of the two signals with an impulse response on the cross-ambiguity function is investigated. Fifth, the effect of signal repetition, or periodicity, on the cross-ambiguity function is studied. Finally, the effect of additive stationary noise on the cross-ambiguity function is determined.

In Section 3.2, a general FSK/PSK radar system diagram is presented that includes the effects of the target transfer function, delay, and motion. This system diagram is analyzed using the properties derived in Section 3.1. In conclusion, is be seen that the interaction between the target and the radar is defined by the correlation of the radar cross-ambiguity function with the down-converted target transfer function.

3.1. The Cross-Ambiguity Function

In this section, the properties of the cross-ambiguity function are discussed. The cross-ambiguity function of a radar is a rigorous mathematical description of a radar's response to an ideal point target moving at a constant range rate. The cross-ambiguity function is therefore a two dimensional function of range delay τ and Doppler frequency f_D. The cross-ambiguity function $\chi_{xy}(\tau,f_D)$ of the signal $x(t)$ with the signal $y(t)$ is defined as

$$\chi_{xy}(\tau, f_D) = \frac{1}{T_d}\int_{-\infty}^{\infty} x(t)\, y(t-\tau)\; e^{j2\pi f_D t}\, dt \tag{3.1}$$

where T_d is the duration of the signal $x(t)$, τ is the time delay between waveforms, and f_D is the Doppler frequency shift induced by the moving target. Equation (3.1) describes the output of the radar receiver for various values of τ and Doppler frequency f_D. Notice that Equation (3.1) is identical to the time average cross-correlation function [4] except for the Fourier transform kernel $e^{j2\pi ft}$.

3.1.A. Physical Limitations on Resolution

It should be noted that the cross-ambiguity function is an accurate representation of the radar response under certain restrictions on the signal duration T_d and bandwidth B_r in relation to the target's velocity v and acceleration a. These restrictions are derived in [1, p. 61] and are given by

$$B_r T_d \leq 0.1 \frac{c}{v} \tag{3.2}$$

and

$$B_r T_d^2 \leq 0.2 \frac{c}{a} \tag{3.3}$$

where c is the speed of light in vacuum. Therefore, the analysis that follows is only valid within the restrictions of Equations (3.2) and (3.3).

An example calculation will now be performed in order to become acquainted with typical velocity and acceleration requirements for a given time-bandwidth product. Consider a radar with a bandwidth of B_r = 300 MHz and a processing time T_d of 100 μsec. According to Equation (3.2), the maximum allowable velocity of a target is

$$v \leq 0.1 \frac{3 \times 10^8}{(300 \times 10^6)(100 \times 10^{-6})} = 1000 \text{ m/sec} \tag{3.4}$$

and the maximum allowable acceleration is

$$a \leq 0.2 \frac{3 \times 10^8}{(300 \times 10^6)(100 \times 10^{-6})^2} = 20 \times 10^6 \ m/sec^2 \ . \qquad (3.5)$$

The acceleration is unreasonably high for any realistic target and is not a limiting factor, but the velocity limit is of interest. The radar signal described above would be limited to processing reflections from targets moving at velocities of less than 1000 m/sec or 1943 kts. It should be noted that if the processing time is reduced, the maximum target velocity will increase.

The velocity resolution of a pulsed radar is given by

$$\Delta v = \frac{c}{2 f_o T_d} \qquad (3.6)$$

where f_o is the carrier frequency of the waveform. For f_o = 2.0 GHz and T_d = 100 μsec, the velocity resolution is

$$\Delta v = \frac{3 \times 10^8}{2 (2.0 \times 10^9) (100 \times 10^{-6})} = 750 \ m/sec \qquad (3.7)$$

which is on the order of the maximum velocity. Therefore, the waveform above cannot resolve the target velocity. Notice, however, that if f_o is increased, then the velocity resolution is increased.

The signal described above is well-suited for measuring range since the range resolution of a signal is given by

$$\Delta R = \frac{c}{2B_r} \tag{3.8}$$

again where B_r is the bandwidth of the signal (for the signal bandwidth of above, the range resolution is 1/2 meter). The product of the range resolution and Doppler resolution is given by

$$\Delta R \Delta v = \frac{c^2}{4 f_o B_r T_d} \quad . \tag{3.9}$$

Therefore, for a fixed time-bandwidth product $B_r T_d$ and carrier frequency f_o, range resolution must come at the expense of Doppler resolution and vice versa. Therefore, a radar with high range resolution cannot also have high Doppler resolution.

Several important fundamental properties of the cross-ambiguity function are now discussed.

3.1.B. Volume Distribution of the Cross-Ambiguity Function

It is of interest to determine the volume beneath the surface of the ambiguity function. This volume is defined by

$$V = \int_{-\infty}^{\infty} \int_{-\infty}^{\infty} \left| \chi_{xy}(\tau, f_D) \right|^2 d\tau \, df_D \quad . \tag{3.10}$$

Following the method shown in [1, pp. 120-122], the volume can be shown to equal

$$V = \chi_{xx}(0,0)\ \chi_{yy}(0,0) \tag{3.11}$$

where

$$\chi_{xx}(0,0) = \frac{1}{T_d} \int_{-\infty}^{\infty} | x(t) |^2 \, dt \tag{3.12}$$

is the normalized energy in $x(t)$ and

$$\chi_{yy}(0,0) = \frac{1}{T_d} \int_{-\infty}^{\infty} | y(t) |^2 \, dt \tag{3.13}$$

is the normalized energy in $y(t)$. Therefore, for fixed signal power, the volume beneath the cross-ambiguity function is fixed. Suppressing the surface of the cross-ambiguity function in one particular region results in an increase elsewhere on the surface.

Two more properties of the cross-ambiguity function are related to the distribution of the volume underneath the function. The first relates the delay-axis function to the volume distribution in Doppler:

$$\int_{-\infty}^{\infty} | \chi_{xy}(\tau, f_D) |^2 \, d\tau = \int_{-\infty}^{\infty} \chi_{xx}^{*}(\tau,0)\ \chi_{yy}(\tau,0)\ e^{-j2\pi f_D \tau} \, d\tau \quad . \tag{3.14}$$

The left side of Equation (3.14) is the integrated sidelobe level (ISL). Therefore, the ISL is the Fourier transform of the product of the autocorrelation functions of the two signals used in the signal processor. From the Wiener-Khinchin theorem, the

integrated sidelobe level is equal to the convolution of the two signal power spectral densities such that

$$ISL\ (\ f_d\ ) = S_{xx}^{*}(\ f_d\ ) * S_{yy}(\ f_d\ ) \quad . \tag{3.15}$$

Therefore, the ISL of a radar signal processing scheme is dependent more upon the power spectral densities of the signals used in the processor than the actual signal type (e.g., linear frequency modulation versus pseudorandom modulation).

The second property relates the Doppler-axis function to the volume distribution in delay:

$$\int_{-\infty}^{\infty} |\ \chi_{xy}(\tau,\ f_D\ )\ |^2\ df_D = \int_{-\infty}^{\infty} \chi_{xx}^{*}(0,\ f_D\ )\ \chi_{yy}(0,\ f_D\ )\ e^{j2\pi f_D \tau}\ df_D \quad . \tag{3.16}$$

Equation (3.16) shows that a signal with a narrow range mainlobe will have energy spread over a broad region in Doppler (broad bandwidth), and likewise a signal with a broad range mainlobe will have its Doppler energy concentrated in a narrow Doppler mainlobe (narrow bandwidth). It should be noted that the majority of the volume beneath the cross-ambiguity function of a pseudorandom signal is contained beneath the pedestal region.

3.1.C. Linearity

The property of linearity is one of the most important properties in systems analysis. This property makes it possible to easily analyze systems with multiple inputs such as target return, clutter, and noise. The cross-ambiguity function of *x(t)*

and $y(t)$ is a linear operation on $x(t)$ and $y(t)$. This can be seen by setting $y(t) = y_1(t) + y_2(t)$ which results in

$$\chi_{xy}(\tau, f_D) = \frac{1}{T_d}\int_{-\infty}^{\infty} x(t)\, y(t-\tau)\, e^{j2\pi f_D t}\, dt \qquad (3.17)$$
$$= \chi_{xy_1}(\tau, f_D) + \chi_{xy_2}(\tau, f_D) \quad .$$

3.1.D. Linear System Effects

A particularly useful property of the cross-ambiguity function is the case for which the signal $y(t)$ has been convolved with a filter impulse response $h(t)$

$$\chi_{xy*h}(\tau, f_D) = \frac{1}{T_d}\int_{-\infty}^{\infty} x(t)\, (y(t-\tau) * h(t))\, e^{j2\pi f_D t}\, dt \quad . \qquad (3.18)$$

This property makes it possible to model distributed targets with a general impulse response function $h(t)$. This impulse response $h(t)$ is referred to as the range profile of the target since it describes how the target behaves in the time (range) domain. Applying the convolution operation to Equation (3.18) yields

$$\chi_{xy*h}(\tau, f_D) = \frac{1}{T_d}\int_{-\infty}^{\infty} x(t) \left(\int_{-\infty}^{\infty} y(t-\tau-u)\, h(u)\, du \right) e^{j2\pi f_D t}\, dt \quad . \qquad (3.19)$$

After switching the order of integration, the cross-ambiguity function becomes

$$\chi_{xy*h}(\tau, f_D) = \frac{1}{T_d} \int_{-\infty}^{\infty} \left(\int_{-\infty}^{\infty} x(t)\, y(t-\tau-u)\, e^{j2\pi f_D t}\, dt \right) h(u)\, du \qquad (3.20)$$

which can be seen to equal

$$\chi_{xy*h}(\tau, f_D) = \frac{1}{T_d} \int_{-\infty}^{\infty} \left(\chi_{xy}(\tau+u, f_D) \right) h(u)\, du \ . \qquad (3.21)$$

Therefore, the interaction between the radar and a target is described completely by the cross-ambiguity function and the target impulse response.

3.1.E. Waveform Repetition

Waveform repetition is often used in radar systems to create a clutter-clear area around the mainlobe of the cross-ambiguity function mainlobe along the Doppler-axis [1, pp. 141-143]. Signal periodicity can be modeled as a convolution of a short-duration repeated signal $x_s(t)$ with a periodic train of impulses. For an ideally periodic train of impulses, there would be infinitely many impulses. But for a study of realistic signals, a finite duration impulse train is used. A periodic signal can therefore be written as

$$x(t) = x_s(t) * \sum_{m=0}^{M-1} \delta(t - m T_p) \qquad (3.22)$$

where T_p is the period of the signal and M is the number of repetitions of the short-term waveform. Equation (3.22) can also be written in terms of a periodic impulse response function $h_p(t)$ as

$$x(t) = x_s(t) * h_p(t) \quad . \tag{3.23}$$

Writing the cross-ambiguity function in terms of the periodic impulse response function $h_p(t)$ yields

$$\chi_{xy}(\tau, f_D) = \frac{1}{T_d} \int_{-\infty}^{\infty} \int_{-\infty}^{\infty} \int_{-\infty}^{\infty} x_s(t-u_1)\, y_s(t-\tau-u_2)\, e^{j2\pi f_D t}\, dt \; h_p(u_1)\, h_p(u_2)\, du_1\, du_2 \; . \tag{3.24}$$

After a change of variable of $z=t-u_1$, Equation (3.24) becomes

$$\chi_{xy}(\tau, f_D) = \frac{1}{MT_d} \int_{-\infty}^{\infty} \int_{-\infty}^{\infty} \int_{-\infty}^{\infty} x_s(z)\, y_s(z-\tau-(u_2-u_1))\, e^{j2\pi f_D z}\, dz \; h_p(u_1)\, h_p(u_2)\, e^{j2\pi f_D u_1}\, du_1\, du_2 \; . \tag{3.25}$$

where the identity $MT_p = T_d$ has been used. By making the substitution of the cross-ambiguity function of the short term waveform imbedded within the integral of Equation (3.25) yields

$$\chi_{xy}(\tau, f_D) = \frac{1}{M} \int_{-\infty}^{\infty} \int_{-\infty}^{\infty} \chi_{xy_s}(\tau-(u_2-u_1)\, , f_D) \; h_p(u_1)\, h_p(u_2)\, e^{j2\pi f_D u_1}\, du_1\, du_2 \; . \tag{3.26}$$

Performing the convolutions and making use of the sifting property of Dirac delta functions yields the following summation

$$\chi_{xy}(\tau, f_D) = \frac{1}{M} \sum_{m=0}^{M-1} \sum_{n=0}^{N-1} \chi_{x_s y_s}(\tau+(m-n)T_p, f_D)\, e^{j2\pi f_D m T_p} . \tag{3.27}$$

Using the substitution of $l = m - n$ casts Equation (3.27) into the separable summation

$$\begin{aligned} \chi_{xy}(\tau, f_D) = {} & \frac{1}{M} \sum_{l=0}^{M-1} \chi_{x_s y_s}(\tau+lT_p, f_D) \sum_{m=l}^{M-1} e^{j2\pi f_D m T_p} \\ & + \frac{1}{M} \sum_{l=-(M-1)}^{-1} \chi_{x_s y_s}(\tau+lT_p, f_D) \sum_{m=0}^{M-1+l} e^{j2\pi f_D m T_p} . \end{aligned} \tag{3.28}$$

The summations over m can be written in closed form by using known properties of geometric series

$$\sum_{m=0}^{M-1} e^{j2\pi f_D m T} = \frac{1-e^{j2\pi f_D M T}}{1-e^{j2\pi f_D T}} \tag{3.29}$$

and Euler's identity. Therefore, Equation (3.28) can be written as

$$\begin{aligned} \chi_{xy}(\tau, f) = {} & \frac{1}{M} \sum_{l=-(M-1)}^{M-1} \chi_{x_s y_s}(\tau+lT_p, f) \\ & \frac{\sin(\pi f (M-|l|)T_p)}{\sin(\pi f T_p)} e^{j\pi f(M+|l|-1)T_p} . \end{aligned} \tag{3.30}$$

Note that the l index locates the periodicities of the mainlobes of the cross-ambiguity function of the short-term functions $x_s(t)$ and $y_s(t)$.

3.1.F. Noise Contamination

The effect of additive stationary noise is now quantified. Since the cross-ambiguity function is a linear transform, the noise can be dealt with separately from

the desired receive signal. Therefore, the noise component of the received signal is given by

$$\chi_{xn}(\tau, f_D) = \frac{1}{T_d} \int_{-\infty}^{\infty} x(t)\ n(t-\tau)\ e^{j2\pi f_D t}\, dt \tag{3.31}$$

where $n(t)$ is a stationary noise contaminant. Assuming that the noise contaminant is a zero mean process, the expected value of the cross-ambiguity function between the reference signal and the noise contaminant is zero:

$$E\{\chi_{xn}(\tau, f_D)\} = \frac{1}{T_d} \int_{-\infty}^{\infty} x(t)\ E\{n(t-\tau)\}\ e^{j2\pi f_D t}\, dt = 0 \tag{3.32}$$

A more important measure of the effect of noise on the cross-ambiguity function is the autocorrelation function of the noise contamination. This is given by

$$E\{\chi_{xn}(\tau_1, f_D)\ \chi_{xn}(\tau_2, f_D)\} = \frac{1}{T_d^2} \int_{-\infty}^{\infty}\int_{-\infty}^{\infty} x(t)\ x^*(t')\ E\{n(t-\tau_1)\ n^*(t'-\tau_2)\}\ e^{j2\pi f_D(t-t')}\, dt\, dt' \tag{3.33}$$

where $n(t)$ is a stationary noise process. By making the substitution of $t=z+t'$ in Equation (3.33), the following equation results

$$E\left\{ \chi_{xn}(\tau_1, f_D)\ \chi_{xn}(\tau_2, f_D)\ \right\} = \frac{1}{T_d{}^2} \int_{-\infty}^{\infty} \int_{-\infty}^{\infty} x^*(t')\ x(t'+z)\ dt' \tag{3.34}$$

$$R_{nn}(z-(\tau_2-\tau_1))\ e^{j2\pi f_D z}\ dz$$

where $R_{nn}(z)$ is the autocorrelation function of the noise contaminant. Noting the autocorrelation function of $x(t)$ in Equation (3.34) and making the substitution of $\Delta=\tau_2-\tau_1$, the autocorrelation function of the cross-ambiguity function equals

$$E\left\{ \chi_{xn}(\tau, f_D)\ \chi_{xn}(\tau+\Delta, f_D)\right\} = \frac{1}{T_d} \int_{-\infty}^{\infty} R_{xx}(z)\ R_{nn}(z-\Delta)\ e^{j2\pi f_D z}\ dz\ . \tag{3.35}$$

Therefore, the autocorrelation function of the noise takes the shape of the convolution of the signal autocorrelation function with the autocorrelation function of the noise. Equation (3.35) will be evaluated for two special cases that are of particular interest: stationary white Gaussian noise and stationary narrowband noise. The white noise process is typical of thermal noise which might occur in the radar receiver while the narrowband noise is typical of an interference type signal such as an in-band emitter.

White noise is defined by an autocorrelation function $R_{nn}(z) = N_o\delta(z)$ where N_o is the noise single sided power spectral density. Under the specific case of white noise, the autocorrelation function of the noise contaminant is given by

$$E\left\{ \chi_{xn}(\tau, f_D)\ \chi_{xn}(\tau+\Delta, f_D)\ \right\} = \frac{N_o}{T_d} R_{xx}(\Delta)\ e^{-j2\pi f_D \Delta}\ . \tag{3.36}$$

Therefore, the noise autocorrelation assumes the shape of the reference signal autocorrelation function. Notice that Equation (3.36) is not a function of τ. This

means that the noise variance is spread uniformly over the entire delay-frequency plane. Notice also that the noise variance decreases as T_d increases for a constant mean square signal value $R_{xx}(0)$. Therefore, for a constant envelope signal, the noise variance is a function of the processing time and additive noise variance only.

The narrowband noise contaminant case is defined by $R_{nn}(z) = N_o \cos(2\pi f_n z)$. Narrowband noise manifests itself in the following manner

$$E\{\chi_{xn}(\tau, f_D)\,\chi_{xn}(\tau+\Delta, f_D)\} = \frac{N_o}{2T_d}\left(S_{xx}(f_D - f_n)\,e^{-j2\pi f_n\Delta} + S_{xx}(f_D + f_n)\,e^{j2\pi f_n\Delta}\right) \tag{3.37}$$

where

$$S_{xx}(f_D) = \int_{-\infty}^{\infty} R_{xx}(z)\,e^{j2\pi f_D z}\,dz \tag{3.38}$$

is the power spectral density of the signal $x(t)$. Notice that narrowband noise does vary as a function of frequency. It causes a contamination that has the same spectral shape as the signal power spectral density except for a simple modulation by the noise contamination frequency. In the delay dimension, there is a phase shift only for complex signals. For a real signal along the zero Doppler axis the shape of the noise carrier wave is seen.

As an example of narrowband noise contamination, consider the case of narrowband contaminant with $N_o = A_i^2$ and with the signal power spectral density $S_{xx}(f)$ uniformly distributed in a bandwidth from $-B_r/2$ to $B_r/2$ and has a uniform amplitude

of $1/B$. This is shown graphically in Figure 3.1. The interference variance at f_D=0 is equal to

$$var\ \{\ \chi_{xn}(\tau,0)\ \} = \frac{A_i^2}{B_r T_d} \quad . \tag{3.39}$$

Therefore, FSK/PSK signaling spreads the narrowband signal over a bandwidth of B_r, and the contamination level is improved by a factor of $B_r T_d$.

3.2. General FSK/PSK Radar System Diagram

A generalized radar block diagram is shown in Figure 3.2. This system implements the cross-ambiguity function of the transmit signal $y(t)$ with a reference signal $x(t)$. For an FSK/PSK radar, the transmit signal is defined by

$$y(t) = \sum_{m=0}^{N-1} a_m \prod \left(\frac{t-mT}{T} \right) \cos\left(2\pi\,(f_m + f_s)\,t\right) \tag{3.40}$$

where a_m is either a 1 or -1, f_m is the baseband frequency of the m^{th} sub-pulse, and f_s is the carrier frequency. The reference signal is defined by

$$x(t) = \sum_{n=0}^{N-1} a_n \prod \left(\frac{t-nT}{T} \right) e^{-j(2\pi(f_n + f_s + f_c)t + \phi_n)} \tag{3.41}$$

where a_n is either a 1 or -1, f_n is the baseband frequency of the n^{th} sub-pulse, f_s is the carrier frequency, f_c is the Doppler correction frequency, and ϕ_n is the phase of the n^{th} sub-pulse.

In general, the transmit signal is delayed τ seconds because of the propagation through the atmosphere at the speed of light c. The signal is also convolved with the

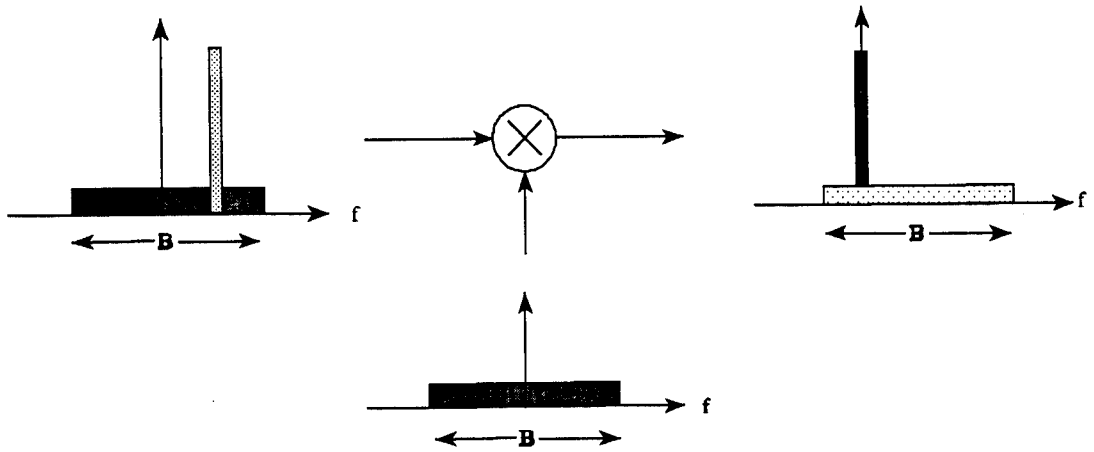

Figure 3.1. Narrowband Noise Contamination in a Pulse Compression System.

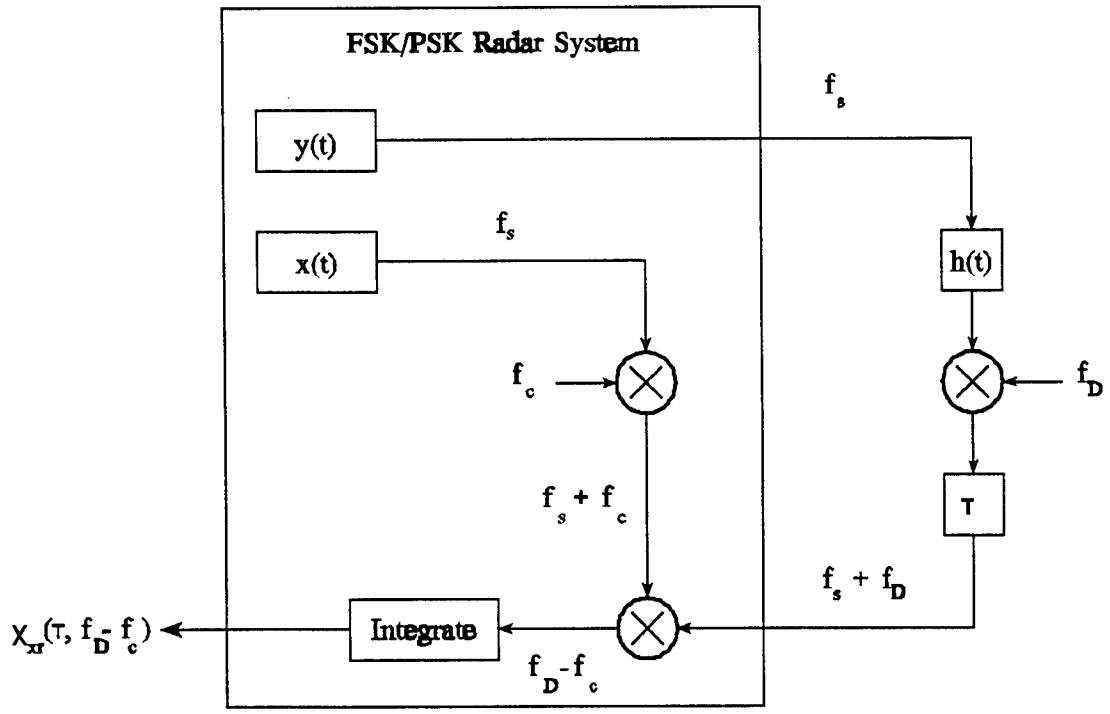

Figure 3.2. FSK/PSK Radar System Block Diagram.

range profile of the target $h(t)$ and Doppler shifted by f_d Hz because of the target motion. With these considerations taken into account, the reflected signal at the input of the receiver is given by

$$r(t) = \left(\sum_{m=0}^{N-1} a_m \prod \left(\frac{t - mT - \tau}{T} \right) \right. \tag{3.42}$$
$$\left. \times \cos \left(2\pi \left(f_m + f_s + f_d \right) t - 2\pi \left(f_m + f_s \right) \tau \right) \right) * h(t) \quad .$$

Referring back to Figure 3.2, it is seen that the output of the radar system is given by

$$\chi_{xr}(\tau, f_D) = \frac{1}{T_d} \int_{-\infty}^{\infty} x(t)\, r(t)\, dt \quad . \tag{3.43}$$

Substituting Equations (3.41) and (3.42) into Equation (3.43) along with the principles derived in Section 3.1 results in

$$\chi_{xr}(\tau, f_D) = \int_{-\infty}^{\infty} \left(\chi_{xy}(u+\tau, f_D - f_c)\, e^{-j2\pi f_s(u+\tau)} \right) h(u)\, du \tag{3.44}$$

where

$$\chi_{xy}(\tau, f_D - f_c) = \sum_{m=0}^{N-1} \sum_{n=0}^{N-1} \chi_{mn}(\tau, f_D - f_c) \quad . \tag{3.45}$$

The function within the summation represents the cross-ambiguity function of each of

the frequency sub-pulses of the signal and is equal to

$$\chi_{mn}(\tau, f_D - f_c) = \frac{1}{2T_d} a_m a_n \int_{-\infty}^{\infty} \prod\left(\frac{t-mT-\tau}{T}\right) \prod\left(\frac{t-nT}{T}\right) \times e^{j2\pi(f_D-f_c+(f_m-f_n))t}\, dt\, e^{-j(2\pi f_m\tau+\phi_n)} \quad (3.46)$$

Evaluating the integral of Equation (3.46) yields

$$\chi_{mn}((m-n+\varepsilon)T, f_D - f_c) = \frac{a_m a_n}{N}(1-|\varepsilon|) \times sinc\{\pi(f_D-f_c+(f_m-f_n)(1-|\varepsilon|)T\}\, e^{j2\pi f(n-\varepsilon/2)T}\, e^{-j(\pi(f_m+f_n)\varepsilon T+\phi_n)} \quad (3.47)$$

where the substitution of $\tau = (m-n+\varepsilon)T$ has been made and $-1 < \varepsilon < 1$. For $|\varepsilon| > 1$, Equation (3.47) is identically equal to zero. Making use of this representation of τ, and letting $l = (m-n)$, Equation (3.47) can be expressed as the following single index summation

$$\chi_{xy}(l+\varepsilon, f_D - f_c) = \begin{cases} \sum_{m=l}^{N-1} \chi_{m(m-l)}(\varepsilon, f_D - f_c) + \sum_{m=l+1}^{N-1} \chi_{m(m-l-1)}(1-\varepsilon, f_D - f_c) & \tau\geq 0,\ l\geq 0,\ \varepsilon:[0,1] \\ \sum_{m=0}^{N+l-1} \chi_{m(m-l)}(\varepsilon, f_D - f_c) + \sum_{m=0}^{N+l-2} \chi_{m(m-l+1)}(-1-\varepsilon, f_D - f_c) & \tau\leq 0,\ l\leq 0,\ \varepsilon:[-1,0] \end{cases} \quad (3.48)$$

Notice that Equations (3.46-3.48) are all considered to be baseband terms because they are all dependent on the baseband frequency terms only. Equation (3.49) shows why this is true. In Equation (3.49), the carrier term f_s is factored out. Writing Equation (3.49) in terms of the correlation integral shows that this separation of the carrier term

results in the down-conversion of the target impulse response to baseband:

$$\chi_{xr}(\tau, f_D - f_c) = \int_{-\infty}^{\infty} \chi_{xy}(\tau+u, f_D - f_c) \left(h(u)\, e^{-j2\pi f_c u} \right) du\, e^{-j2\pi f_c \tau} \quad . \quad (3.49)$$

3.3. Conclusions

The volume beneath the surface of the cross-ambiguity function is constant for constant power signals. Therefore, reductions in ambiguity function volume in one region result in increases in other regions. This means that if the ISL for some specific Doppler frequency is reduced, then the ISL will be increased for other Doppler frequencies. Signal repetition causes the Doppler response of the repeated signal to be multiplied by a weighting function that results in a sharper mainlobe in Doppler at the expense of range ambiguities. In other words, the ISL is reduced in the moving target region of the cross-ambiguity function, but the stationary target ISL is increased.

The response of a radar to an arbitrary target range profile is given by the correlation of the baseband signal cross-ambiguity function with the down-converted target range profile. Therefore, the response of the radar to a given target is dependent not only on the target range profile, but also on the radar signal processor itself. This means that the effective radar cross section of a target can be enhanced by designing a signal processor that excites an maximum response.

Additive white noise becomes distributed uniformly over the entire delay and frequency plane. The variance of the additive white noise decreases as the processing

time increases. The processing time, however, can only be increased within the confines of the limitation placed on the time-bandwidth product by maximum target velocity. Narrowband noise contamination results in a modulated signal spectrum contamination. Therefore, this contamination is a function of signal spectral shape. If a narrowband contamination is introduced to the receiver signal processor, the signal processor tends to spread the energy out over the entire bandwidth of the signal (which is much larger than the contamination) thus reducing the effect of the noise.

3.4. References

1. A. W. Rihaczek, Principles of High Resolution Radar, Peninsula Publishing, Los Altos, CA, 1985.

2. P. M. Woodward, Probability and Information Theory, with Applications to Radar, Pergamon Press, New York, 1953.

3. W. A. Gardner, Statistical Spectral Analysis, A Nonprobabalisitic Theory, Prentice-Hall Publishing, 1988.

4. A. Papoulis, Probability, Random Variable, and Stochastic Processes, Third Edition, McGraw-Hill Publishing, 1991.

CHAPTER IV

PROBABILISTIC ANALYSIS OF THE FSK/PSK CROSS-AMBIGUITY FUNCTION

In this chapter, the FSK/PSK cross-ambiguity function is analyzed probabilistically as a random process. The function is analyzed for two different regions; the mainlobe region and the sidelobe (or pedestal) region. The mainlobe region is that portion of Equation (3.48) for which l=0 and $|f| < 1/T_d$. The sidelobe region is that portion of Equation (3.48) for which $l \neq 0$ and/or $|f| > 1/T_d$. Probabilistic analysis of these functions is required since the frequency and phase sequences within a signal are inherently random. Therefore, the function is best quantified in general by its mean (or expected value) and variance. The expected value of the cross-ambiguity function describes the shape of the function on the average whereas the variance describes how the realized function deviates from the expected value on the average. It is assumed that the frequency and phase sequences are stationary random sequences. The requirement of stationarity is necessary for the analysis that follows and is also a valid assumption for signals that are random from signal-to-signal.

4.1. Mainlobe Analysis

The mainlobe of the of the cross-ambiguity function of an FSK/PSK radar signal is given by

$$\chi_{xy}(\tau,f) = \sum_{m=0}^{N-1} \chi_{mm}(\tau, f) + \sum_{m=1}^{N-1} \chi_{m(m-1)}(1-\tau, f)\, u(\tau) + \sum_{m=0}^{N-2} \chi_{m(m+1)}(1+\tau, f)\, u(-\tau) \tag{4.1}$$

where $u(\tau)$ is the unit step function and $f=f_D-f_c$.

Taking the expectation of the sub-pulse cross-ambiguity functions with respect to a_m and a_n yields

$$E_{a_m a_n}\{\chi_{mn}(\tau, f)\} = \begin{cases} \dfrac{(1-|\varepsilon|)}{N}\, sinc\{\pi f(1-|\varepsilon|)T\}\, e^{j2\pi mfT} e^{-j2\pi\varepsilon T}\, e^{-j(2\pi f_m \varepsilon T + \phi_m)} & m=n \\ 0 & m\neq n \end{cases} \tag{4.2}$$

assuming equal likelihood of +1 or -1 for a_m. From this knowledge, the expectation of Equation (4.1) with respect to a_m and a_n can be written as

$$E_{a_m a_n}\{\chi_{xy}(\tau, f)\} = \sum_{m=0}^{N-1} \chi_{mm}(\tau, f) \quad . \tag{4.3}$$

Now, taking the expectation with respect to the sub-pulse frequencies f_m and phases ϕ_m, the expected function of the mainlobe is given by

$$E_{a_m a f_m \phi_m}\{\chi_{xy}(\varepsilon, f)\} = \frac{1}{N}(1-|\varepsilon|)\, sinc\{\pi f(1-|\varepsilon|)T\}\, e^{-j2\pi f\varepsilon T} \sum_{m=0}^{N-1} e^{j2\pi m f T}\, E_{f_m \phi_m}\{e^{-j(2\pi f_m \varepsilon T+\phi_m)}\} \tag{4.4}$$

which simplifies to

$$E_{a_m a f_m \phi_m}\{\chi_{xy}(\varepsilon, f)\} = \frac{1}{N}(1-|\varepsilon|)\, sinc\{\pi f(1-|\varepsilon|)T\}\, e^{-j2\pi f\varepsilon T} \frac{\sin(\pi N f T)}{\sin(\pi f T)}\, e^{j\pi(N-1)fT} \sum_{k=0}^{K-1} p_k\, e^{-j(2\pi f_k \varepsilon T+\phi_k)} \tag{4.5}$$

where K is the number of oscillators used to construct the signal, p_k is the probability that the k^{th} oscillator f_k is selected within the burst, and ϕ_k is the phase associated with the k^{th} oscillator.

The mainlobe variance is now derived. The variance is important because it describes the mean square error between any realization of an FSK/PSK cross-ambiguity function mainlobe and the mean mainlobe function given in Equation (4.5). The variance of the mainlobe of the cross-ambiguity function is found from the following equation

$$var\{\chi_{xy}(\varepsilon, f)\} = E_{a_m a_n f_m \phi_m}\left\{\left|\sum_{m=0}^{N-1} \chi_{mm}(\varepsilon, f)\right|^2\right\}$$

$$- \left| E_{a_m a_n f_m \phi_m}\{\chi_{xy}(\varepsilon, f)\}\right|^2 + E_{a_m a_n f_m \phi_m}\left\{\left|\sum_{m=1}^{N-1} \chi_{m(m-1)}(1-\varepsilon, f)u(\varepsilon)\right|^2\right\} \quad (4.6)$$

$$+ E_{a_m a_n f_m \phi_m}\left\{\left|\sum_{m=0}^{N-2} \chi_{m(m+1)}(-1-\varepsilon, f)\, u(-\varepsilon)\right|^2\right\} .$$

Substituting in the individual functions into Equation (4.6) and collecting terms yields the following

$$var\{\chi_{xy}(\varepsilon, f)\} =$$

$$\frac{1}{N}(1-|\varepsilon|)^2\, sinc^2\{\pi f(1-|\varepsilon|)T\}\left[1 - \left|\sum_{k=0}^{K-1} p_k\, e^{-j(2\pi f_k \varepsilon T + \phi_k)}\right|^2\right] \quad (4.7)$$

$$+ \frac{(N-1)}{N^2}|\varepsilon|^2 \sum_{k=0}^{K-1}\sum_{i=0}^{K-1} p_k\, p_i\, sinc^2\{\pi(f-(f_k - f_i)|\varepsilon|\, T\} .$$

Notice that the variance is upper bounded by $1/N$. The longer the sequence, the lower the variance. Therefore, as the sequence length increases, the realized cross-ambiguity function converges to the expected function Equation (4.5).

4.2. Sidelobe Analysis

The sidelobe region of the FSK/PSK radar signal cross-ambiguity function for positive lag values is given by

$$\chi_{xy}(l+\varepsilon, f) = \sum_{m=l}^{N-1} \chi_{m(m-l)}(\varepsilon, f) + \sum_{m=l+1}^{N-1} \chi_{m(m-l-1)}(1-\varepsilon, f) \quad . \tag{4.8}$$

Using Equation (4.2), the expected value of Equation (4.8) is found to be equal to zero. Therefore, the variance of Equation (4.8) is given by

$$\begin{aligned} var\left\{ \chi_{xy}(l+\varepsilon, f) \right\} &= \sum_{m=l}^{N-1} E_{a_m a_j f_m \phi_m} \left\{ \left| \chi_{m(m-l)}(\varepsilon, f) \right|^2 \right\} \\ &+ \sum_{m=l+1}^{N-1} E_{a_m a_j f_m \phi_m} \left\{ \left| \chi_{m(m-l-1)}(1-\varepsilon, f) \right|^2 \right\} \quad . \end{aligned} \tag{4.9}$$

Equation (4.9) can also be expressed as

$$\begin{aligned} &var\left\{ \chi_{xy}(l+\varepsilon, f) \right\} = \\ &\frac{(N-1)}{N^2} (1-|\varepsilon|)^2 \sum_{k=0}^{K-1} \sum_{i=0}^{K-1} p_i p_k \, sinc^2 \left\{ \pi(f-(f_k-f_i))(1-|\varepsilon|)T \right\} \\ &+ \frac{(N-l-1)}{N^2} |\varepsilon|^2 \sum_{k=0}^{K-1} \sum_{i=0}^{K-1} p_i p_k \, sinc^2 \left\{ \pi(f-(f_k-f_i))|\varepsilon|T \right\} \quad . \end{aligned} \tag{4.10}$$

Equation (4.10) was derived for the sidelobes characterized by values of $l>0$. It is however valid for both positive and negative values of l. Again notice that the variance of the sidelobes decreases approximately as $1/N$.

4.3. Integrated Sidelobe Level Analysis

A more important result obtained from Equation (4.10) is the integrate sidelobe level (*ISL*) given by

$$ISL\ (\ |f| \ll 1/T\ ) = \int_{-\infty}^{\infty} var\ \{\ \chi_{xy}(\tau, |f| \ll 1/T\ )\ \}\ d\tau \quad . \tag{4.11}$$

The ISL is important because it is related to the variance (power) of the ground clutter return. Substituting Equation (4.10) into Equation (4.11) and evaluating the integral yields the following equation describing the ISL in terms of the frequency selection probabilities:

$$ISL\ (\ |f| \ll 1/T\ ) = 2\left[\ \sum_{k=0}^{K-1} \frac{p_k^2}{3} + \sum_{\substack{i,k \\ i\neq k}}^{K-1} \frac{p_i\ p_k}{2(\pi(i-k))^2}\ \right] \quad . \tag{4.12}$$

Notice that the ISL is not a function of the sequence length. This results from the fact that the randomized FSK/PSK waveform uniformly spreads its sidelobe energy in range. As the sequence length increases, the variance of the sidelobes decreases accordingly. The ISL remains constant however, since the domain of integration is increased in a proportionally.

In Chapter III, the effect of periodicity (of period T_p) on the cross-ambiguity function was investigated. From the results of Equation (4.12) and (3.29), it can be seen that the ISL of an FSK/PSK waveform that is repeated M times is given by

$$ISL_p\ (\ |f\ | \ll 1/T\ ) = ISL\ (\ f\ )\ PER\ (\ f\ ,\ M\ ) \tag{4.13}$$

where

$$PER\ (f, M) = \frac{1}{M^2} \sum_{l=-(M-1)}^{M-1} \left(\frac{\sin\left(\pi f (M - |l|) T_p\right)}{\sin\left(\pi f T_p\right)} \right)^2 \qquad (4.14)$$

assuming nonoverlapping waveforms. A plot of Equation (4.14) for M = 2, 4, 8, and 16 is shown in Figure 4.1. As is shown in Figure 4.1, the zero frequency term is increased by approximately 10 dB/decade with increasing M while the nonzero frequency terms are decreased approximately as 10 dB/decade with increasing M.

4.4. Conclusions

The mean value of the cross-ambiguity function is non-zero only in the mainlobe. Additionally, the variance of the cross-ambiguity function is upper bounded by $1/N$ at the mainlobe, and the variance falls off linearly with the distance from the mainlobe to zero at its outer delay boundary. Even though the variance of the sidelobes can be decreased by increasing the sequence length, the ISL of the cross-ambiguity function is unaffected since the sidelobe energy is simply spread over a larger area. Additionally, repetition of waveforms has the effect of increasing the zero Doppler region ISL while the moving target portion is decreased. Therefore, a clear area can be created by repeating waveforms.

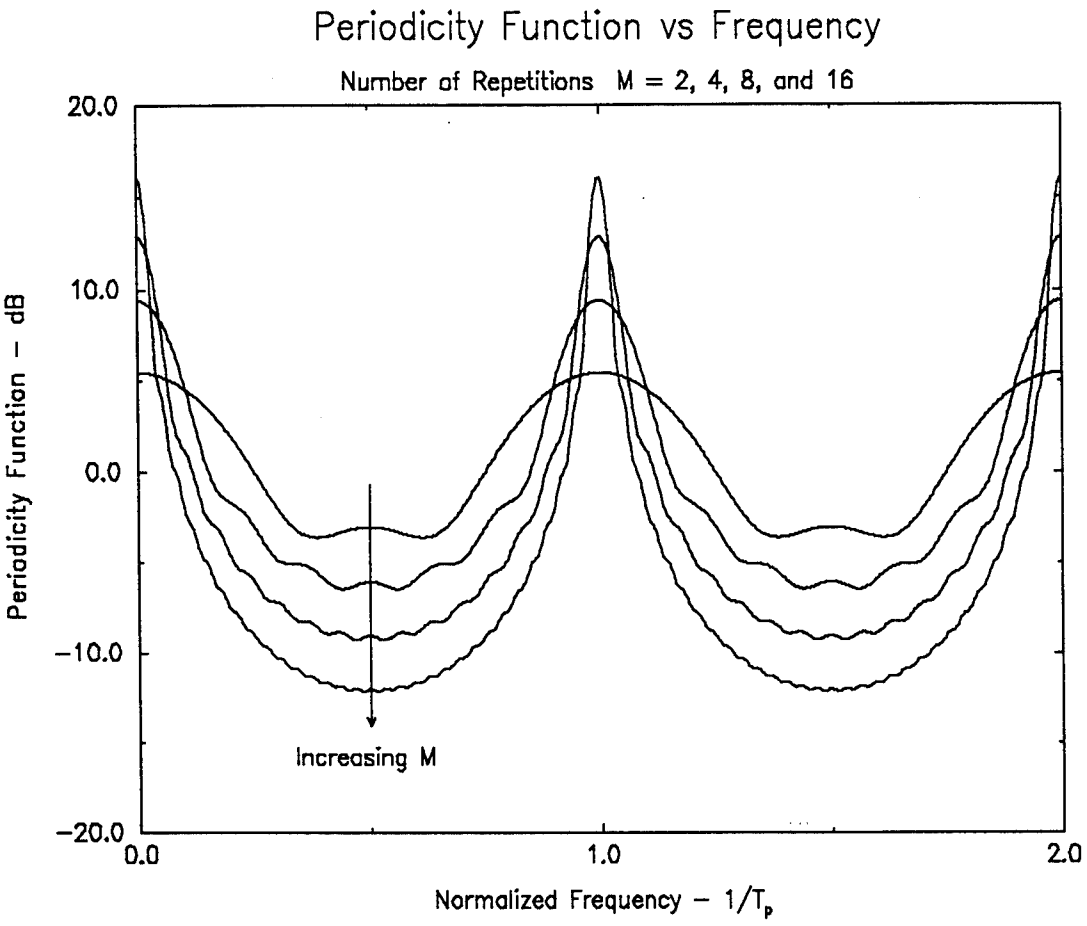

Figure 4.1. Periodicity Function in dB Versus Frequency for Various Values of M.

CHAPTER V

MATCHED FSK/PSK SIGNAL TIME-BANDWIDTH PRODUCT

In Chapter II, it was seen certain factors that contribute to the LPI performance of a radar signal processor: the time-bandwidth product of the transmit signal and the effective radar cross section of the target. The higher the time-bandwidth product, the better the LPI performance of the radar. In this chapter, the effective time-bandwidth product of an FSK/PSK radar signal is derived. The time-bandwidth product is determined by first calculating the effective bandwidth of the FSK/PSK transmit signal power spectral density. The effective bandwidth of the signal power spectral density is developed based on the signal's noise equivalent bandwidth [1].

5.1. FSK/PSK Radar Signal Power Spectral Density

The power spectral density of a signal describes how the signal power is distributed in the frequency domain on the average. The power spectral density of a signal $y(t)$ is defined by [1]

$$S_{yy}(\omega) = \frac{E\left\{ \left| Y(\omega) \right|^2 \right\}}{T_d} \tag{5.1}$$

where $E\{\}$ is the expected value operator, T_d is the signal duration, and $Y(\omega)$ is the Fourier transform of $y(t)$ defined by

$$Y(\omega) = \int_{-\infty}^{\infty} y(t)\, e^{-j\omega t}\, dt \quad . \tag{5.2}$$

Mathematically, the power spectral density of a signal is equal to the limit of Equation (5.1) as T_d grows to infinity. For the purposes of this study, however, only finite-duration signals are of interest. Therefore, Equation (5.1) will be termed the finite-duration power spectral density of the transmit signal.

The transmit signal of the radar is defined by Equation (3.40). Evaluating Equation (5.3) with Equation (3.40) as the argument of the integral yields

$$\begin{aligned} Y(\omega) = {} & \frac{1}{2} \sum_{n=0}^{N-1} a_n\, T\, sinc\left\{ \left[\omega - \left(\omega_n + \omega_s \right) \right] \frac{T}{2} \right\} e^{-j(\omega-(\omega_n+\omega_s))\, nT/2} \\ & + \frac{1}{2} \sum_{n=0}^{N-1} a_n\, T\, sinc\left\{ \left[\omega + \left(\omega_n + \omega_s \right) \right] \frac{T}{2} \right\} e^{-j(\omega+(\omega_n+\omega_s))\, nT/2} \quad . \end{aligned} \tag{5.3}$$

Taking the expected value with respect to the random FSK code and the random PSK code of the magnitude squared of Equation (5.3) yields

$$\begin{aligned} E\left\{ \left| Y(\omega) \right|^2 \right\} = {} & \frac{NT^2}{4} \sum_{k=0}^{K-1} p_k\, sinc^2\left\{ \left[\omega - \left(\omega_k + \omega_s \right) \right] \frac{T}{2} \right\} \\ & + \frac{NT^2}{4} \sum_{k=0}^{K-1} p_k\, sinc^2\left\{ \left[\omega + \left(\omega_k + \omega_s \right) \right] \frac{T}{2} \right\} \end{aligned} \tag{5.4}$$

where p_k's represent the probability of selecting oscillator k. Now, dividing through by the duration NT of the signal yields the finite-duration power spectral density

$$S_{yy}(\omega) = \frac{T}{4}\sum_{k=0}^{K-1} p_k \, sinc^2\left\{\left[\omega - \left(\omega_k + \omega_s\right)\right]\frac{T}{2}\right\} + \frac{T}{4}\sum_{k=0}^{K-1} p_k \, sinc^2\left\{\left[\omega + \left(\omega_k + \omega_s\right)\right]\frac{T}{2}\right\} \quad . \tag{5.5}$$

Notice that the power spectral density of the signal takes the shape of the probability density function of the frequency selection process. Mathematically, the term finite-duration power spectral density is an oxymoron. By definition, power signals are infinite in duration (persistent). In actuality, $y(t)$ is an energy signal because only a finite duration portion of the signal is processed in any processing interval. For the purposes of this study, it will be assumed that the actual signal exists for infinity, but only a finite-duration portion of the signal is of interest. Therefore, Equation (5.5) is valid for the analysis that follows.

5.2. Equivalent Bandwidth

Equation (5.5) can take on any arbitrary shape that has the properties of a valid probability density function. Therefore, the bandwidth of the power spectral density is a difficult parameter to define. The bandwidth could be defined to be $(\omega_{K-1}-\omega_0)$ since that is the maximum possible bandwidth in which the signal could possibly exist. A definition of filter bandwidth that is often used in signal processing analysis is the noise equivalent bandwidth of a signal. A pictorial representation of noise equivalent bandwidth is shown in Figure 5.1 and mathematically by [1]

$$B_e = \frac{1}{2\pi \, \max\{S_{yy}(\omega)\}} \int_{-\infty}^{\infty} S_{yy}(\omega) \, d\omega \quad . \tag{5.6}$$

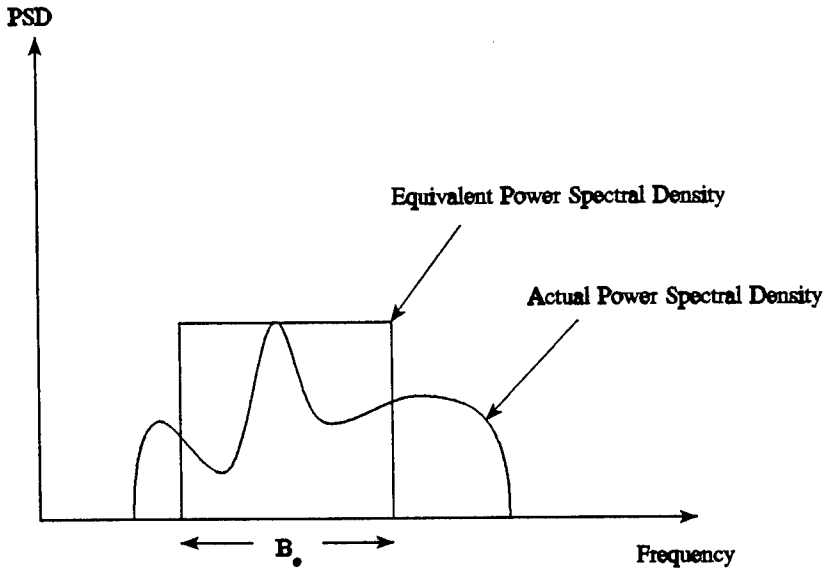

Figure 5.1. Equivalent Bandwidth of a Signal.

Equation (5.6) assumes that the oscillator frequencies are separated by at least $1/T$ Hz. In other words, the different frequency sub-pulse power spectral densities do not overlap. From Equation (5.5), the maximum value of the power spectral density function is equal to one fourth of T times the maximum probability of frequency occurrence

$$\max\{ S_{yy}(\omega) \} = \frac{T}{4} \max\{ p_k \} \quad . \tag{5.7}$$

Additionally, the integral of Equation (5.6) is in a form that is tabulated in many integral tables. The value of the integral can be found to equal

$$\int_{-\infty}^{\infty} S_{yy}(\omega)\, d\omega = \frac{\pi}{2} \sum_{k=0}^{K-1} p_k = \frac{\pi}{2} \quad . \tag{5.8}$$

Therefore, according to Equation (5.6), the equivalent bandwidth of an FSK/PSK radar signal is given by

$$B_e = \frac{1}{T \max\{ p_k \}} \quad . \tag{5.9}$$

Equation (5.9) can be evaluated for two extreme probability density functions in order to become acquainted with the equivalent bandwidth. The first density function is a uniform distribution in which all frequencies occur with probability $1/K$. Under this condition, the equivalent bandwidth is given by

$$B_e = \frac{K}{T} \quad . \tag{5.10}$$

The second density function that is of interest is one in which only a single frequency is used. Under this density function, the equivalent bandwidth becomes

$$B_e = \frac{1}{T} \quad . \tag{5.11}$$

Both of these equivalent bandwidth calculations have results that are intuitively obvious.

5.3. Equivalent Time-Bandwidth Product

Since the duration of the FSK/PSK radar signal is equal to the number of pulses time the duration of each pulse, the equivalent time-bandwidth product is equal to

$$B_e T_d = \frac{N}{\max\{ p_k \}} \quad . \tag{5.12}$$

It should be noted that the equivalent time-bandwidth product should be used to evaluate the LPI performance of the radar signal. It should not be used to determine the maximum target velocity that can be processed by the radar. For the velocity limitation, it should always be assumed that all frequencies will be utilized equally often. In other words, for determining the maximum velocity that the radar can process, the following equation should be used

$$B_r T_d = NK \quad . \tag{5.13}$$

It should also be noted that the maximum time-bandwidth product possible occurs for a signal that uses all sub-pulse frequencies with equal likelihood. Therefore, as a signal takes on any shape other than a uniform shape, the equivalent time-bandwidth product, and the associated LPI performance is reduced. A measure of LPI performance degradation due to a nonuniform transmit signal power spectral density can be defined as the ratio of Equation (5.13) to (5.12)

$$L_{LPI} = \frac{B_e T_d}{B_r T_d} = \frac{1}{K \max\{ p_k \}} \quad . \tag{5.14}$$

Notice that a value of L_{LPI} less than unity represents an LPI performance degradation.

5.4. Conclusions

The power spectral density of an FSK/PSK radar signal is defined by the probability density function of the frequency selection random process. Since the power spectral density can take on any shape that is a valid probability density function, the bandwidth of the signal is somewhat difficult to parameterize. For the purposes of LPI performance, the equivalent bandwidth of the radar signal is used. This equivalent bandwidth of a signal is equal to the bandwidth of a signal with equal power to the original signal that has an ideal bandlimited shape and a magnitude equal to the peak value of the actual signal power spectral density. The equivalent bandwidth is maximum for a signal that utilizes each available oscillator with equal likelihood (uniform power spectral density). The equivalent bandwidth is bounded between $1/T$ and K/T where K is the number of oscillators available and T is the pulsewidth.

5.5. References

1. G. R. Cooper and C. D. McGillem, Probabilistic Methods of Signal and System Analysis, Second Edition, Holt, Rinehart, and Winston, 1986.

CHAPTER VI

MATCHED FSK/PSK SIGNAL DESIGN

In this chapter, the probabilistic analysis of the FSK/PSK cross-ambiguity function will be used to develop design techniques for Matched FSK/PSK radar signals. Matched FSK/PSK radar signals are FSK/PSK signals in which the mainlobe of the cross-ambiguity function has been specifically shaped to become a matched filter for a given target range profile. The design technique will be derived from Equation (4.5). First the special case of the FSK/PSK cross-ambiguity function mainlobe at zero frequency will be analyzed. This will be shown to be of the form of a discrete Fourier series. The discrete Fourier series representation will allow the mainlobe of the FSK/PSK cross-ambiguity function to be designed to approximate the shape of any arbitrary time-limited function. A step-by-step example involving computer simulations will be used to illustrate the concept.

6.1. FSK/PSK Cross-Ambiguity Function as a Fourier Series

In this section, the mainlobe of the FSK/PSK cross-ambiguity function for the case of zero frequency deviation will be analyzed to show that it is of the form of a discrete Fourier series. From Equation (4.5), the expected value of the mainlobe of an FSK/PSK radar signal cross-ambiguity function is given by

$$E_{a_m a_n f_m}\{\chi_{xy}(\varepsilon, f)\} = \frac{(1-|\varepsilon|)\,T}{N}\, sinc\{\pi f(1-|\varepsilon|)T\}\, e^{-j2\pi f\varepsilon T} \frac{\sin(\pi NfT)}{\sin(\pi fT)}\, e^{j\pi(N-1)fT} \sum_{k=0}^{K-1} p_k e^{-j(2\pi f_k \varepsilon T+\phi_k)} \tag{6.1}$$

again where K is the number of oscillators used to construct the signal, p_k is the probability that the k^{th} oscillator of frequency f_k is chosen within the signal burst, and ϕ_k is the phase of the k^{th} oscillator. If the values of f_k are chosen to be integer multiples of the pulse rate

$$f_k = \frac{k}{T} \tag{6.2}$$

then the summation of Equation (6.1) is of the form of a discrete Fourier series (DFS). It is of interest to express Equation (6.1) in a more convenient form of the product of a closed form window function and a DFS,

$$E_{a_m a_n f_m}\{\chi_{xy}(\varepsilon, f)\} = W(\varepsilon, f) \sum_{k=0}^{K-1} p_k\, e^{-j(2\pi k\varepsilon+\phi_k)} \tag{6.3}$$

where

$$W(\varepsilon, f) = \frac{(1-|\varepsilon|)\,T}{N}\, sinc\{\pi f(1-|\varepsilon|)T\}\, \frac{\sin(\pi NfT)}{\sin(\pi fT)}\, e^{j\pi(N-1-2\varepsilon)fT} \,. \tag{6.4}$$

For values of $f \ll 1/NT$, Equation (6.4) is approximately equal to

$$W(\varepsilon,0) = (1-|\varepsilon|)\,T \,. \tag{6.5}$$

Therefore, the expected value of the cross-ambiguity function for $f \approx 0$ is given by

$$E_{a_m a_n f_m}\{\chi_{xy}(\varepsilon,0)\} = W(\varepsilon,0)\sum_{k=0}^{K-1} p_k\, e^{-j(2\pi k\varepsilon+\phi_k)} \quad . \tag{6.6}$$

Equation (6.6) is clearly of the form of a discrete Fourier series with a triangular windowing function $W(0,\varepsilon)$.

6.2 Properties of the Discrete Fourier Series

For the purposes of this study, the discrete Fourier series representation of the function $f(\varepsilon)$ will be defined as

$$f(\varepsilon) \approx \sum_{k=0}^{K-1} b_k\, e^{-j(2\pi k\varepsilon+\phi_k)} = f_{DFS}(\varepsilon) \tag{6.7}$$

where $-1/2 < \varepsilon < 1/2$. Using the orthogonality property of the complex exponential, the weights b_k and phases ϕ_k are determined by the following

$$b_k e^{-j\phi_k} = \int_{-1/2}^{1/2} f(\varepsilon)\, e^{j2\pi k\varepsilon}\, d\varepsilon \quad . \tag{6.8}$$

The DFS representation of a signal will now be demonstrated with an example. For this example, define

$$f(\varepsilon) = .5\delta(\varepsilon) - .5\delta(\varepsilon-.25) \tag{6.9}$$

where $\delta(\varepsilon)$ is the Dirac delta function. Assume that the function is to be approximated with 8 complex exponentials ($K=8$). Now, the weights b_k and the phases ϕ_k can be determined from Equation (6.8) and are given by

$$b_k = \left| \sin\left(\frac{\pi k}{4}\right) \right| \tag{6.10}$$

and

$$\phi_k = \left(\frac{k-2}{4} + u\left[\sin\left\{\frac{\pi k}{4}\right\} \right] \right)\pi \quad . \tag{6.11}$$

Table 6.1 shows the values of $f(\varepsilon)$ and $f_{DFS}(\varepsilon)$ for 8 discrete values of ε. Notice that the actual signal is approximated exactly for the 8 match points shown. A plot of the series evaluated at 128 values of ε within the defined interval is shown in Figure 6.1. As can be seen from Figure 6.1, the DFS functions approximate the original function exactly at 8 match points. The DFS does not match the signal over the entire interval. The reason that this occurs is that only 8 complex exponentials are being used to represent a function that is actually represented by infinitely many sinusoids because of its infinite bandwidth. In general, the DFS will match the original function at K points equally spaced between $-1/2 < \varepsilon < 1/2$ where K is the number of frequencies summed together to form the estimate. A bandlimited function could, however, be represented exactly.

6.3. Matched FSK/PSK Signal Design Example

In this Section, an FSK/PSK signal will be designed that will be matched to function of Equation (6.9). The expected value of the cross-ambiguity function is shown in Figure 6.2. Two things should be noticed from the Figure. First, the DFS has been scaled. Second, the mainlobe of the expected value of the FSK/PSK cyclic cross-correlation function has been windowed by the triangular windowing function.

Table 6.1. Values of the Function $f(\varepsilon)$ and $f_{DFS}(\varepsilon)$ for 8 Equally Spaced Values of ε.

ε	$f(\varepsilon)$	$f_{DFS}(\varepsilon)$
-.5	0	0
-0.375	0	0
-0.25	0	0
-0.125	0	0
0	0.5	0.5
0.125	0	0
0.25	-0.5	-0.5
0.375	0	0

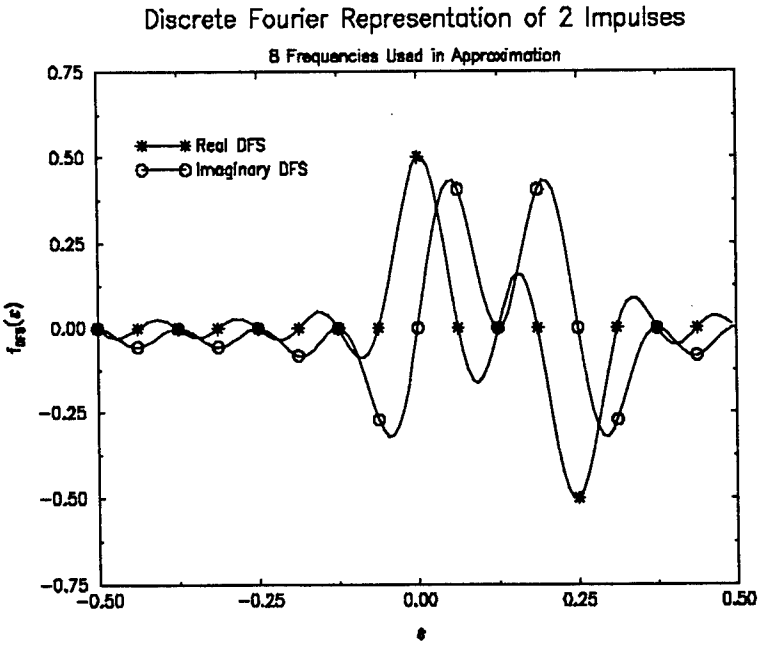

Figure 6.1 DFS Approximation to Equation (6.9).

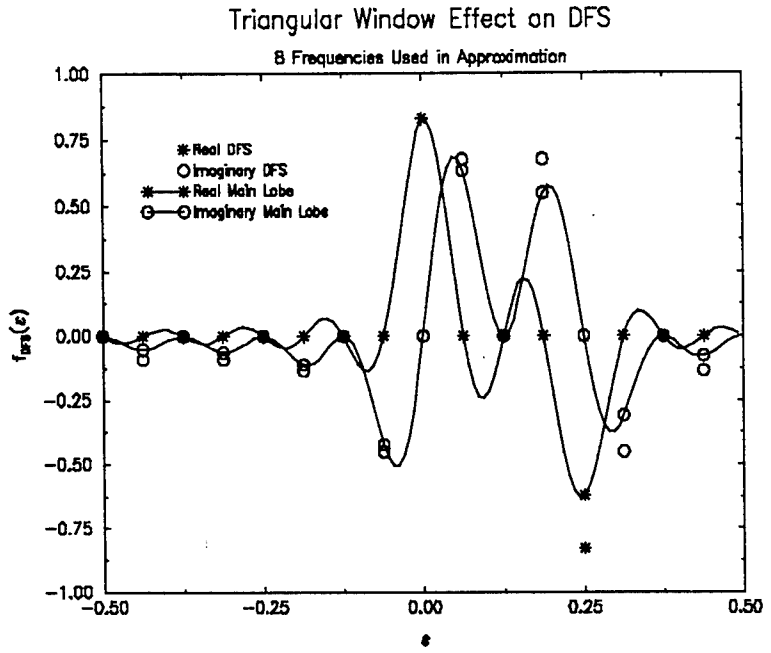

Figure 6.2. Scaled DFS of Equation (6.9) and the Expected Value of the Mainlobe of the Matched FSK/PSK Cross-Ambiguity Function.

The scaling results from the fact that the Fourier weights must sum to unity in order to satisfy the constraints of a probability density function. Therefore, an FSK/PSK signal that has an arbitrary cross-ambiguity function mainlobe can be constructed using the DFS theory derived in the previous section. Two sources of error between the desired result and the realized result are the effect of the triangular windowing function and the variance of the realized main lobe. The windowing is a deterministic functional error and the variance is a random noise-like error.

Figures 6.3.a and 6.3.b show a realization of the mainlobe of an $N=64$ pulse $K=8$ frequency Matched FSK/PSK cross-ambiguity function designed to be matched to the function of Equation (6.9). Figure 6.3.a shows the real component of the cyclic cross-correlation function and Figure 6.3.b shows the imaginary component. Three

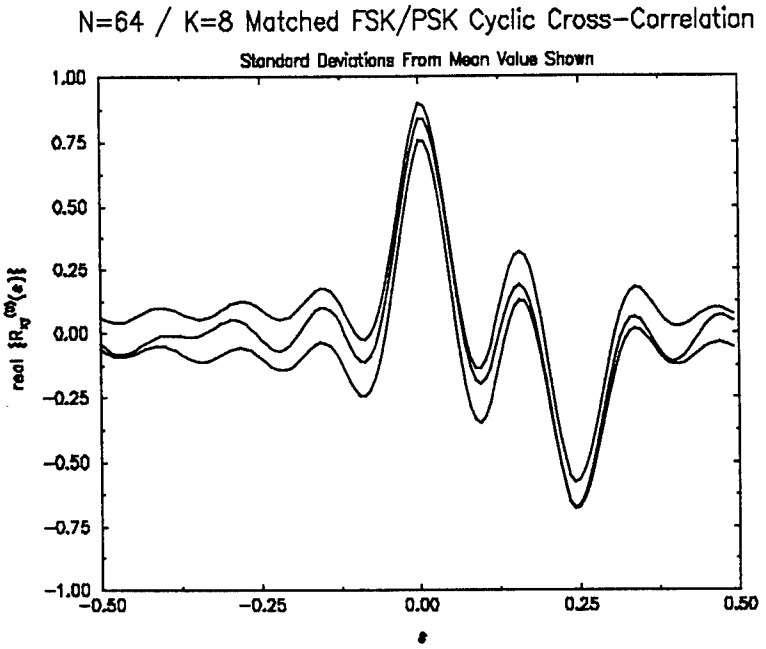

Figure 6.3.a. Real Component of the Realized Matched FSK/PSK Cross-Ambiguity Function and Standard Deviations for N=64 and K=8.

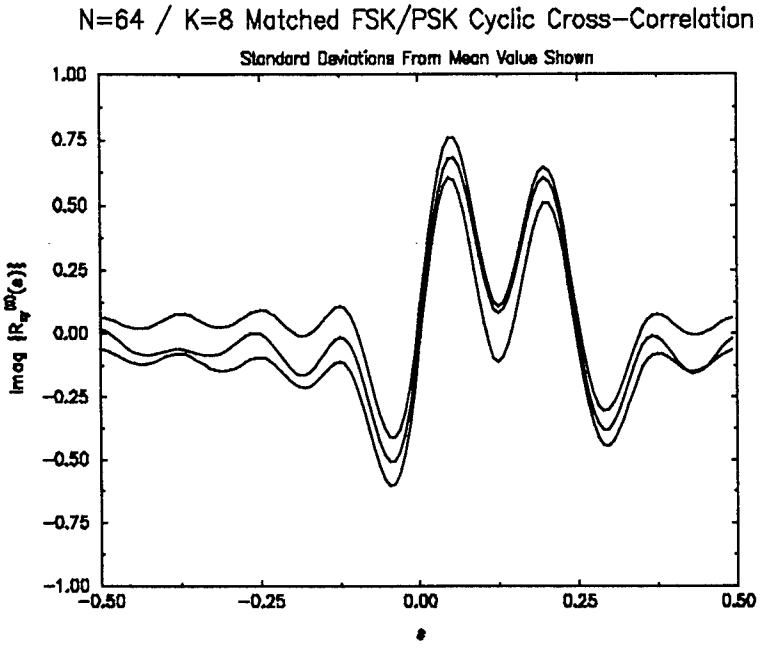

Figure 6.3.b. Imaginary Component of the Realized Matched FSK/PSK Cross-Ambiguity Function and Standard Deviations for N=64 and K=8.

curves are shown in each figure: the realized function, the expected function plus the standard deviation function, and the expected function minus the standard deviation function. As can be seen from Figures 6.3.a-b, the realized functions stay within the previously derived standard deviation function where the standard deviation is defined as the square root of the variance. Therefore, Figures 6.3.a and 6.3.b verify the expected value Equation (4.5) and the variance Equation (4.7).

The magnitude squared of the error between the expected Matched FSK/PSK cross-ambiguity function and the actual realized Matched FSK/PSK cross-ambiguity function of Figures 6.3.a-b is shown in Figure 6.4. As can be seen from Figure 6.4, the realized error (or variance) loosely follows the mainlobe variance derived in the previous chapter. Figure 6.5 shows the average realized variance of 300 random Matched FSK/PSK cross-ambiguity functions each for N=64, 128, 256, and 512 pulses. As predicted by Equation (4.7), the mainlobe variance decreases as $1/N$. Additionally, Equation (4.7) is verified since the shape of the variance curve is closely tracked by the realized variance values. It should be reiterated that Figure 6.4 shows a single realization of a random process (the error between the realized mainlobe and the expected mainlobe) while Figure 6.5 shows an average of 300 realizations. The curve of Figure 6.4 is not expected to follow exactly with the derived mean squared error since it is only a single realization.

6.4. Conclusions

The mean value of the cross-ambiguity function mainlobe range response is of the form of a discrete Fourier series. The weights of the discrete Fourier series are

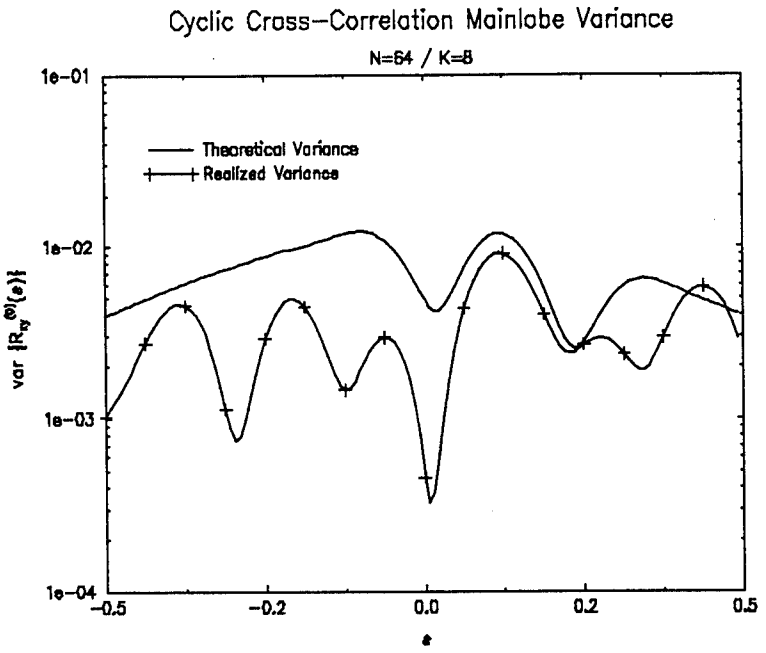

Figure 6.4. Squared Error of the Realized Matched FSK/PSK Cross-Ambiguity Function Along with the Expected Error Function.

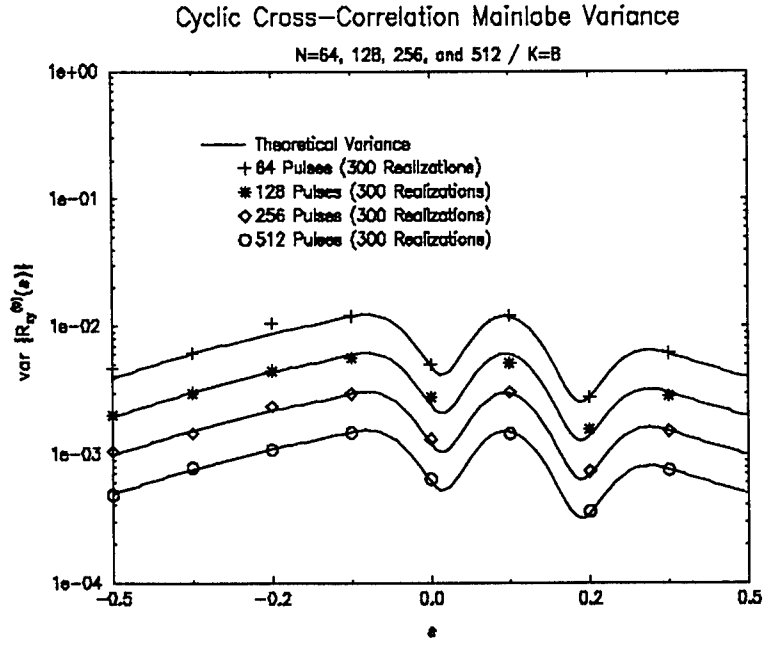

Figure 6.5. Average Realized Squared Error Functions and Expected Error Functions for N=64, 128, 256, and 512 Pulses.

defined by the probability density function of the frequency selection process, and the phases are given by the sub-pulse phases. Using known properties of the discrete Fourier series, FSK/PSK signals can be designed to approximate any arbitrary mainlobe cross-ambiguity function range response. This makes it possible to design signals that excite a maximum response from any arbitrary radar target based on knowledge of the target range profile $h(t)$. Additionally, computer simulations verify the results of Chapter III: the variance of the mainlobe response decreases with increasing sequence length. The utility of this signaling scheme will be demonstrated in the next chapter.

CHAPTER VII

COMPARATIVE ANALYSIS OF MATCHED FSK/PSK

In this chapter, matched FSK/PSK signaling is compared with two radar signaling schemes: a baseline system that utilizes a uniform spectrum signal with a receiver matched to the transmitted signal and a matched filter system that utilizes a post processing filter matched to the target to filter the output of the baseline system. The baseline system is referred to as a current technology system because its signal processor is matched only to the transmit signal. The matched filter system is a future technology system since it makes use of target-specific scattering information (the range profile). The analysis begins with an analysis of the radar-target interaction (effective radar cross section) of the baseline system, a white noise contamination analysis of the baseline system, and a clutter contamination analysis of the baseline system. Next, the effective target radar cross section, white noise contamination, and ground clutter contamination of the matched filter radar is analyzed in a similar fashion. The matched FSK/PSK radar system is analyzed for the same three conditions above to develop equations for comparison with the other two methods. A general mathematical comparison follows the analysis of the three radar technologies which are quantified by performance ratios, or performance improvements. Finally,

the performance improvements are characterized for six example target spectra predicted by a radar cross section prediction code.

7.1. Analysis of the Baseline System

The baseline system transmits an FSK/PSK signal with a frequency probability density function defined by

$$p_k = \frac{1}{K} \tag{7.1}$$

where K is the number of frequencies used by the radar signal. Therefore, according to Equation (6.6), the ambiguity function of the radar is approximately given by

$$\chi_{xx}(\varepsilon\ ,\ 0) = \frac{1}{K} \sum_{k=0}^{K-1} e^{j2\pi k\varepsilon} \quad . \tag{7.2}$$

Equation (7.2) has an impulse-like ambiguity range delay function. It is assumed that the target has a range profile defined by

$$h(\varepsilon) = \sum_{k=0}^{K-1} \sqrt{\sigma_k}\ e^{j(2\pi k\varepsilon + \phi_k)} \tag{7.3}$$

where σ_k is the radar cross section of the target at the k^{th} frequency, and the target imparts a phase shift of ϕ_k on the k^{th} frequency component of the signal. From the correlation property of Equation (3.49), the maximum possible output of the radar for a range delay value of ε=0 is given by

$$\max_{\varepsilon} \left| \chi_{xr}(\varepsilon , 0) \right| = \frac{1}{K} \max_{\varepsilon} \left| \sum_{k=0}^{K-1} \sqrt{\sigma_k} \; e^{j(2\pi k\varepsilon + \phi_k)} \right| \quad . \tag{7.4}$$

It should be noted that the squared value of the maximum output voltage is equivalent to the effective radar cross section σ of the target used in Equation (2.1).

The variance of an additive white noise contaminant is given by Equation (3.36) to be

$$R_{nn}(0) = \frac{N_o}{T_d} \tag{7.5}$$

where N_o is the power spectral density of the channel noise and T_d is the duration of the signal. From Equation (4.12), the ISL of the signal with the frequency distribution defined by Equation (7.1) is given approximately by

$$ISL \approx \sum_{k=0}^{K-1} p_k^2 = \frac{1}{K} \quad . \tag{7.6}$$

Therefore, the output of the baseline radar has been defined for the effective radar cross section (7.4), additive noise (7.5), and clutter contamination (7.6). The clutter contamination, for the purposes of this comparative study, will be defined as the ratio of the effective target radar cross section to the integrated sidelobe level. Or, as the ratio of the square of Equation (7.4) to Equation (7.6)

$$\frac{S_b}{C} = \frac{1}{K} \left(\max_{\varepsilon} \left| \sum_{k=0}^{K-1} \sqrt{\sigma_k} \; e^{j(2\pi k\varepsilon + \phi_k)} \right| \right)^2 \quad . \tag{7.7}$$

7.2. Matched Filtering

A matched filter implementation is now investigated. A matched filter implementation involves a radar that utilizes the baseline signaling scheme with the frequency probability density function defined by Equation (7.1). As in the previous section, the output of the radar is given by Equation (7.4). The matched filter radar system differs from the baseline system in that it filters the range profile (measured by the baseline radar) with a filter impulse response defined by

$$h_m(\varepsilon) = \frac{\sum_{k=0}^{K-1} \sqrt{\sigma_k}\; e^{j(2\pi\varepsilon k + \phi_k)}}{\sqrt{\sum_{k=0}^{K-1} \sigma_k}} \quad . \tag{7.8}$$

The denominator term of Equation (7.8) is a normalization factor to give the filter a unity noise bandwidth [1]. From linear system theory, it is known that the output of the matched filter for $\varepsilon=0$ is equal to the convolution of the filter impulse response of Equation (7.8) with the cross-ambiguity function of Equation (7.4)

$$\chi_{xr}(0,0) = \frac{\sum_{k=0}^{K-1} \sigma_k}{K\sqrt{\sum_{k=0}^{K-1} \sigma_k}} \quad . \tag{7.9}$$

As above with Equation (7.4), the squared value of the output voltage is equal to the effective target radar cross section of the target σ. It should be noticed that Equation (7.9) does not contain any phase terms. This results from the fact that the matched filter is phase matched to the target, and therefore, realigns all of the phase variations

in the target spectrum. In other words, all contributions to the target spectrum are added in phase with one another (added constructively).

For the baseline radar, the autocorrelation function of the noise process at the input of the matched filter is given by Equation (3.36) to be

$$R_{nn}(\varepsilon) = \frac{N_o}{T_d} \sum_{k=0}^{K-1} \frac{1}{K} e^{j2\pi\varepsilon k} \quad . \tag{7.10}$$

From stochastic processes theory [1], the autocorrelation function of the noise process output from the matched filter defined by Equation (7.10) is given by

$$R_{n'n'}(\varepsilon) = \frac{N_o}{K\,T_d} \frac{\sum_{k=0}^{K-1} \sigma_k\, e^{j2\pi\varepsilon k}}{\sum_{k=0}^{K-1} \sigma_k} \quad . \tag{7.11}$$

The mean squared noise output voltage (the noise power) output from the matched filter is given by

$$R_{n'n'}(0) = \frac{N_o}{K\,T_d} \quad . \tag{7.12}$$

Therefore, the noise variance of the baseline radar (7.5) is K times that of the matched filtered case.

To determine the effect of the matched filter on the clutter return, it is assumed that the clutter can be modeled as additive white noise. In other words, the autocorrelation function of the clutter return can be modeled according to (7.11) as

$$R_{cc}(\varepsilon) = ISL \sum_{k=0}^{K-1} \frac{1}{K} e^{j2\pi\varepsilon k} \tag{7.13}$$

where the ISL is given in Equation (7.6). Following the white noise analysis procedure from above, the actual effect of the clutter variance is equal to

$$R_{cc}(0) = \frac{ISL}{K} = \frac{1}{K^2} \quad . \tag{7.14}$$

Therefore, the signal to clutter ratio for the matched filter case is

$$\frac{S_m}{C} = \frac{\chi_{xr}^2(0,0)}{R_{cc}(0)} = \sum_{k=0}^{K-1} \sigma_k \quad . \tag{7.15}$$

7.3. Matched FSK/PSK Radar

The matched FSK/PSK radar is said to be matched to a target if the probability density function of the frequency selection process has a shape that is proportional to the magnitude of the target's voltage reflection coefficients at each of the frequencies. In equation form, the probability density function is given by

$$p_k = \frac{\sqrt{\sigma_k}}{\sum_{k=0}^{K-1} \sqrt{\sigma_k}} \quad . \tag{7.16}$$

The numerator of Equation (7.16) describes the shape of the probability density function and the denominator is a normalizing factor required of a valid probability density function. The cross-ambiguity function for the matched FSK/PSK radar waveform, as defined by Equation (6.6), is therefore equal to

$$\chi_{xy}(\varepsilon, 0) = \sum_{k=0}^{K-1} p_k \, e^{j(2\pi\varepsilon k + \phi_k)} \tag{7.17}$$

where the p_k's are as defined above in Equation (7.16) and the phase terms ϕ_k are also given in Equation (7.16). It is of interest to determine the value of the output signal for zero delay. In other words, when the cross-ambiguity function is perfectly aligned with the target range profile of Equation (7.3). Therefore, according to Equation (3.49), the peak response for $\varepsilon=0$ equals

$$\chi_{xr}(0, 0) = \frac{\sum_{k=0}^{K-1} \sigma_k}{\sum_{k=0}^{K-1} \sqrt{\sigma_k}} \quad . \tag{7.18}$$

As with the previous two radar examples, Equation (7.18) is the square root of the effective target radar cross section of the target σ.

It is now of interest to investigate white noise contamination of a matched FSK/PSK radar. According to Equation (3.36), for the case of the matched FSK/PSK radar, noise autocorrelation function equals

$$R_{nn}(\varepsilon) = \frac{N_o}{T_d} \sum_{k=0}^{K-1} p_k \, e^{j2\pi\varepsilon k} \tag{7.19}$$

where the p_k's are as given above in Equation (7.16), N_0 is the channel noise power spectral density, and T_d is the waveform duration. For the case of $\varepsilon=0$, the mean noise output power is

$$R_{nn}(0) = \frac{N_o}{T_d} \tag{7.20}$$

since the probabilities sum to unity. Notice that this is the same as for the baseline case above (7.5).

From Equation (4.12), the ISL of a matched FSK/PSK radar is given approximately by

$$ISL = \frac{\sum_{k=0}^{K-1} \sigma_k}{\left(\sum_{k=0}^{K-1} \sqrt{\sigma_k} \right)^2} \quad . \tag{7.21}$$

Therefore, the signal to clutter ratio (as defined by the ratio of effective radar cross section of the target to integrated sidelobe level) is given by

$$\frac{S_M}{C} = \frac{\chi_{xr}^2(0,0)}{ISL} = \sum_{k=0}^{K-1} \sigma_k \quad . \tag{7.22}$$

Notice that the signal to clutter ratios of the matched FSK/PSK radar (7.22) and the matched filter radar (7.15) are identical.

7.4. Comparison of Results

In this section, the results obtained in the previous three sections are compared. The signaling schemes are compared in three categories: effective target radar cross section (radar cross section enhancement), additive noise contamination level, and signal to clutter ratio.

A gain can be defined that is the ratio of the matched FSK/PSK effective target radar cross section obtained from Equation (7.18) to the effective target radar cross section of the baseline radar from Equation (7.4). This ratio describes the target enhancement obtained by utilizing matched FSK/PSK signaling. It should be noted that this is a power gain and therefore translates into a signal to noise ratio improvement. The target enhancement of matched FSK/PSK is therefore given by

$$E_b = \left| \frac{K \sum_{k=0}^{K-1} \sigma_k}{\left(\sum_{k=0}^{K-1} \sqrt{\sigma_k} \right) \left(\max_{\varepsilon} \left| \sum_{k=0}^{K-1} \sqrt{\sigma_k}\, e^{j(2\pi k\varepsilon + \phi_k)} \right| \right)} \right|^2 . \qquad (7.23)$$

It can be seen that Equation (7.23) is always greater than or equal to

$$E_b \geq \left| \frac{K \sum_{k=0}^{K-1} \sigma_k}{\left(\sum_{k=0}^{K-1} \sqrt{\sigma_k} \right)^2} \right|^2 = E_b^{\min} . \qquad (7.24)$$

Notice that the enhancement is target dependent because the matched FSK/PSK radar system utilizes target-specific information while the baseline system does not.

A gain can also be defined that is the ratio of the matched FSK/PSK effective target radar cross section to the matched filter target radar cross section. This is given by the squared ratio of Equation (7.18) to Equation (7.9) and is equal to

$$E_m = \left| \frac{K \sqrt{\sum_{k=0}^{K-1} \sigma_k}}{\sum_{k=0}^{K-1} \sqrt{\sigma_k}} \right|^2 \quad . \tag{7.25}$$

There is considered to be a performance improvement due to matched FSK/PSK signaling over a matched filter radar if

$$\sqrt{\sum_{k=0}^{K-1} \sigma_k} > \frac{1}{K} \sum_{k=0}^{K-1} \sqrt{\sigma_k} \quad . \tag{7.26}$$

Using the triangle inequality, the left-hand side of Equation (7.26) represents the hypotenuse while the right-hand side represents the average side length. Therefore, Equation (7.26) is satisfied since the hypotenuse is always greater than the average side length. Therefore, the effective radar cross section is always greater for the Matched FSK/PSK radar than for the matched filtered radar.

Target enhancements for two example target radar cross section distributions can now be calculated: a uniform spectral distribution and an impulsive spectral distribution. For the uniform distribution, $\sigma_k = c$ and $\phi_k = 0$ for all k from 0 to K-1 where K is the number of frequencies in the signal. For this specific case, the matched FSK/PSK target enhancement to baseline radar target enhancement is given by

$$E_b = 1 \quad . \tag{7.27}$$

The enhancement of the two radar targets is identical since the target spectrum is identical to the baseline radar transmit signal spectrum. In other word, the baseline radar is matched to the uniform spectrum target. Likewise, the enhancement of matched FSK/PSK radar over matched filter radar is

$$E_m = K \quad . \tag{7.28}$$

The matched filter radar suffers a loss in target enhancement for the impulsive target even though the transmit signal is matched to the target. This is a result of the unity noise bandwidth of the filter. In other words, the filter tends to attenuate the target return, but as will be seen later, the noise is attenuated by the same amount. For the impulsive target distribution the target spectrum equals $\sigma_m = c$ for some integer m and is zero otherwise. For this impulsive spectral distribution, the matched FSK/PSK target enhancement over the baseline radar is equal to

$$E_b = K^2 \quad . \tag{7.29}$$

The target enhancement for this spectral distribution is quite large. The reason for this improvement is that the baseline signal only has one frequency component reflected whereas the matched FSK/PSK signal only transmits in the frequency band reflected by the target. The target enhancement of matched FSK/PSK over matched filtering is given by

$$E_m = K^2 \quad . \tag{7.30}$$

Therefore, the target enhancement is dependent upon the distribution of the target radar cross section in frequency. The target enhancement is greater for the impulsive spectral distribution (uniform in range) than for the uniform spectral (impulsive in range) radar cross section distribution. This is a result of the effective utilization of the transmitter power for the matched FSK/PSK radar.

From the noise analysis of the previous sections, the improvement in signal to noise ratio of the matched FSK/PSK radar SNR_M over the baseline radar SNR_b is simply given by Equation (7.23) since the noise contamination levels are the same for each of the two systems. From Equations (7.12), (7.20), and (7.25), the improvement in signal to noise ratio of the matched FSK/PSK radar system SNR_M over that of the matched filter radar SNR_m is given by

$$\frac{SNR_M}{SNR_m} = \frac{E_m}{K} = \left(\frac{K \sqrt{\sum_{k=0}^{K-1} \sigma_k}}{\sum_{k=0}^{K-1} \sqrt{\sigma_k}} \right)^2 \frac{1}{K} = E_b^{\min} \quad . \tag{7.31}$$

For the two example distributions from above, the signal to noise ratio improvements are

$$\frac{SNR_M}{SNR_b} = E_b = 1 \tag{7.32}$$

and

$$\frac{SNR_M}{SNR_m} = \frac{E_m}{K} = \frac{K}{K} = 1 \tag{7.33}$$

for the uniform spectral distribution, and

$$\frac{SNR_M}{SNR_b} = E_b = K^2 \tag{7.34}$$

and

$$\frac{SNR_M}{SNR_m} = \frac{E_m}{K} = \frac{K^2}{K} = K \tag{7.35}$$

for the impulsive spectral distribution. This is intuitively pleasing since the uniform spectral distribution matches the signal transmitted of the baseline implementation (in other words, the target-specific information is the same for all targets). Therefore, no performance improvement should be expected. The performance improvement associated with the impulsive spectral distribution is also logical since the radar would be transmitting only in the spectral region in which the target reflects.

The signal to clutter performance of the matched FSK/PSK system (7.22) is identical to that of the matched filter system (7.15). It should be remembered that the matched filtering implementation has an additional layer of signal processing over the matched FSK/PSK radar and hence is more complex in the receiver whereas matched FSK/PSK is more complex in the transmitter. The matched FSK/PSK radar system requires that the signal be transmitted and processed through the correlation processor. The matched filter implementation requires that the output of the correlator be matched filtered to enhance the target.

The ratio of the matched FSK/PSK signal to clutter ratio to the baseline signal to clutter ratio is equal to

$$\frac{S_M / C}{S_b / C} = \frac{K \sum_{k=0}^{K-1} \sigma_k}{\left(\max_{\varepsilon} \left| \sum_{k=0}^{K-1} \sqrt{\sigma_k}\ e^{j(2\pi k\varepsilon + \phi_k)} \right| \right)^2} > E_{b_{min}} \quad . \tag{7.36}$$

From Equations (7.27) and (7.29), it is known that Equation (7.36) varies between one for the uniform spectral distribution and K for the impulsive spectral distribution. Therefore, either matched FSK/PSK signaling or matched filtering provide a gain over the baseline radar in all environments due to the use of target-specific information.

7.5. Example Performance Gains for Predicted Target Signatures

The calculations in the previous examples are for some extreme theoretical distributions. It is of interest to calculate the performance improvements for some predicted signatures of actual aircraft models. Table 7.1 shows the performance improvements in dB for six different aircraft targets. The target spectra (σ_k's and ϕ_k's) are predicted for the models using Xpatch1 [2] which is an optical region electromagnetic signature prediction code. The signatures are taken over an azimuthal sweep from 5° to 15° off nose-on in 10 equally spaced steps and in elevation from -5° to 5° above the waterline in 10 equally spaced steps. There are a total of 100 signatures for each target. Each signature is predicted within a bandwidth from 2.0 to 2.3 GHz (1/2 meter range resolution), and there are 64 frequencies in each signature.

In Table 7.1, the first column represents the mean value of the improvement in signal to additive noise power of a matched FSK/PSK radar over a baseline radar in dB. This is calculated by the following equation

$$\overline{E_b} = 10 \log_{10} \left(E \{ E_b \} \right) \tag{7.37}$$

where $E\{\}$ is the ensemble average over all azimuth and elevation values, and E_b is calculated from Equation (7.23) for each azimuth and elevation value.

Column two represents similar values of improvement in signal to noise ratio for the matched FSK/PSK radar over the matched filter radar. The equation evaluated in column two is given by

$$\overline{E_m} = 10 \log_{10} \left(E \left\{ \frac{E_m}{K} \right\} \right) \tag{7.38}$$

where E_m^2/K is calculated using Equation (7.31).

Column three represents the improvement in the signal to clutter ratio by using matched FSK/PSK or matched filtering over the baseline radar system. Column three is calculated using the following equation:

$$\overline{S/C} = 10\log_{10} \left(E \left\{ \frac{S_M / C}{S_b / C} \right\} \right). \tag{7.41}$$

where the ratio in the argument of the logarithm is calculated using Equation (7.36).

Table 7.1. Realized Performance Improvements and Losses for Matched FSK/PSK and Matched Filtering.

Target #	E_b	E_m	S/C	L_{LPI}
1	6.2	0.9	5.3	-3.1
2	4.2	0.8	3.3	-2.7
3	3.0	0.5	2.4	-2.1
4	5.6	0.9	4.7	-3.2
5	3.6	0.8	2.8	-2.7
6	3.6	0.7	2.8	-2.5
Units	dB	dB	dB	dB

Column four of Table 7.1 shows the expected LPI performance losses due to the reduction in effective bandwidth that results for utilizing matched FSK/PSK signaling. This loss is calculated using Equation (5.19) and is given by

$$L_{LPI} = 10\ log10\left(E\left\{ L_{LPI} \right\} \right) \quad . \tag{5.40}$$

The data in Table 7.1 show that the performance improvement achieved by making use of target-specific information is significant. For the matched FSK/PSK signal to noise ratio data (column one), the mean improvement over the baseline radar is in a range of between 3 dB and 6 dB. In other words, the average signal to noise ratio is doubled or even quadrupled depending on the target. For clutter limited environments, the mean signal to clutter ratios (column three) are improved by a factor of between 2.4 dB and 5.3 dB. This improvement is not quite as large as those seen for the additive noise environments, but they are still significant improvements. The

data in column two show that the mean improvement realized by utilizing matched FSK/PSK instead of matched filtering is minimal. They range from a 0.5 dB improvement to 0.9 dB. Column four shows the LPI performance loss due to the reduction in effective bandwidth due to matched FSK/PSK. It appears that typical losses are in a range of 2 dB to 3 dB. Therefore, the overall LPI performance improvement achieved by utilizing matched FSK/PSK radar over the baseline radar is in a range of between 1 dB and 3 dB on the average.

Figures 7.2 and 7.2 give some insight into the enhancement and loss values encountered in Table 7.1. Figure 7.1 shows a typical range profile and spectrum for Target 1 while Figure 7.2 shows a typical range profile and spectrum for Target 3. From Table 7.1, Target 1 is seen to have the highest enhancement and signal to clutter improvement of all targets. Conversely, Target 3 has the worst enhancement and signal to clutter improvement. The reason for these results can be seen by comparing Figure 7.1 with Figure 7.2. The range profile of Target 1 is more distributed in range (spectrum is more concentrated in frequency) than the profile of Target 3. This means that greater target enhancement should occur for Target 1 since its spectrum is less uniform in frequency (more distributed in range). Additionally, it should be noted that the spectra of both targets are broadbanded and uniform. This is the reason the enhancements and signal to clutter ratio improvements are closer to unity than K. This spectral uniformity is a characteristic of optical region target scattering (impulsive in range, broadband in frequency) and therefore, large gains (> 10 dB) should not be expected for optical region targets.

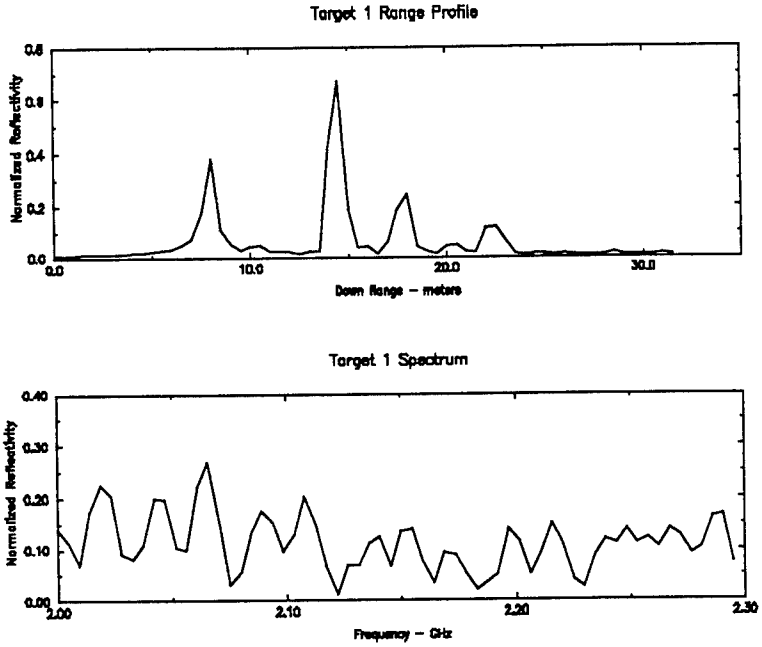

Figure 7.1. Target 1 Range Profile and Spectrum.

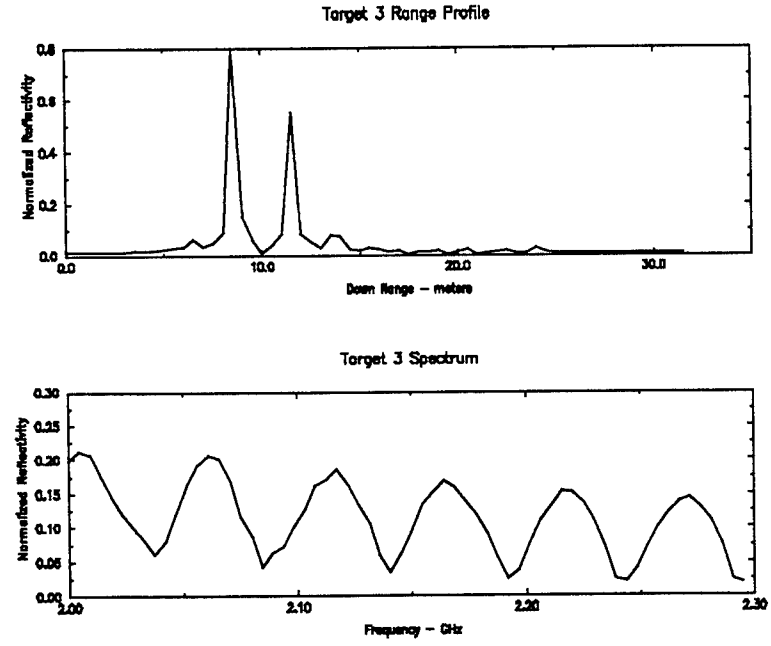

Figure 7.2. Target 3 Range Profile and Spectrum.

7.6. Conclusions

Matched FSK/PSK radar and the matched filter radar both yield performance that is superior to the baseline radar based on an analysis of the signal to noise ratio and the signal to clutter ratio. The performance increase is dependent upon the target spectral content since the matched FSK/PSK radar and the matched filter radar both make use of target-specific information. The theoretical matched FSK/PSK signal to noise ratio is between 1 and K^2 times that of the baseline radar. Additionally, the matched FSK/PSK signal to clutter ratio is theoretically between 1 and K times that of the baseline radar depending on the spectrum of the target. Therefore, a significant performance increase can potentially be obtained by utilizing target-specific information in the design of a radar signal.

Based on the calculations in Section 7.5, expected values of signal to noise ratio improvement for actual optical region targets are typically between 3 dB and 6 dB. Additionally, the use of target-specific information results in typical signal to clutter improvements of between 2 dB and 5 dB. Even though these improvements are significant, they are much less than the theoretically possible improvements. This is a result of the basically uniform spectral signature of optical region radar targets. The spectral signatures have a uniform broadband shape because of the impulse-like temporal characteristic of optical region radar targets.

In an additive white noise environment, matched FSK/PSK radar outperforms both the baseline system and the matched filter system. This performance increase results from an efficient use of transmitter power. The matched FSK/PSK radar

transmits power only in regions that scatter efficiently. In other words, a radar that transmits an impulse-like signal wastes power in spectral regions that do not reflect transmitter power. The overall performance gain is dependent upon the target reflection characteristics, and the gain is bounded between 1 and K where K is the number of frequencies.

The results of calculations based on predicted target signatures show that the realized matched FSK/PSK signal to noise ratio improvement relative to the matched filter radar is typically less than 1 dB. Therefore, it seems that matched FSK/PSK performance is not significantly better than matched filtering for a actual optical region target. Additionally, with the matched filter implementation, there is no LPI performance degradation due to a transmit bandwidth reduction.

In a ground clutter limited environment, matched FSK/PSK radar performance is identical to matched filtering radar. This results from the fact that the ISL of the matched FSK/PSK radar signal increases identically with the target enhancement of matched FSK/PSK over matched filtering. It should be noted, that matched FSK/PSK requires one less layer of receiver signal processing than matched filtering because the matched FSK/PSK signaling scheme has the additional layer of signal processing built into the waveform. This post processing could be a limiting factor if a large range search (large number of range bins) is required because of the computational overhead of performing the discrete convolutions. According to [3], an N_c point convolution (N_c is the number of output range bins) requires approximately

$$3N_c \log_2 N_c \tag{7.43}$$

complex floating point operations when an efficient FFT-based convolution routine is used. For example, a 1024 point output result requires approximately 31,000 complex floating point operations. This translates into 775 μsec of processing time for a 40 Mflop processor. It should be remembered that the 775 μsec is required for the convolution alone. This does not include any other computer tasking that might be required such as Doppler processing.

With regard to the overall LPI performance, the matched FSK/PSK radar trades 2 dB to 3 dB in LPI performance in order to obtain an additional 3 dB to 6 dB in signal to noise ratio performance. This is a positive overall LPI improvement of between 1 dB and 2 dB over the baseline radar. The reason that this loss occurs is that the matched FSK/PSK radar must reduce its equivalent transmitter bandwidth to transmit only in highly reflective regions. Therefore, the equivalent time-bandwidth product is reduced.

It should be reiterated that both the matched FSK/PSK radar and the matched filter radar perform better than the baseline radar in both white noise environments and ground clutter limited environments. This performance improvement is a result of target enhancement. This target enhancement requires knowledge about the target's scattering characteristics. Since this knowledge is typically not known a priori, a technique for determining the target spectral characteristics must be developed. This is the focus of the remainder of this study.

7.6. References

1. G. R. Cooper and C. D. McGillem, Probabilistic Methods of Signal and System Analysis, Second Edition, Holt, Rinehart, and Winston Publishing, 1986.

2. Xpatch1 User's Manual.

3. E. O. Brigham, The Fast Fourier Transform and Its Applications, Prentice-Hall Publishing, 1988.

CHAPTER VIII

GRADIENT DESCENT METHOD FOR DESIGNING OPTIMUM RADAR SIGNALS

In previous chapters, the pulse compression radar processing technique designated matched FSK/PSK was analyzed. This processing technique makes it possible to design signals with compressed main lobes of arbitrary pre-designed shapes. Since the response of a radar to a given target is given by the correlation of the compressed main lobe with the target range profile (for a high range resolution radar signal), it is possible to design a signal that will excite an optimum response from a target. A problem arises with this method because the design of a signal to excite the optimum response requires a priori knowledge of the target. Typically, the range profile will not be known a priori and therefore, it is desirable to have a method for iteratively designing the optimum signal based on previous radar returns in real time. This chapter focuses on a method that is derived based on the technique of gradient descent.

First, a brief outline of the required background information is given so that the problem can be properly formulated. Next, the optimum signal is derived for a randomly varying target range profile. An iterative solution to the analytic problem is then derived that is based on gradient descent [1]. Algorithm implementation within

the framework of a radar is discussed next. Finally, the results of computer simulations are used to illustrate the effectiveness of the algorithm on high range resolution radar targets in various environments: additive white noise, correlated and uncorrelated random range variation, and correlated and uncorrelated random angle variation. Conclusions about the usefulness of the algorithm as a target learning, or measurement technique are discussed.

8.1. Background

A block diagram of a high range resolution radar system utilizing a cross-correlation receiver is shown in Figure 3.1. The response of a high range resolution radar range profile *h(t)* to a radar utilizing a cross-correlation receiver is defined by

$$\chi_{xr}(\tau, f) = \int_{-\infty}^{\infty} \chi_{xy}(\tau + u, f)\, h(u)\, du \tag{8.1}$$

where the cross-ambiguity function $\chi_{xy}(\tau)$ is given by Equation (6.6).

An optimum radar, or matched radar is defined as a radar that utilizes a cross-ambiguity that maximizes

$$|\chi_{xr}(0, 0)|^2 = \int_{-\infty}^{\infty}\int_{-\infty}^{\infty} \chi_{xy}(u,0)\, \chi_{xy}^{*}(v,0)\, h(u)\, h^{*}(v)\, du\, dv \quad . \tag{8.2}$$

It is useful to cast the equation above into a vector representation. The vector representation of the cross-ambiguity function is

$$\chi = \left[\chi_{xy}(u_0)\ \chi_{xy}(u_1)\ \ldots\ldots\ \chi_{xy}(u_{N-1}) \right]^T \tag{8.3}$$

where the subscripts designate the various sample points and T designates the vector transposed. Likewise, for the target range profile is given by

$$\boldsymbol{h} = \left[h(u_0)\ h(u_1)\ \ldots\ldots\ h(u_{N-1}) \right]^T \quad . \tag{8.4}$$

Equation (8.2) becomes

$$\left|\chi(0,0)\right|^2 = \chi^H \boldsymbol{h}\,\boldsymbol{h}^H \chi \tag{8.5}$$

where the superscript H designates the complex conjugate transpose. Therefore, it is desired to maximize Equation (8.5) with respect to χ. For generality, it is assumed that the vector **h** is a random process described by a correlation matrix C defined by

$$\boldsymbol{C} = E\left\{\boldsymbol{h}\,\boldsymbol{h}^H\right\} \tag{8.6}$$

where E represents the ensemble average operator. Therefore, Equation (8.5) becomes

$$\left|\chi(0,0)\right|^2 = \chi^H \boldsymbol{C} \chi \tag{8.7}$$

where **C** is the target correlation matrix.

8.2. Analytic Approach to Optimization

Equation (8.7) must now be maximized. It is of interest to maximize the squared voltage value (as opposed to the signal-to-noise ratio) since the white noise contamination of a pulse compression waveform depends only on the processing interval and not the compressed main lobe shape. The typical approach to maximizing a functional is to take the derivative with respect to the control function, and then

solve for the value of the control function for which the derivative is zero. It is also required that the energy of the cross-ambiguity function be constrained to some constant value α. This is a constrained extremization problem, therefore a Lagrange multiplier must be used. Using the Lagrange multiplier, the following equation must be maximized

$$\tilde{\chi}_{xr}(\chi) = \chi^H C \chi + \lambda(\alpha - \chi^H \chi) \tag{8.8}$$

where λ is known as the Lagrange multiplier. The optimum solution to Equation (8.8) is obtained by solving

$$\frac{\partial \tilde{\chi}_{xr}(\chi)}{\partial \chi} = 2C\chi - 2\lambda\chi = 0 \quad . \tag{8.9}$$

Therefore, the optimum vector χ_{opt} is obtained from the following

$$C\chi_{opt} = \lambda\chi_{opt} \quad . \tag{8.10}$$

Equation (8.10) is simply a statement of the well-known eigenvalue problem where χ_{opt} is an eigenvector of C and λ is its associated eigenvalue. It can be shown that the optimum solution of Equation (8.10) occurs when χ_{opt} is the eigenvector of C associated with the principal eigenvalue λ of C. χ_{opt} is also known as the principal component of the correlation matrix C. The principal component can be thought of as pointing in the direction of the maximum variation of the random process **h** [2].

Equation (8.10) suggests how to design a signal based on a target correlation matrix. This correlation matrix is typically not known a priori. Therefore, an iterative solution must be obtained that will iteratively approximate the optimum solution.

8.3. Gradient Descent Iterative Solution

An iterative method for maximizing Equation (8.8) is described in this section. First an initial guess of χ_0 is assumed. Also, it is assumed that all subsequent estimates of the optimum solution will be better than the previous estimate. In equation form, the previous assumption yields

$$\tilde{\chi}_{xr}(\chi_0) \leq \tilde{\chi}_{xr}\,(\,\chi_0 + \Delta\chi\,) \quad . \tag{8.11}$$

Expanding $\tilde{\chi}_{xr}$ about χ_0 as a Taylor series and retaining only the linear term yields the following linearized equation

$$\tilde{\chi}_{xr}\,(\,\chi_0 + \Delta\chi\,) \approx \tilde{\chi}_{xr}\,(\,\chi_0\,) + \Delta\chi\,\frac{\partial\,\tilde{\chi}_{xr}}{\partial\,\chi} \quad . \tag{8.12}$$

Substituting Equation (8.12) into Equation (8.11) gives the following inequality

$$\tilde{\chi}_{xr}\,(\,\chi_0\,) \leq \tilde{\chi}_{xr}\,(\,\chi_0\,) + \Delta\chi\,\frac{\partial\,\tilde{\chi}_{xr}}{\partial\,\chi} \quad . \tag{8.13}$$

Equation (8.13) is always satisfied if the increment $\Delta\chi$ is given by

$$\Delta\chi = \mu\,\frac{\partial\,\tilde{\chi}_{xr}}{\partial\,\chi} \tag{8.14}$$

where μ is the learning rate. Therefore,

$$\chi_{k+1} = \chi_k + \mu\,\frac{\partial\,\tilde{R}}{\partial\,\chi} \tag{8.15}$$

where the subscript designates the iteration index. Using the partial derivative of the functional from the previous section, Equation (8.15) becomes

$$\chi_{k+1} = \chi_k + 2\mu C\chi_k \quad . \tag{8.16}$$

Another crucial component of the iterative solution involves normalizing χ_{k+1} after each step with the following energy normalizing equation

$$\chi_{k+1} = \frac{\chi_{k+1}}{\sqrt{\chi^H_{k+1}\chi_{k+1}}} \quad . \tag{8.17}$$

This normalization process is required since the optimization problem is a constrained optimization.

It is important to note that the algorithm defined by Equations (8.16) and (8.17) is known as plain Hebbian Learning [2] in the field of Neural Sciences. The learning technique can be thought of as a reinforced learning technique in that it tends to converge to the vector that points in the direction of maximum variation (variance). It will also point in the direction of the vector input that is introduced to the algorithm most often. The learning machine paradigm of the iterative design algorithm yields significant intuitive insight into the operation of the algorithm.

8.4. Implementation Issues

Equation (8.16) provides a method for designing the optimum radar cross-ambiguity function. The technique requires the target correlation matrix C to be measured. Therefore, a technique for measuring C must be determined. From Equation (8.6),

$$\boldsymbol{C} = E\{\boldsymbol{h}\,\boldsymbol{h}^{H}\} \tag{8.18}$$

and

$$\boldsymbol{C}\,\chi = E\{\boldsymbol{h}\,\boldsymbol{h}^{H}\}\,\chi \quad . \tag{8.19}$$

Now, define

$$\begin{aligned} \tilde{\boldsymbol{C}}\,\chi &= \boldsymbol{h}\,(\,\boldsymbol{h}^{H}\,\chi\,) \\ &= \boldsymbol{h}\,c^{*} \end{aligned} \tag{8.20}$$

where c is a scalar that is a measure of the cross-correlation between **h** and χ. The radar can measure c by transmitting the complex conjugate of χ and conjugating the received voltage for zero delay. **h** can be measured if the radar transmits a signal with an impulse-like cross-ambiguity function. Therefore, a plausible implementation of the gradient descent algorithm derived in the previous section would be the following:

1) Transmit the complex conjugate of χ_k and receive c,
2) Transmit an impulse like waveform and receive **h**, and
3) Form the next estimate of the optimum waveform from

$$\chi_{k+1} = \chi_k + 2\,\mu\,c^{*}\,\boldsymbol{h} \quad . \tag{8.21}$$

The algorithm above requires that the optimum waveform be transmitted only half of the time. The other half of the time, an impulse-like sub-optimum signal must be transmitted. This is required only during the waveform design procedure. In other words, the radar would operate in a design mode until the signal is designed (i.e., K

iterations). After the K^{th} iteration, the radar would operate using only the designed optimum waveform. This aspect is illustrated in the following computer simulations.

8.5. Computer Simulation of the Gradient Descent Method

In this section, the gradient descent signal design technique derived in the previous sections is illustrated using computer simulations. These simulations will model the effects of additive white noise, correlated and uncorrelated random range motion, and correlated and uncorrelated random angular motion. A listing of the Matlab© [3] script used in the study can be found in Appendix A.

The target range profile used in the simulations is that of an aircraft-like target generated by Xpatch1 [4]. The range profiles consist of 64 data points and they are valid within the bandwidth of 2.0 to 2.3 GHz. Therefore, they have a .5 meter resolution. The angular variation is between 5° and 15° in azimuth at 10° below the waterline in elevation. These angular locations were chosen since they are typical of a closing target. Additionally, it was found that the incident angle, at least on a broad scale, had little to do with the performance of the algorithm.

The performance metric is the squared error between the estimated range profile (optimum signal) and the actual range profile

$$\begin{aligned} e_k^2 &= (\chi_k - \boldsymbol{h})^H (\chi_k - \boldsymbol{h}) \\ &= 2 \left(1 - \left| \chi_k^H \boldsymbol{h} \right| \right) \end{aligned} \tag{8.22}$$

where

$$\chi_k^H \boldsymbol{h} \tag{8.23}$$

is the cross-correlation between the estimated profile and the actual range profile. It has been assumed that

$$\chi_k^H \chi_k = \boldsymbol{h}^H \boldsymbol{h} = 1 \quad . \tag{8.24}$$

The actual squared error value in Equation (8.22) would replace the magnitude operator with an operator that would include the real part only. The magnitude operator is used for this case since the phase error is not of interest, only the shape. Also notice that the iterative algorithm maximizes the component of Equation (8.23) and therefore Equation (8.22) is minimized. Therefore, the gradient descent algorithm minimizes the squared error between the optimum signal and the actual target range profile. This means that the gradient descent technique is optimal for target measurement as well as target excitation.

8.5.A. Additive White Noise Effects

Figure 8.1 shows the effect of the learning rate on the removal of additive white Gaussian noise. This plot shows the mean square error versus the number of iterations for three values of learning rate: μ=0.2, 0.1, and 0.05. The average of 100 independent trials is shown for each value of the learning parameter μ. The signal to noise ratio of each measurement is unity where the signal to noise ratio is defined by

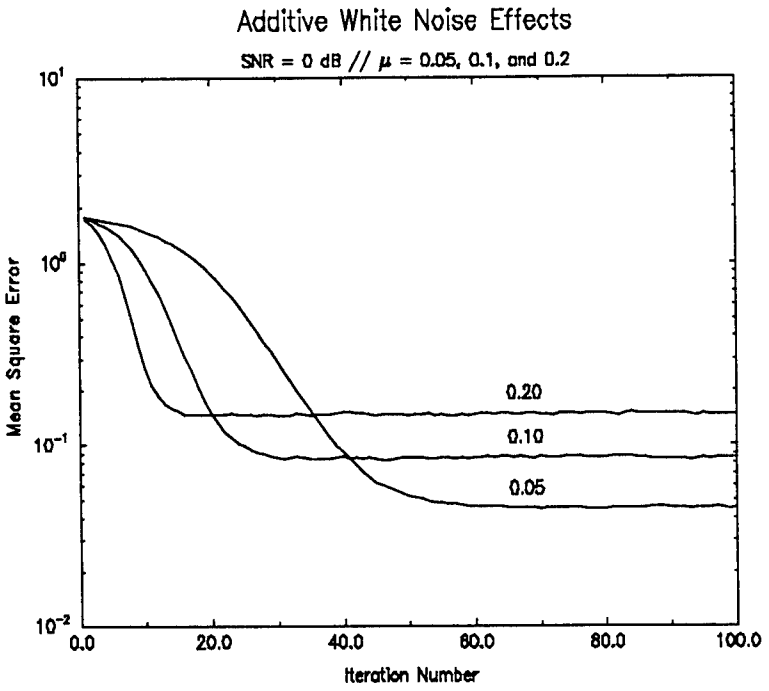

Figure 8.1. Mean Squared Error Versus the Number of Iterations for Three Different Learning Rates.

$$SNR = \frac{1}{\boldsymbol{n}^H \boldsymbol{n}} \tag{8.25}$$

where $\boldsymbol{n}$ is the vector of 64 independent Gaussian random variables. From the plot it can be seen that the gradient descent technique converges to its minimum value after $1/\mu$ iterations, and the mean square error converges to approximately a value of μ. Figure 8.2 shows the effect of additive noise for a fixed learning rate. The plot shows the mean square error for three different signal to noise ratios: SNR = 6 dB, 0 dB, and -6 dB. The learning rate is a constant value of $\mu = 0.1$. An average of 100 independent trials is shown for each curve. It can be seen from the Figure that the mean square error of the estimate improves at 10 dB/decade with signal to noise ratio.

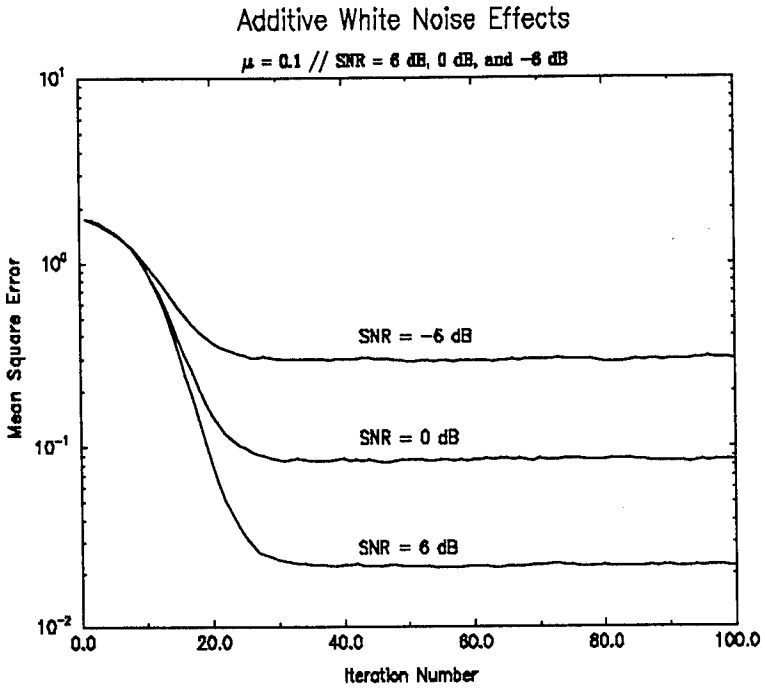

Figure 8.2. Mean Squared Error Versus the Number of Iterations for Three Additive White Noise Variances.

Additionally, the learning time (convergence time) is not appreciably affected by the noise contamination level.

8.5.B. Random Range Motion Effects

The effects of correlated random range motion on the squared error are shown in Figure 8.3. Correlated range errors are of interest because they model the errors that might occur with a range tracking control loop. The range errors will be correlated because the radar has a finite servo bandwidth. The simulated range errors are modeled by a Gaussian noise vector that has been low pass filtered with a second order Butterworth filter [5]. In the test, the learning rate is fixed at a value of $\mu = 0.1$. For this series of tests, the variance of the range errors is fixed at 0.1 squared range

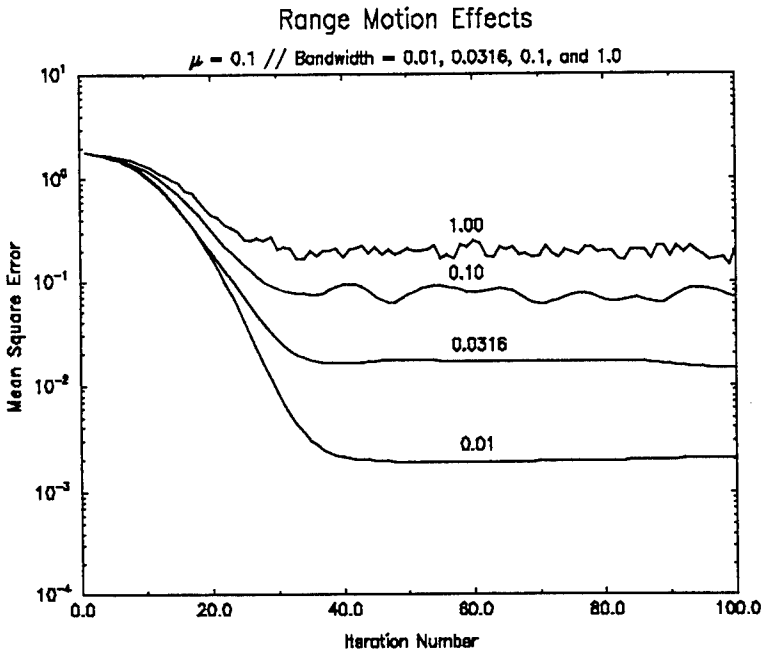

Figure 8.3. Mean Squared Error Versus the Number of Iterations for Various Range Tracker Servo Bandwidths and Fixed Range Tracker Error Variance.

resolution cells. The plot shows the mean square error for three values of bandwidth: B = 0.01, 0.0316, 0.1 (5 dB increments), and 1.0 (uncorrelated). It should be noted that the decorrelation times for each of the bandwidths are 100, 32, 10, and 1 iterations, respectively. Additionally, since the gradient descent technique converges within approximately 10 iterations, the technique converges before the range errors decorrelate for the two lower bandwidth simulations (B = 0.01 and B = 0.0316). From the curves in Figure 8.3, the mean square error appears to increase as 20 dB/decade with servo bandwidth for the two lower bandwidth cases. This means that the accuracy of the range profile estimates is dependent upon the bandwidth of the random motion. Additionally, the 20 dB/decade change suggests that the error is strongly

related to iteration-to-iteration variation of the motion (the time derivative of the range motion error).

Figure 8.4 shows the effect of varying the variance of the range tracker error while holding the servo bandwidth of the tracker constant. For this test, the normalized bandwidth is held at a constant value of B = 0.0316. The variance of the range tracking error is set to values of 0.0316, 0.1, and 0.316 (5 dB increments). From the plot, it can be seen that the mean square error of the range profile estimate increases as 10 dB/decade with increasing range tracker error variance. Since the range profile estimation error increases 20 dB/decade with servo bandwidth and 10 dB/decade with range tracker error variance, it is reasonable to assume that the mean square error of the range profile estimate is dependent upon the derivative of the range tracker error signal and not the range tracking error itself.

The effect of the learning rate on the mean square range profile error in a range motion environment is shown in Figure 8.5. As is shown in Figure 8.5, as long as the learning parameter is greater than the bandwidth, the mean square error decreases with increasing learning rate. In other words, the learning rate should be set so that the gradient descent technique converges faster than the range tracker errors decorrelate. Additionally, it appears that the mean square range profile error decreases as 20 dB/decade with increasing learning rate.

8.5.C. Random Angle Motion Effects

In this section, the effect of angular scintillation on the gradient descent method is investigated. From Chapter II, angular motion has two effects on the range

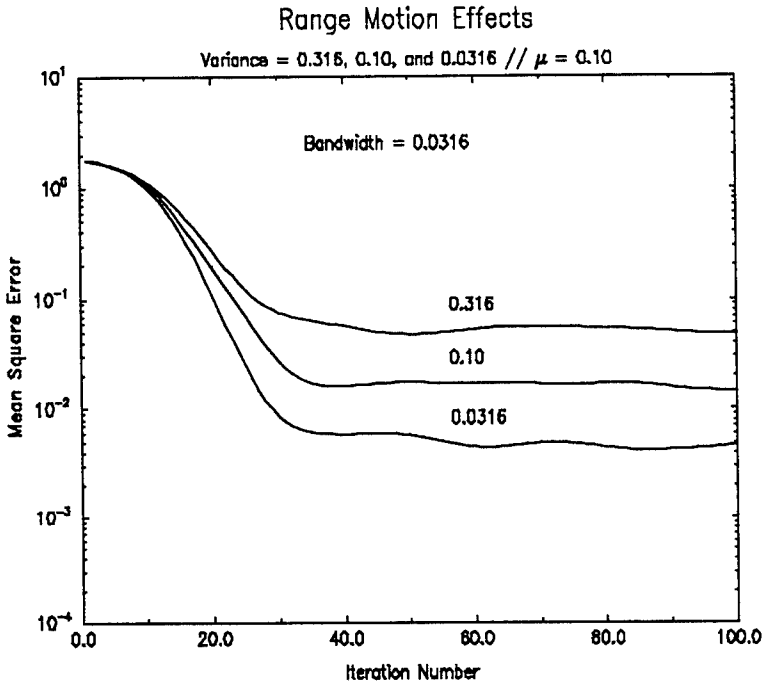

Figure 8.4. Mean Squared Error Versus the Number of Iterations for Three Values of Range Tracker Error Variance with a Fixed Servo Bandwidth.

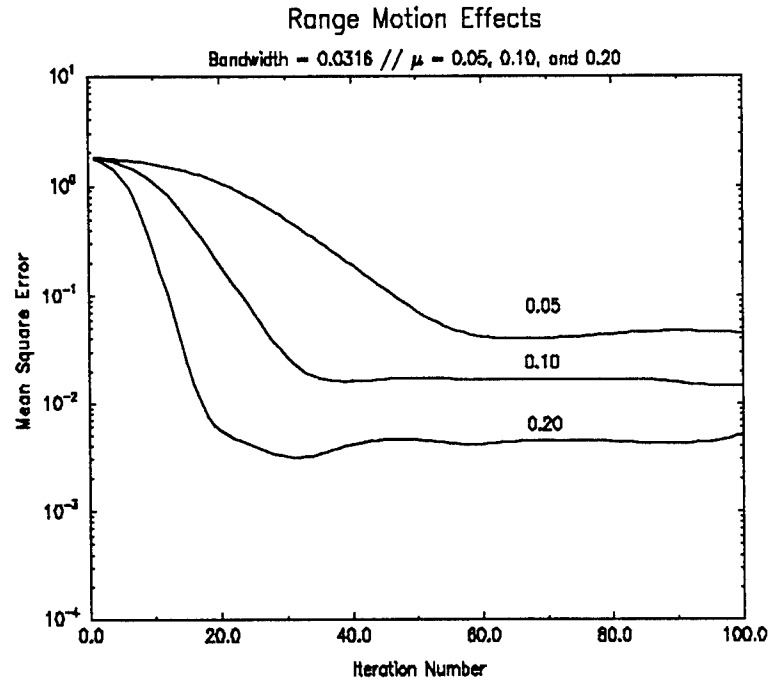

Figure 8.5. Mean Squared Error Versus the Number of Iterations for Three Values of Learning Rate and Fixed Range Tracker Error Variance.

profile: a phase modulation effect and an envelope effect. From Equation (2.21), the phase modulation varies significantly for a 15 meter length target at approximately 2 GHz if the angle varies by more than 0.14°. Additionally, from Equation (2.22) with ΔR = 0.5 meters, the range envelope varies significantly if the angle varies by any more than 1.92°. As in the previous section, angle motion is modeled by a second order Butterworth low pass filtered Gaussian random process. The variance of the process is held constant to 0.1 squared degrees (standard deviation of 0.316°). The curves of Figure 8.6 represent averages of 100 independent simulations with the bandwidth B = 0.01, 0.0316, 0.1 (5 dB steps), and 1.0 (uncorrelated). The range profiles are generated by Xpatch1 at 5° below waterline in elevation and from 5° to 15° in azimuth sampled every 0.1° to satisfy Equation (2.23). The range profiles for azimuth angles between the calculated points are determined by linear interpolation of the calculated points.

Figure 8.6 shows that the mean square error of the range profile estimation increases approximately as 20 dB/decade with the bandwidth of the angle motion when the range errors do not decorrelate within a learning period of approximately 10 iterations. This is similar to the phenomenon seen in Figure 8.4 for the range tracking errors. Therefore, as with the range tracking errors, it appears that the rate of change in the target incident angle is the most important factor in range profile estimation.

Figure 8.7 shows that the mean square error of the range profile estimation increases as 10 dB/decade with the variance of the angle motion (assuming fixed bandwidth). This trend, along with those of Figure 8.6, suggests that the rate of

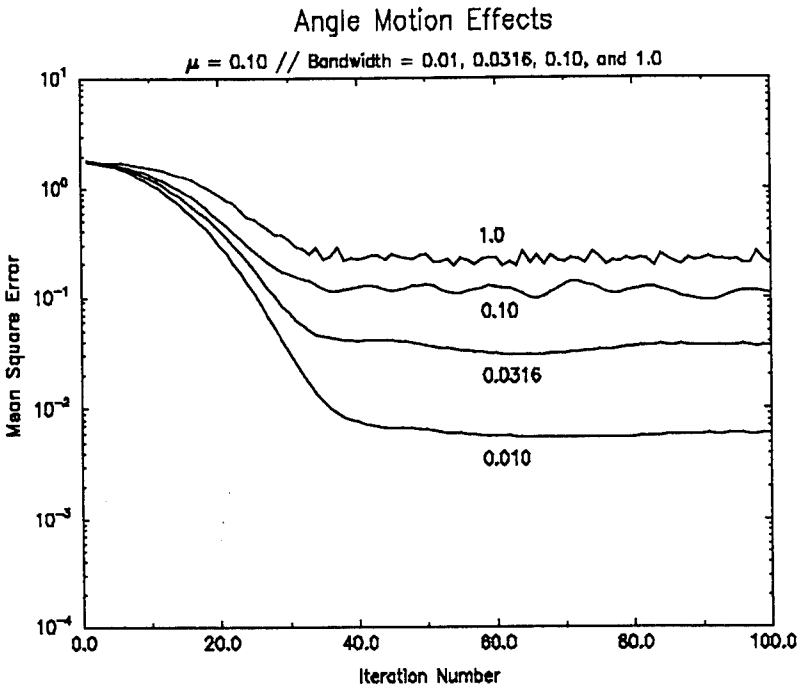

Figure 8.6. Mean Squared Error Versus the Number of Iterations for Various Angle Motion Bandwidths and Fixed Motion Variance.

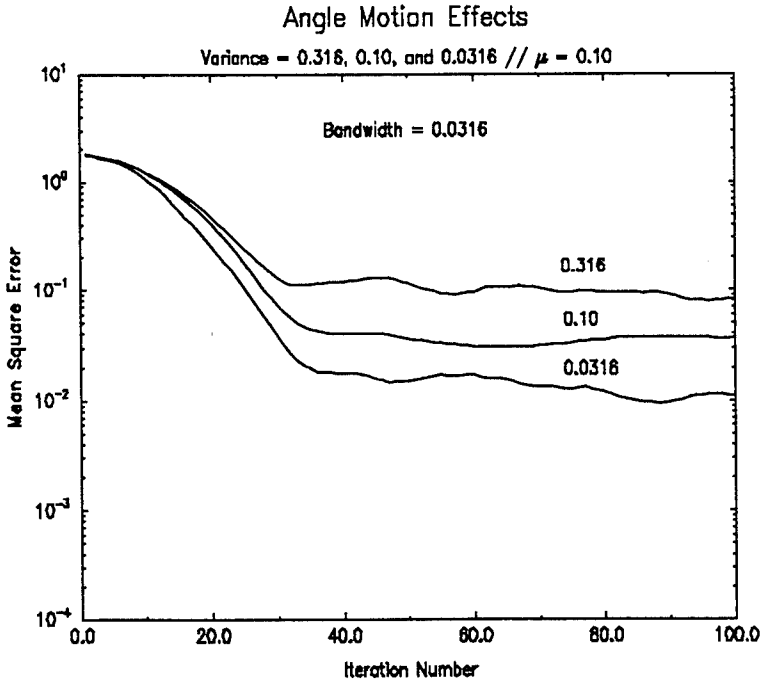

Figure 8.7. Mean Squared Error Versus the Number of Iterations for Three Values of Angle Motion Variance and Fixed Motion Bandwidth.

change of the target incident angle is more important that the variance of the process. Again, this is identical to the error sources associated with range tracking errors.

Figure 8.8 shows the effect of changing the learning rate while maintaining a fixed motion bandwidth of B=0.0316 and an angular motion variance of 0.1 squared degrees. As above with the range errors, the higher the learning rate, the lower the mean square range profile error. This also suggests that the source of error is in the rate of change of the range profile due to angular motion.

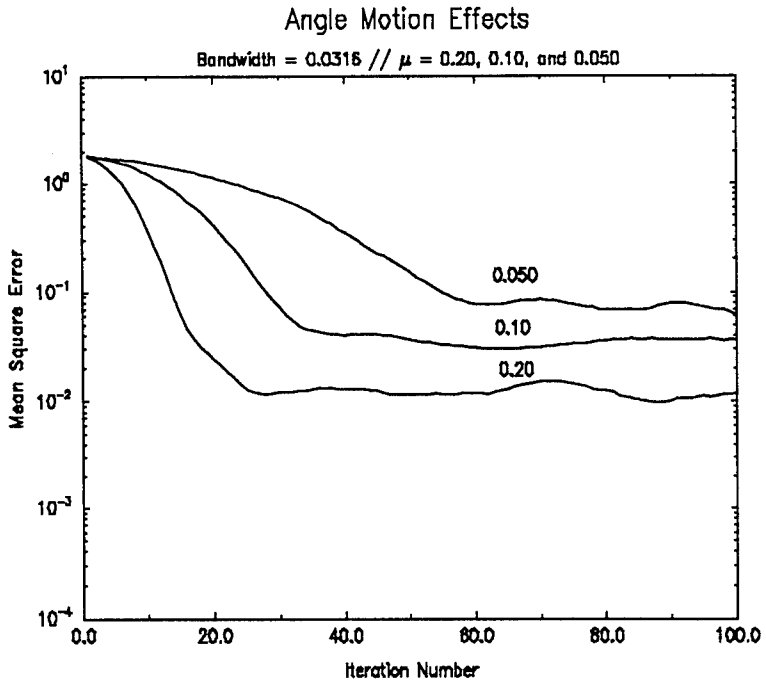

Figure 8.8. Mean Square Error Versus the Number of Iterations for Three Values of Learning Rate and Fixed Motion Variance.

8.6. Conclusions

In this chapter, an iterative signal design technique was derived and simulated. The derivation was based on the well known method of gradient descent. The

computer simulations were used to develop an understanding of the performance of the algorithm in order to determine a possible design philosophy for the technique.

From the simulations it was seen that there are basically two types of errors that are associated with the iterative technique: additive noise errors and target profile fluctuation errors. The additive noise errors are representative of additive white noise, jamming, and ground clutter contamination. The target profile fluctuation errors result from the fact that the target range profile is itself a random process. The target is a random process since the range to the target and the aspect angle of the target are constantly changing by unknown amounts.

The iterative algorithm handles the two types of errors in different ways. Additive errors are minimized by reducing the learning rate. In other words, the lower learning rate causes the additive noise components to be averaged out. Target range profile fluctuation errors are reduced by increasing the learning rate. This allows the iterative algorithm to effectively track the range profile. If the learning rate is set too low, the estimated target range profile converges to an average range profile because of the random fluctuations. Therefore, a simple algorithm design rule would be to set the learning parameter in such a way as to minimize the errors due to the additive noise components without increasing the errors due to target range profile fluctuation. This, of course, will depend on the level of additive noise contamination and the fluctuation rate of the target. If the target is slowly fluctuating, then the target can be extracted from a harsh additive noise environment. If, on the other hand, the target is

fluctuating rapidly, only a minimal amount of additive noise removal can be accomplished.

It should also be pointed out that the performance metric (the mean square error), is calculated based on the present value of the range profile, while the estimated range profile represents the average range profile. Therefore, the performance metric is biased toward non-fluctuating targets. The actual representation of the target range profile may be better than the performance metric implies.

In this chapter, only one target was used for the simulations (Target 1 from Chapter VII). From other simulations, not shown in this study, the algorithm appears to perform similarly on various targets.

8.7. References

[1] S. J. Orfanidis, *Optimum Signal Processing: An Introduction*, pp. 408-410, McGraw-Hill Publishing Co., 1988.

[2] J. Hertz, A. Krogh, and R. G. Palmer, *Introduction to the Theory of Neural Computing*, pp. 197-215, Addison-Wesley Publishing Co., 1991.

[3] Matlab® Reference Guide, The MathWorks, Inc., 1992.

[4] Xpatch User's Manual

[5] Signal Processing Toolbox User's Guide, For Use with Matlab®, The MathWorks, Inc, 1992.

CHAPTER IX

SUMMARY AND CONCLUSIONS

The purpose of this study was to develop a signal processing scheme that would combine the separate research efforts of low probability of intercept signaling, low altitude low observable target tracking, and noncooperative target recognition into a single research effort. The end result of this fusion is a new radar design concept designated adaptive FSK/PSK signaling. An adaptive FSK/PSK radar system makes use of matched FSK/PSK signals in conjunction with a gradient descent adaptive signal design algorithm. matched FSK/PSK signals are ultra wideband pseudorandom multiple frequency bi-phase modulated signal sequences that have spectral content specifically matched to the target under track. This use of target-specific information in the design of radar signals is the salient point of this research effort. It allows for more efficient use of signal power and results in a performance improvement over existing radar technologies that are matched to the transmit signal only. Since the spectral content of the target is not known a priori, the target range profile must be learned by the radar. This matching of the signal to the target is accomplished through the use of an iterative (adaptive) algorithm that is based on gradient descent. Once the radar has adapted to the target (learned the target), the range profile of the target is known and target identification can take place based on the learned range

profile. Therefore, an adaptive FSK/PSK radar system can be thought of as a learning system as opposed to a measurement system. In other words, the radar measurement is improved as a result of the learning process.

9.1. Conclusions

The pseudorandom sequence structure of the matched FSK/PSK signal, along with its high time-bandwidth product, makes the radar inherently difficult to detect. Therefore, the signals can be classified as low probability of intercept. Additionally, since the transmitter power is used in a most effective manner (signal efficiency is maximized by target matching), lower peak power signals can be utilized by the radar. This results in an additional improvement in LPI performance.

In an additive noise environment, matched FSK/PSK signaling provides a signal processing gain over a baseline radar that utilizes a signal with an impulse-like ambiguity function. This performance improvement results from the fact that the signal power is utilized in an efficient manner and the target reflection is enhanced without enhancing the additive noise. The level of signal processing gain is dependent upon the spectral complexity of the target. If the target reflects all frequencies equally well, little processing gain is seen. On the other hand, if the target reflectivity is concentrated in a few isolated frequency bands, then the processing gain can be large (on the order of the square of the number of frequencies used in the signal).

In a ground clutter limited environment, matched FSK/PSK signaling performs better than conventional radar technologies that do not take into account any target specific information. This occurs because the matched FSK/PSK radar system is

capable of achieving a theoretical target enhancement of between 1 and K^2 while the integrated sidelobe level is increased by a factor of between 1 and K where K is the number of frequencies used in the construction of the signal. Therefore, in a clutter limited environment, adaptive FSK/PSK radar systems can achieve performance improvement factors of between 1 and K. It should be noted that a matched FSK/PSK radar system and a conventional radar system using a matched filter post-processor are able to achieve identical performance in a clutter limited environment.

Analysis of predicted real target signature data shows that the use of target-specific information in the design of the radar signal typically yields average signal to noise ratio improvements of between 3 dB and 6 dB depending on the target. In a clutter limited environment, typical improvements are between 2 dB and 5 dB. These improvements are closer to the low end of the theoretically possible performance improvements. This is result of the uniform nature of optical region target spectra. The gains, however, are significant and provide a significant performance increase. It should be pointed out that in the resonance region, greater gains are expected since resonance region spectra are typically impulse-like.

The adaptation algorithm derived in Chapter VIII provides a method of not only designing the optimum signal to excite the maximum response from the target, but also for measuring the best mean squared estimate of the target range profile. Through computer simulations, it can be seen that the adaptation algorithm removes additive noise. The level of noise removal is dependent on the value of the learning parameter. The smaller the learning parameter (slower the learning rate), the better the

mean squared estimate. The simulations also show that the random fluctuations of the target range profile due to random range motion and random incidence angle motion increase the mean squared error of the estimate. If the learning rate is high enough for the adaptive algorithm to learn the target range profile before the profile decorrelates, then the errors are small. If on the other hand, the target decorrelates more rapidly than the algorithm can learn, range profile estimation errors are increased. This results in decreased target enhancement due to matched FSK/PSK signaling. It should be pointed out that the performance metric used in this study (the mean squared range profile error) is biased towards stationary (nonfluctuating) targets. It is difficult to ascertain the deleterious effects of range profile fluctuations on an actual target identification algorithm. The effects may be insignificant since the adaptation algorithm determines a best mean squared fit to the second order statistics of the random target fluctuation process within the learning period of the algorithm. It is of interest to note that a linear averaging scheme would yield a zero result for range profile estimation since the phase angle of the returns is random from measurement to measurement.

In conclusion, adaptive FSK/PSK signaling radar is an excellent platform for fulfilling the future mission of radar: low probability of intercept noncooperative target recognition. It utilizes low probability of intercept signals in a spectrally adaptive manner. The ability of the radar to adapt its spectrum makes it possible to enhance targets thus improving system performance in additive noise environments and ground clutter limited environments. Finally, the adaptation scheme derived in this study is

capable of extracting the range profile of the target under track. This is important for target identification since it is the range profile that is the feature vector used by most target identification algorithms.

9.2. Future Work

The purpose of this study was to fuse three existing research efforts into a single new integrated effort. Therefore, significant work remains to be done in this new research area. Three questions are of particular interest. First, there are several techniques for optimizing functions other than gradient descent [1]. It would therefore be of interest to investigate other optimization techniques within the framework of adaptive FSK/PSK radar. Second, algorithms exist for optimizing the spanning phase sequence of a signal in order to minimize a known clutter distribution [2]. It is of interest to determine if theses clutter minimization techniques could be applied to adaptive FSK/PSK. Third, it is of interest to determine the allowable target variation in range and velocity versus processing time requirements to determine the allowable performance envelope for the iterative radar.

It is also of interest to point out some other areas of applicability of matched FSK/PSK signaling that were not addressed specifically in this study. This work can be applied to any area of active sensor signaling such as underwater sonar for close-range mine detection, ultrasound diagnostics in the field of medicine, fault detection in the inspection of composite materials in heavy industry, and also in the area of laser radar. Additionally, matched FSK/PSK signaling could be utilized in the field of spread spectrum communications through harsh fading channels. This application

would require that the transmitter transmit only in spectral regions that are not severely attenuated thus improving the signaling efficiency.

9.3. References

1. D. A. Pierre, Optimization Theory with Applications, John Wiley & Sons, Inc., 1969.

2. T. E. Richardson, Utilization of Optimum Discrete Phase Modulated Waveforms in Ground-Based Radars, Ph.D. Dissertation, University of in Alabama Huntsville, 1985.

APPENDIX A

VARIOUS MATLAB SCRIPTS AND FORTRAN PROGRAM LISTINGS

```
%  CAR_hebb.m
%
%  B. J. Skinner
%  5 November 1994
%  Mississippi State University
%
%  This program simulates the gradient descent signal
%  design technique derived in Chapter VII.  The range
%  profiles used in the simulation are generated by
%  xpatch1, and the matlab script read_data_11.m must
%  be run to read in the xpatch1 frequency domain data.
%  The matlab script trans_data.m must then be run to
%  transform the data into the time domain.  The data
%  files are aspect dependent in azimuth.  Interpolation
%  is used to determine the range profile for angle data
%  that is not predicted by xpatch.  The azimuth angle
%  variation is modeled as a 2nd order Butterworth
%  low pass random process.  The range to the target
%  is also modeled using a 2nd order Butterworth low
%  pass random process to simulate a range tracking
%  system with random errors.


%  This portion of the script reads in all needed data from
%  the user.
Mbig=2*K;

k=menu('SELECT LEARNING RATE','mu=1','mu=.5',.........
     'mu=.1','mu=.05','mu=.01');
if k==1
      mu=1;
  elseif k==2
      mu=.5;
  elseif k==3
      mu=.1;
  elseif k==4
      mu=.05;
  elseif k==5
      mu=.01;
end

k=menu('SELECT SNR','-6 dB','-3 dB','0 dB',......
      '3 dB','6 dB','9 dB','infinite');
var=sqrt(2.^(-k+3)/K);
if k==7
   var=0;
end

h1=zeros(K,1);

k=menu('SELECT THE NUMBER OF ITERATIONS','50',......
```

```
    '100','200','400','800');

Nit=50*2^(k-1);

k=menu('SELECT TRAINING EPOCHS','1','10',.......
   '100','1000');
Nave=10.^(k-1);

clear m_rec1
clear m_rec2
clear m_rec3

for epoch=1:Nave

%For each averaging realization, a new angle track is
%created.
   angle_bw_s=0.0316;
   angle_sigma_s=1.779;
   [b_az, a_az]=butter(2,angle_bw_s);
   az_pntr1=filtfilt(b_az,a_az,angle_sigma_s*......
      randn(1,8*Nit))+beam_sector;
   l1=5*Nit;

%For each averaging realization, a new range track is
%created.
   rng_bw=.0316;
   rng_sigma=0.0;
   [b_rng, a_rng]=butter(2,rng_bw);
   rng_pntr1=filtfilt(b_rng,a_rng,rng_sigma*randn(1,8*Nit));
   l2=5*Nit;


%Re-initialize all used vectors.
   chi=[zeros(1,K/2-1) 1 zeros(1,K/2)]';
   az=az(1,:);
   score=zeros(1,Nit);
   shift=zeros(1,Nit);
   avging=zeros(size(chi));
   avg_prof=zeros(size(chi));

%Clear required memory.
   clear h2
   clear rec1
   clear rec2
   clear corr_score_chi
   clear corr_score_avg
   clear rec_pwr
   clear min_score

%Interpolation of the angle data.
%This should be used only when the angle does
```

```
%not vary with the simulation.  Otherwise, comment
%it out as shown below.  It should only be done
%to speed up the program.
%  for m=1:K
%  h2(m)=interp1(az,real(ll(m,:)),az_pntr1(ll+1)....
%          ,'linear')+j*interp1(az,imag(ll(m,:))....
%          ,az_pntr1(ll+1),'linear');
%  end
%  h_prof=h2';


for i=1:Nit

  ll=ll+1;
  l2=l2+1;


%Calculate angle interpolation.  Should be
%commented out when angle does not vary within
%the simulation.  Most time consuming part of
%the code.
  clear h2
  for m=1:K
    h2(m)=interp1(az,real(ll(m,:))....
          ,az_pntr1(ll+1),'linear')....
          +j*interp1(az,imag(ll(m,:))....
          ,az_pntr1(ll+1),'linear');
    end
    h_prof=h2';

%Calculate frequency domain modulation for range shifting.
%This is done by first calculating the range dependent
%linear phase shift in the frequency domain.  This
%Modulation is then multiplied by the FFT of the target
%range profile, and the product is inverse-FFT back into
%the range domain. This makes it possible to shift the
%range profile a fraction of a resolution cell.
   phase2=exp(j*2*pi*(fo/B+(0:(K-1))/K)*rng_pntr1(l2+1));
   h2=ifft(fft(h_prof).*phase2');


%Renormalize the range profile.
  h2=h2/sqrt(h2'*h2);

%Add in white Gaussian noise.
  noise2=(var)/sqrt(2)*.....
         (randn(size(h2))+j*randn(size(h2)));

%Gradient descent design method.
   chi=chi+2*mu*(h2+noise2)*(h2+noise2)'*chi;
   chi=chi/sqrt(chi'*chi);
```

```
   clc

%Calculate performance Metrics.
   corr_score_chi(i)=max(abs(ifft(fft(abs(chi)).*....
      conj(fft(abs(ref_prof))))));

  [corr_score_chi(i) corr_score_avg(i)]
  perf=[i 2*(1-corr_score_chi(i))]

end


%Plot range track erros.
  figure(1)
  subplot(2,1,1)
  plot(1:Nit,rng_pntr1(5*Nit+1:12))
  axis([1 Nit -1 1])
  grid on
  subplot(2,1,2)
  plot(1:Nit,az_pntr1(5*Nit+1:12))
  axis([1 Nit beam_sector-1 beam_sector+1])
  grid on


%Plot the learning curve
  figure(2)
  subplot(2,1,1)
  plot(1:64,abs(chi))
  axis([1 64 0 1])
  subplot(2,1,2)
  loglog(1:Nit,2*(1-corr_score_chi),1:Nit,rec_pwr.^2)
  axis([1 Nit .0001 1])

if epoch==1
  m_rec2=2*(1-corr_score_chi);
  m_rec3=rec_pwr.^2;
else
  m_rec2=[m_rec2; 2*(1-corr_score_chi)];
  m_rec3=[m_rec3; rec_pwr.^2];
  figure(3)
  loglog(1:Nit,mean(m_rec2),1:Nit,mean(m_rec3))
  axis([1 Nit .0001 1])
end

end
```

```
%read_data_lin.m
%  This program is used to read in an Xpatch1 data
%  and form it into a usable Matlab matrix.  All four
%  polarizations are retained (VV, VH, HV, and HH).
%  The Xpatch output data must be pre-processed by
%  the FORTRAN program named field_mat.for

%Read in the data file.
m_file=input('Enter the .lin filename:  ','s');
m_file_i=[m_file '.lin'];
fid=fopen(m_file_i,'r');
disp('Reading the datafile')
[N]=fscanf(fid,'%d %d %d',[3 1])
X=fscanf(fid,'%g %g %g %g %g %g %g %g %g %g %g',[11 inf]);
fclose(fid)

%Strip out the data into separate vectors.
disp('Stripping')
el=X(1,:);
az=X(2,:);
f=X(3,:);
LL=X(4,:)+j*X(5,:);
LR=X(6,:)+j*X(7,:);
RL=X(8,:)+j*X(9,:);
RR=X(10,:)+j*X(11,:);

clear X

N_freq=N(1);
N_el=N(2);
N_az=N(3);

%Reshape the data vectors into matrices
disp('Reshaping')
el=reshape(el,N_freq,N_el*N_az);
az=reshape(az,N_freq,N_el*N_az);
f=f(1:N_freq);
LL=reshape(LL,N_freq,N_el*N_az);
LR=reshape(LR,N_freq,N_el*N_az);
RL=reshape(RL,N_freq,N_el*N_az);
RR=reshape(RR,N_freq,N_el*N_az);
```

```
%trans_data.m
%  This program converts the frequency domain data
%  generated by read_data_lin into time domain range
%  profile vectors.

%Transform the data into the time domain.
disp('Transforming')
for i=1:N_el*N_az
  ll(:,i)=fftshift(ifft(LL(:,i)));
  lr(:,i)=fftshift(ifft(LR(:,i)));
  rl(:,i)=fftshift(ifft(RL(:,i)));
  rr(:,i)=fftshift(ifft(RR(:,i)));
end

%Normalize the data to unit energy.
pll=ones(N_freq,1)*(std(ll).^(-1))/sqrt(N_freq);
plr=ones(N_freq,1)*(std(lr).^(-1))/sqrt(N_freq);
prl=ones(N_freq,1)*(std(rl).^(-1))/sqrt(N_freq);
prr=ones(N_freq,1)*(std(rr).^(-1))/sqrt(N_freq);
ll=pll.*ll;
lr=plr.*lr;
rl=prl.*rl;
rr=prr.*rr;
```

```
%  params.m
%  This matlab script contains the initial constants
%  required by the CAR_hebb.m simulation script.

B=300e6;
N=1024;
K=64;
fo=2.0e9;
c=3e8;

T=K/B;
Td=N*T;

beam_sector=10;
```

```
%This matlab script reads in a data file containing
%radar cross section data and calculates the target
%enhancement, signal to clutter improvement, and
%LPI performance loss due to Matched FSK/PSK signaling.
%This program is used to calculate the data contained
%in Table 7.1.

m_file=input('Enter the .lin filename:  ','s');
m_file_i=[m_file '.lin'];
fid=fopen(m_file_i,'r');
disp('Reading the datafile')
[N]=fscanf(fid,'%d %d %d',[3 1])
X=fscanf(fid,'%g %g %g %g %g %g %g %g %g %g %g',[11 inf]);
fclose(fid)

disp('Stripping')
el=X(1,:);
az=X(2,:);
f=X(3,:);
LL=X(4,:)+j*X(5,:);
LR=X(6,:)+j*X(7,:);
RL=X(8,:)+j*X(9,:);
RR=X(10,:)+j*X(11,:);

clear X

N_freq=N(1);
N_el=N(2);
N_az=N(3);

disp('Reshaping')

el=reshape(el,N_freq,N_el*N_az);
az=reshape(az,N_freq,N_el*N_az);
f=f(1:N_freq);
LL=reshape(LL,N_freq,N_el*N_az);
LR=reshape(LR,N_freq,N_el*N_az);
RL=reshape(RL,N_freq,N_el*N_az);
RR=reshape(RR,N_freq,N_el*N_az);

num=sum(abs(LL).^2);
den1=max(abs(ifft(LL)));
den2=sum(abs(LL));

Eb=(num./den1./den2).^2;
Em=N_freq*num./den2;
sc=num./(den1.^2)/N_freq;
L=1/N_freq./max(abs(LL)./(ones(N_freq,1)*den2));

perf=[10*log10(mean(Eb))  10*log10(max(Eb));.....
      10*log10(mean(Em))  10*log10(max(Em));......
```

```
10*log10(mean(sc)) 10*log10(max(sc));.....
10*log10(mean(L))  10*log10(min(L))]
```

```
C  FIELD_MAT.F
C  THIS FORTRAN PROGRAM READS IN AN XPATCH1 DATA FILE
C  AND CONVERTS THE DATA INTO A FORM THAT IS EASILY
C  PROCESSED BY THE MATLAB SCRIPT READ_DATA_LIN.M.
C  ADDITIONALLY, THE VERTICAL POLARIZED DATA IS CONVERTED
C  INTO CIRCULAR POLARIZED DATA IF NEEDED.

      COMPLEX VV, VH, HV, HH
      COMPLEX RR, RL, LR, LL
      COMPLEX J

      REAL F, AZ, EL

      INTEGER N_FREQ, N_AZ, N_EL, N_POINTS
      CHARACTER*50 JUNK
      CHARACTER F_FILE*13, M_FILE*13, L_FILE*13
      CHARACTER*5 FILE

C*************************************************************
C         GET THE REQUIRED DESCRIPTION FROM THE USER
C*************************************************************
      PRINT *,'ENTER THE TARGET FILENAME.FIELD'
      READ (*,*) FILE

      PRINT *,'ENTER THE NUMBER OF FREQUENCIES'
      READ (*,*) N_FREQ

      PRINT *,'ENTER THE NUMBER OF AZIMUTH ANGLES'
      READ (*,*) N_AZ

      PRINT *,'ENTER THE NUMBER OF ELEVATION ANGLES'
      READ (*,*) N_EL

      N_POINTS=N_FREQ*(N_AZ+1)*(N_EL+1)
         F_FILE=FILE // '.field'
         M_FILE=FILE // '.cps'
      L_FILE=FILE // '.lin'
         print *,F_FILE, M_FILE, L_FILE

      PRINT *,''
      PRINT
*,'================================================'   PRINT
*,'THE FILE TO BE PROCESSED IS        ',F_FILE
      PRINT *,'THE OUTPUT FILE IS                  ',M_FILE
      PRINT *,'THE NUMBER OF FREQUENCIES IS        ',N_FREQ
      PRINT *,'THE NUMBER OF AZIMUTH ANGLES IS     ',N_AZ+1
      PRINT *,'THE NUMBER OF ELEVATION ANGLES IS   ',N_EL+1
      PRINT *,'THE NUMBER OF DATA POINTS IS        ',N_POINTS
      PRINT
*,'================================================'
```

```
C*************************************************************
C       OPEN FILES FOR PROCESSING
C*************************************************************
     OPEN(UNIT=1, FILE=F_FILE)
     OPEN(UNIT=2, FILE=M_FILE)
        OPEN(UNIT=3, FILE=L_FILE)

C*************************************************************
C       READ THE DATA, PROCESS IT AND WRITE IT OUT          *
C*************************************************************
     J=CMPLX(0.000,1.000)

     WRITE(2,*) N_FREQ, N_AZ+1, N_EL+1
     WRITE(3,*) N_FREQ, N_AZ+1, N_EL+1
     DO 1 ICOUNT=1,5
 1      READ(1,*) JUNK

     ICOUNT=0
 10  READ(1,*,END=100) EL, AZ, EL, AZ, F, VV, VH, HV, HH
     ICOUNT=ICOUNT+1

     LL=.5*((HH-J*VH)-J*(HV-J*VV))
     LR=.5*((HH-J*VH)+J*(HV-J*VV))
     RL=.5*((HH+J*VH)-J*(HV+J*VV))
     RR=.5*((HH+J*VH)+J*(HV+J*VV))

     WRITE(2,*) EL, AZ, F, REAL(LL), AIMAG(LL),
     1     REAL(LR), AIMAG(LR),
     2     REAL(RL), AIMAG(RL),
     3     REAL(RR), AIMAG(RR)

        WRITE(3,*) EL, AZ, F, REAL(VV), AIMAG(VV),
     1     REAL(VH), AIMAG(VH),
     2     REAL(HV), AIMAG(HV),
     3     REAL(HH), AIMAG(HH)


     GOTO 10

 100 PRINT *,'ALL DONE'
     PRINT *,'YA KNOW..... THERE WERE ',ICOUNT,' DATAPOINTS'

     END
```